

Space for Shore

ESA EOEP-5
Coastal Erosion

Deliverable 1.3 Product Validation Plan



DOCUMENT HISTORY			
VERSION	AUTHORS	DATE	NOTE
0.0	SANDRA FERNÁNDEZ, UNIVERSITY OF AVEIRO VIRGINIE LAFON, I-SEA	19/11/2019	FIRST DRAFT
1.0	SANDRA FERNÁNDEZ, UNIVERSITY OF AVEIRO VIRGINIE LAFON, OLIVIER REGNIERS, NICOLAS DEBONNAIRE, I-SEA KERSTIN STELZER, BROCKMANN CONSULT ; GEORGIA KALOUSHI, TERRA SPATIUM ; SORIN CONSTANTIN, TERRA SIGNA ; MARTIN GADE, UNIVERSITY OF HAMBURG ; ISSAAK PARCHARIDIS, HAROKOPIO UNIVERSITY OF ATHENS	7/01/2019	FIRST RELEASE
2.0	SANDRA FERNÁNDEZ, UNIVERSITY OF AVEIRO VIRGINIE LAFON, I-SEA KERSTIN STELZER, BROCKMANN CONSULT ; GEORGIA KALOUSHI, TERRA SPATIUM ; ISSAAK PARCHARIDIS, HAROKOPIO UNIVERSITY OF ATHENS	11/01/2019	SECOND RELEASE
3.0	VIRGINIE LAFON, I-SEA	22/01/2019	THIRD RELEASE INCLUDING CLARIFICATIONS ASKED BY ESA





Summary

1	Introduction.....	5
1.1	Scope of the document.....	5
1.2	Reference documents.....	5
2	Validation of remotely sensed indicators of Coastal Erosion: Background	6
2.1	Objectives	6
2.2	State of the Art	6
2.2.1	Bathymetry.....	6
2.2.2	Waterlines (including middle of swash zones)	6
2.2.3	Dune foot	7
2.2.4	Cliff lines (apex and foot)	7
2.2.5	Submerged sandbars.....	8
2.2.6	Tidal flat – creek position changes	8
2.2.7	Top-of-the-cliff vertical movement	8
3	Validation methods implemented during phase 1	9
3.1	2D Morphological indicators (waterlines, dune foot, cliff foot, cliff apex and submerged sand bars, intertidal creek indicators).....	9
3.1.1	Quantitative approach n°1: the baseline method.....	9
3.1.2	Quantitative approach n°2: distance from GPS surveys.....	10
3.1.3	Qualitative approach.....	10
3.2	3D Morphological indicators.....	11
3.2.1	Nearshore bathymetry	11
4	Experiments carried out during phase 1: Data, results and discussion	14
4.1	Middle of Swash Zone.....	14
4.1.1	Detection based on optical data – algorithm 2b adapted.....	14
4.1.2	Detection based on SAR data – algorithm 2d adapted.....	18
4.2	Waterline	19
4.2.1	Detection based on optical data – algorithm 2a	19
4.2.2	Detection based on optical data – algorithm 2b and 2c.....	22
4.2.3	Detection based on SAR data (algorithm 2d)	28
4.3	Dune foot.....	29
4.3.1	Detection based on optical data – algorithm 3a	29
4.3.2	Detection based on optical data – algorithm 3h	30
4.4	Cliff lines (cliff apex, cliff foot)	33
4.4.1	Detection based on optical data – algorithm 3i	33
4.5	Bathymetry	35
4.5.1	Detection based on optical data – algorithm 4a	35
4.5.2	Detection based on optical data – algorithm 4b	37
4.5.3	Detection based on SAR data – algorithm 4c	42
4.6	Submerged sandbars	45
4.6.1	Detection based on optical data – algorithm 6a	45
4.7	Summary: validation actions performed during year 1 and planned for the year 2.....	46



5	Validation Plan for Phase 2	50
5.1	Current products.....	50
5.1.1	Water line detection using band ratios (algorithm 2a)	50
5.1.2	Waterline detection based on optical imagery (algorithm 2b)	51
5.1.3	Middle of swash zone based on optical imagery (algorithm 2b – adapted).....	52
5.1.4	Middle of swash zone based on SAR imagery (algorithm 2d - adapted).....	53
5.1.5	Waterline detection based on SAR imagery (algorithm 2d).....	55
5.1.6	Dune foot based on textural analysis of VHR optical data (algorithm 3a)	55
5.1.7	Dune foot extraction based on VHR imagery-derived DEM (algorithms 1a + 3b).....	57
5.1.8	Cliff lines extraction based on VHR imagery-derived DEM (algorithm 1a + 3c)	57
5.1.9	Cliff lines extraction based on VHR/HR imagery-derived DEM (algorithm 1b + 3c).....	59
5.1.10	Manual linear feature extraction from DEMs (algorithm 3d).....	59
5.1.11	Beach width (algorithm 3e).....	60
5.1.12	Top-of-the cliff vertical movements (algorithm 3f).....	61
5.1.13	Intertidal creek morphological characteristics (algorithm 2e, 3g and 5c).....	64
5.1.14	Dune foot extraction using supervised classification (algorithm 3h)	65
5.1.15	Cliff line extraction using supervised classification (algorithm 3i)	67
5.1.16	Bathymetry (algorithm 4c)	69
5.1.17	Submerged sand banks (algorithm 6a).....	70
5.1.18	Mapping change of sandbars (algorithm 6b)	70
5.2	New products.....	71
5.2.1	Dune foot extraction using SAR data (3j)	71
5.2.2	Maximum swash zone excursion (run-up)	72
5.3	Synthesis of the planned validation actions	73
6	References	78



1 INTRODUCTION

1.1 Scope of the document

This document provides an overview of the methodologies for validation of current indicators produced by the Space for Shore Consortium as well as the prospect of methodologies for validation of indicators or algorithms that were not tested during phase 1. Additionally, the validation results obtained for some indicators produced at different POC sites during the first phase of the project are also presented. These results disclose the necessity of future work (*e.g.*, field surveys at some POC sites, new techniques of field data acquisition).

All the details about the plan are presented in the fifth section of the present document.

Since the validation activities are numerous, a general summary of the planned actions and expected results is finally reassembled.

1.2 Reference documents

This document refers to the coastal erosion indicators requested by the end-users engaged in the project. The indicators are listed, detailed and described into the following deliverables:

- A. Dehouck, V. Lafon, A. Robinet, K. Stelzer, I. Serban, S. Constantin, G. Kalousi, P. Baptista, 2019. ESA EOEP-5 Coastal Erosion - Requirement Baseline. Space for Shore Consortium, V7.0, 22/08/2019.
- K. Stelzer, A. Dehouck, I. Serban, G. Kalousi, P. Baptista, 2019. ESA EOEP-5 Coastal Erosion – User Requirement Document Book. Space for Shore Consortium, V1.0, 23/04/2019.
- K. Stelzer, A. Robinet, V. Lafon, O. Regniers, B. Beguet, A. Dehouck, P. Baptista, S. Fernández, G. Kalousi, I. Serban, I. Echave, M. Gade, K. Bantouvaki, I. Parcharidis, 2019. ESA EOEP-5 Coastal Erosion – Technical Specification. Space for Shore Consortium, V1.1, 13/08/2019.



2 VALIDATION OF REMOTELY SENSED INDICATORS OF COASTAL EROSION: BACKGROUND

2.1 Objectives

The main goals of the validation activities are as follows:

- (1) to improve Technical Specification Report (many algorithms do not have validation results);
- (2) to drive the development of some innovative algorithms;
- (3) to present objectively the accuracy of the produced indicators;
- (4) to convince the end-users the products delivered fit their expectations.

2.2 State of the Art

This section summarizes the methods found in the literature for validation of remotely sensed indicators namely, bathymetry, waterlines, dune foot, cliff lines (foot and apex), cliff vertical movements, submerged sandbars and tidal flat (namely creek position changes).

2.2.1 Bathymetry

Satellite Derived Bathymetry (SDB) has achieved a great worldwide development (*e.g.*, Almar et al., 2019; Caballero and Stumpf, 2019; Casal et al., 2019; Chénier et al., 2019; Evagorou et al., 2019; Mavraeidopoulos et al., 2019; Misra et al., 2019; Pereira et al., 2019; Sagawa et al., 2019). The satellite derived bathymetry needs to be compared with the available field bathymetry and accuracy assessments are required in order to identify methodological approaches which perform best (Chénier et al., 2019). This validation can be done comparing satellite derived water depths and measured ones at different points (Mavraeidopoulos et al., 2019) or at different contour lines (Pereira et al., 2019). It can be also mapped the difference between satellite derived and measured water depths (Hamylton et al., 2015; Evagorou et al., 2019).

2.2.1.1 3D rasters

As described in many studies (*e.g.*, Evagorou et al., 2019; Pereira et al., 2019; Sagawa et al., 2019), the accuracy of satellite derived bathymetry is usually estimated by comparing the results with field data after applying a tidal correction to bring both data in the same tidal reference. Once the field data has been resampled at the resolution of the satellite data, a pixel by pixel comparison can be carried out. Scatterplots, statistics (bias, RMSE, mean absolute error, mean relative error, etc.), transect plots, difference histogram or difference maps are among the most common validation outputs.

2.2.1.2 Depth contour lines

Pereira et al. (2019) evaluated the accuracy of the satellite derived bathymetry comparing the calculated depth contour lines (*i.e.* isobaths) with the field bathymetry. The calculated isobaths were corrected considering the astronomical tidal elevation at time of image acquisition to make possible the comparison with the bathymetry survey. Furthermore, the relative error of water depth was estimated.

2.2.2 Waterlines (including middle of swash zones)

Waterlines are one of the indicators of shoreline (Toure et al., 2019 and references therein) and the waterlines can be considered as:

- Instant tidal levels and wetting limits such as:
 - water line (swash line) that is the interface between the body of water and the slope of the beach. It refers to the limit of the foam of the swash (the rush of seawater up the beach after the breaking of a wave)



- wet/dry line (wet/sand line) that represents the end of the swash at high tide and during the ebb tide and it migrates to the sea and marks the land side limit of the sands darkened by the breaking of a wave
 - high water line that defines the level of the last high tide and thus, corresponds to the upper wetting limit of the foreshore by the previous open sea
 - high tide wrack line that consists in the line of debris left on the beach by high tide
 - mean high water line (average high-water line)
- Tidal datums such as:
 - mean sea level
 - mean high water line
 - mean spring high water line
 - mean higher high-water line
 - mean low water line
 - mean low water spring tide mark
 - lowest astronomical sea level

Waterlines satellite derived techniques have been widely used (*e.g.*, García-Rubio et al., 2015; Cenci et al., 2017; Luijendijk et al., 2018; Oyedotun et al., 2018; Cabezas-Ramadán et al., 2019; Di Lucio et al., 2019; Esmail et al., 2019; Toure et al., 2019; Vos et al., 2019). Waterlines satellite derived need to be compared with the corresponding field waterlines to determine the accuracy of the methodological approaches. Furthermore, as satellite images are acquired at any stage of tide, a simple tidal correction must be applied to each waterline extracted from satellite image to enable comparison (García-Rubio et al., 2015; Vos et al., 2019).

2.2.3 Dune foot

Similarly, to satellite derived waterlines, the estimation of the detection accuracy of dune foot lines relies entirely on its comparison with a field data acquired at a date close to the satellite image. From an operational point of view, an approach such as the perpendicular transect method available in the R package AMBUR or in the ArcGIS plugin DSAS is often used (*e.g.*, Jackson et al., 2012; Kaliraj et al., 2014; Lafon et al., 2014).

2.2.4 Cliff lines (apex and foot)

Changes on the cliff lines, apex and foot, result from a combination of different processes and can be assessed through “traditional” state-of-the-art satellite photogrammetric techniques, while the validation of such products is usually performed by comparing these satellite derived lines with measured lines (on the ground) on specific points (Nunes et al., 2009; Redweik et al., 2009; Rosser et al., 2005).

In most cases the cliff lines are collected during a in-situ GPS survey techniques (Real Time Kinematic, L1/L2 frequencies) with a mean horizontal accuracy of a few centimetres (Nunes et al., 2009). While, the past years with the massive emergence of UAV platforms and relevant data handling and management techniques, several UAV-derived data (over specific areas) could also been used for validation purposes for satellite-derived results in extended areas (Nikolakopoulos et al., 2019).

These UAV platforms brought also new digital photogrammetry techniques, termed Structure-from-Motion (SfM), that have reinvigorated the use of photography from land-based and/or airborne platforms to measure landscape topography and changes (Warrick, 2017). Most applications of SfM include photographic and ground control surveys to build three-dimensional point clouds or two-dimensional height fields, that could also be used for validation purposes as well. Airborne lidar measurements can be used as an alternative. DEM (Digital Elevation Model), instead of DSM (Digital Surface Model) are recommended to retrieve the morphology of the cliffs.



Meantime, other traditional surveying methods could also be used for collecting 3D points over cliff lines, with state-of-the-art terrestrial laser scanning techniques (Rosser et al., 2005). The results of this publication demonstrate that terrestrial laser scanning can be used to quantify cliff failures to a previously unobtainable precision.

In cases where historical cliff lines are produced (past years), of course with the use of archive/legacy satellite imagery (usually high-resolution imagery), then the proposed validation methods could also be performed with lines produced by pre-existing aerial photos (Redweik et al., 2009; Marques et al., 2011). For example, in Marques et al. (2013) use state-of-the-art methods that include special procedures to enable the extraction of accurate data from old aerial photographs, and validated by systematic stereo photograph interpretation, helped by oblique aerial photographs observation and field surveys.

Cliff line horizontal motion is generally studied by 4 different approaches:

- The baseline approach (Dolan et al., 1978), similar to the one described for waterline and dune foot validation;
- The dynamic segmentation approach (Liu, 1998 ; Li et al., 2001 ; Srivastava et al, 2005) ;
- The area-based approach (Costa, 2000; Ali, 2003);
- The approach based on buffers and the non-linear least square estimation (Heo et al., 2009).

2.2.5 Submerged sandbars

The methodology used to validate the results of the sandbars positions extractions from satellite data relies on the one described in Tatui and Constantin (2020). For each of the sandbar crest position available as *in-situ* measurement, a corresponding location estimated using the satellite imagery is identified. For each point, the distance to a baseline (almost parallel to the sandbars) is computed. The difference between these two distances is then computed in order to assess how different are the satellite estimations from the in-situ observations.

2.2.6 Tidal flat – creek position changes

Remote sensing in combination with *in-situ* surveying are effective and flexible means of monitoring tidal flats. The *in-situ* surveying can include: ground-based video imaging that enables the determination of three-dimensional real-world positions from time-series frame-images but it only covers a local area and/or airborne imaging (e.g., airborne light detection and ranging-LIDAR) that allows to cover a big area (Wang et al., 2019).

The Wadden Sea is regularly recorded by airborne images which are rectified to orthophotos. They are the basis of creek line extraction and will be used as verification data sets. Until now it is not known that the position of tidal is mapped on ground. In addition, we could not find reference in the literature of validation works already performed for this particular indicator.

2.2.7 Top-of-the-cliff vertical movement

The PS-InSAR technique allowed to perform a pre- and a post-event displacement analysis on the general rock massif stability, evaluating the state of activity of long-term ground displacements. For the validation of ground motion many scientists use a monitoring system based on remote sensing techniques, such as radar interferometry ground-based and terrestrial laser scanning, in order to monitor the ground deformation of the investigated area and to evaluate the residual risk (Frodella et al., 2016). More specific for the top of the cliff movement validation the Martino et al. (2014) use field-based geomechanically investigations and remote geostructural investigations via a terrestrial laser scanner (TLS).



3 VALIDATION METHODS IMPLEMENTED DURING PHASE 1

(This section describes how has been performed the validation. It should contain a table with the different indicators indicating if they are 2D or 3D because there are two approaches for validation: planimetric and altimetric)

3.1 2D Morphological indicators (waterlines, dune foot, cliff foot, cliff apex and submerged sand bars, intertidal creek indicators)

3.1.1 Quantitative approach n°1: the baseline method

The quantitative planimetric approach implemented during phase 1 for waterline, dune and cliff lines, middle of swash zone and submerged sandbars consists in computing the distance between measured *in-situ* and satellite derived lines. The distance between lines or points is estimated with Digital Shoreline Analysis (DSAS) software that is an add-in to ESRI ArcGIS desktop (Himmelstoss et al., 2018; Thieler et al., 2009), or by using in-house developed methodologies. The required inputs are the lines (*i.e.* produced indicators such as waterline, dune foot, cliff foot, cliff apex, ...), or points (submerged sandbars), the baseline (*i.e.* reference line from all distances are calculated) and the cross-shore transects spaced from a baseline (Figure 1). The cross-shore transect spacing is site dependent and for that reason, each regional partner must decide it keeping in mind that the total number of transects guarantee the representative of the calculations. The output is the distance of lines from baseline and the difference between measured and satellite derived lines is obtained as (Eq.1):

Distance between lines =

$$\text{Distance to baseline of in-situ measured line} - \text{Distance to baseline of satellite derived line} \quad (\text{Eq.1})$$

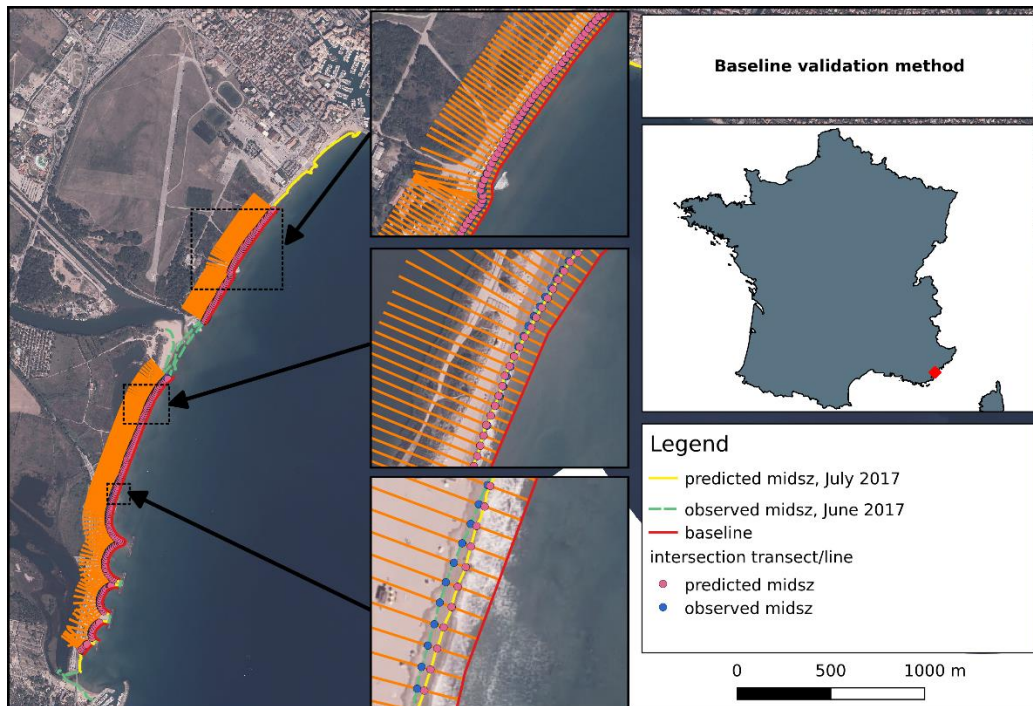


Figure 1: Map with the baseline, the measured and satellite derived lines and the cross-shore transects.



3.1.2 Quantitative approach n°2: distance from GPS surveys

The approach is described in section 2.2.5, p. 8.

3.1.3 Qualitative approach

As an alternative to quantitative approaches was also implemented a qualitative planimetric approach. This approach consists in the comparisons with high resolution images in Google Earth (Figure 2) or airborne orthophotos. These are performed by using the historic images and overlaying them with the extracted waterlines lines.



Figure 2: Google Earth image close to the satellite overpass of Sentinel-2 in 2018 overlaid with waterline (wet/dry line) derived from Sentinel-2.

In addition to these images, airborne orthophotos that have been provided by the user (Germany) have been used for overlaying the waterlines satellite derived and perform a visual inspection.

Tidal creek lines extracted from satellite imagery are compared with airborne orthophotos. Furthermore, an intercomparison is performed between optically derived indicators and indicators based on SAR images. Figure 3 shows the overlay of optically derived creek position on a Sentinel-1 image for cross-checking



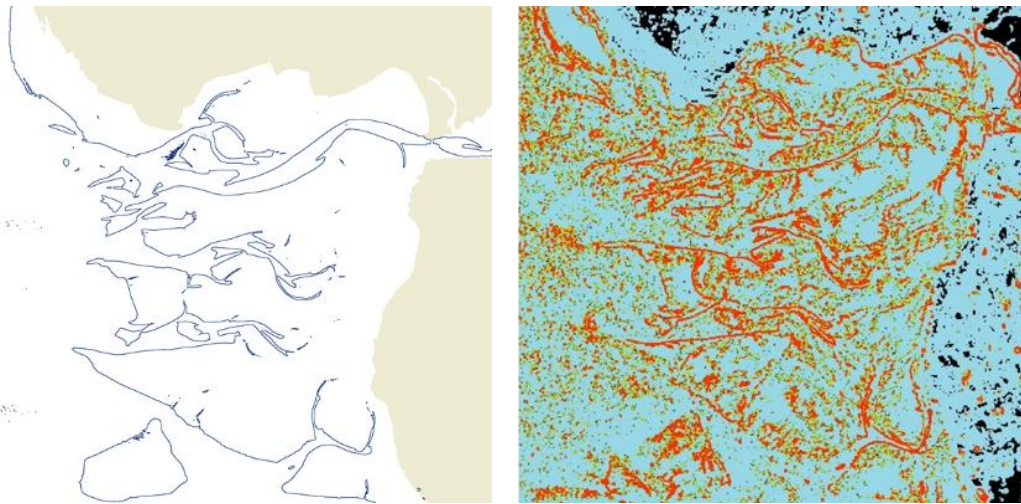


Figure 3: Intercomparison of the optic and SAR algorithms for the tidal creek position for the year 2018.

3.2 3D Morphological indicators

3.2.1 Nearshore bathymetry

3.2.1.1 3D rasters (altimetric approach)

Prior to the validation, available field bathymetric data are resampled at the spatial resolution of the satellite image. If multiple data are available within a same pixel, a criterion based on the standard deviation is used to discard data located over steep gradients. Besides, the satellite derived bathymetry is also corrected to take the tide level into account and bring the result to the same tidal reference as field data. If a calibration step is necessary, the pre-processed dataset is split in half, one set is used for the calibration and the other for the validation.

Several validation outputs are produced. First, a scatterplot between field data and the estimated depth is computed to represent how both data depending on the depth (Figure 4).

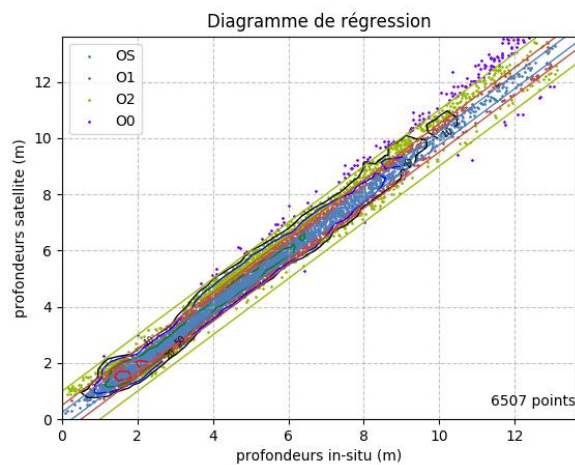


Figure 4: Regression diagram between field data and satellite derived bathymetry with isolines and dots corresponding to OHI orders (blue line and dots: ± 0.25 m – Special Order, red line and dots – Order 1: ± 0.5 m, green line and dots – Order 2: ± 1 m, purple dots – Order 0: $> \pm 1$ m).



Second, an absolute difference map (Satellite derived depth – Observed depth) is computed in order to identify more or lesser accurate areas (Figure 5). Finally, statistics, such as bias, RMSE, absolute mean error and relative mean error are computed and stored.

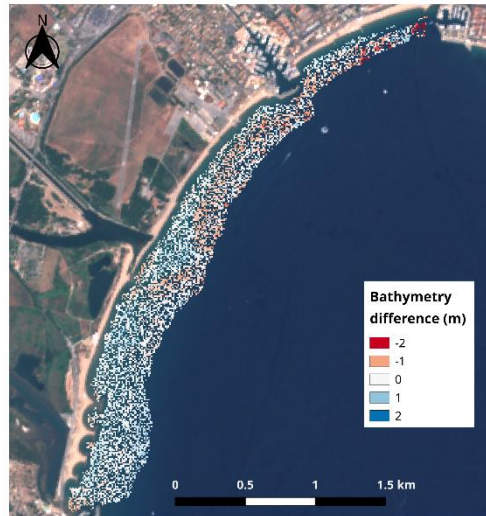


Figure 5: Example of a difference map between satellite derived bathymetry and observed bathymetry.

3.2.1.2 Depth contour lines (altimetric approach)

A set of nearshore depth contour lines (*i.e.* isobaths) 5m spaced from 15 m to 35 m below mean sea level are considered to compare the observed and satellite derived bathymetry as in Pereira et al. (2019). The values of depth at the location of the measured isobaths are extracted from the satellite derived bathymetry (Figure 6). Then, the depth differences are computed from satellite and measured bathymetry (Eq.2):

$$\text{Depth difference} = \text{Depth observed} - \text{Depth satellite derived} \quad (\text{Eq.2})$$



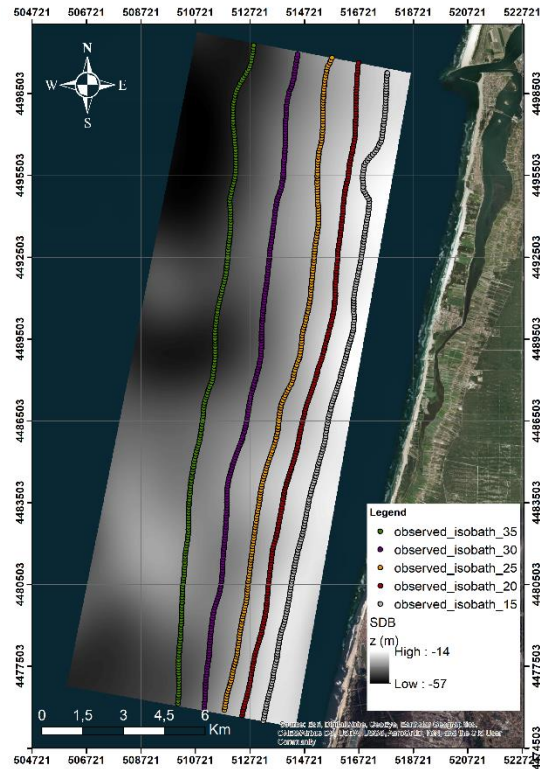


Figure 6 : Map of the satellite derived bathymetry (SDB) with the observed isobaths from 15 to 35 m depth referred to mean sea level.



4 EXPERIMENTS CARRIED OUT DURING PHASE 1: DATA, RESULTS AND DISCUSSION

4.1 Middle of Swash Zone

4.1.1 Detection based on optical data – algorithm 2b adapted

4.1.1.1 Background

A set of waterlines are computed for a short period of time (2 months) and then averaged to estimate the middle of swash zone. Waterline detection uses a combination of a classification approach and a thresholding method (Vos et al., 2019). First a threshold is determined by plotting the distribution of a water index among sand and water pixels. Then, a marching square algorithm (Lorensen et al., 1987) is used to find the line on the water index corresponding to that threshold.

This method has been applied to numerous images and sensors during phase 1. An extensive validation experiment has been carried out. We will present the validation made for VHR sensors, SPOT5, then for Sentinel-2 and Landsat-8.

4.1.1.2 VHR sensors

4.1.1.2.1 Data

Tests have been performed for Worldview and Pleiades at Hyères and Saint Raphaël, respectively. For Hyères, the year 2011 was considered. A remotely sensed shoreline derived from an image acquired the 5th of May and was compared to GPS surveys carried out during summer 2011 over a total distance of 2.49 km.

For Saint Raphaël, the image was acquired in July 2017 and the GPS survey in June 2017 over a total distance of 2.28 km.

4.1.1.2.2 Results

Comparison between predicted and observed middle of swash zones at Hyères and Saint Raphaël are detailed in Figure 7 and Figure 8, respectively.

In both cases, the bias is lower than 1 m and the RMSE lower than 2 m. Maximum errors rarely exceed 5 m.

Therefore, the uncertainty on the detected middle of swash zone based on VHR images is of the order of the pixel size, and of the GPS survey best achievable accuracy. Main discrepancies between the GPS survey and the remotely sensed middle of swash zone are observed in the vicinity of groins.

Thus, it can be concluded that the detection of the middle of swash zone based on VHR imagery satisfies coastal managers monitoring needs in microtidal regions, even if one single image is used, even when the image acquisition time and period is not constrained.



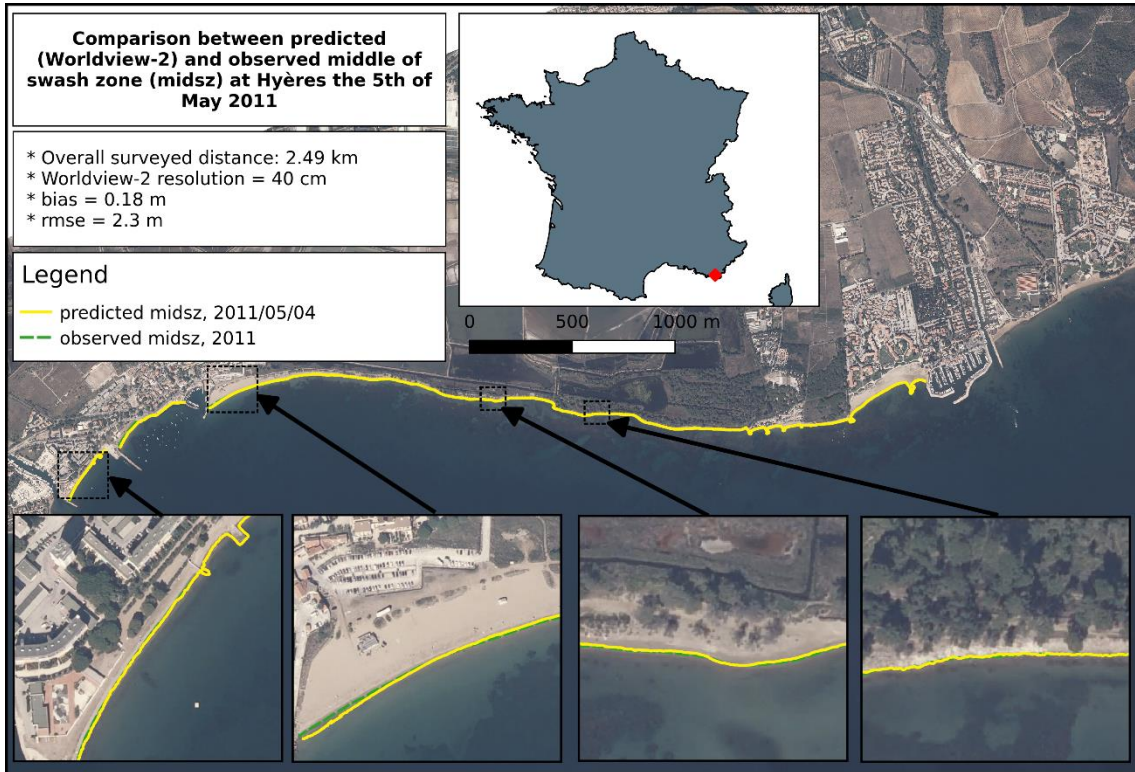


Figure 7 : Comparison between predicted (WorldView-2) and observed middle of swash zone at Hyères the 5th of May

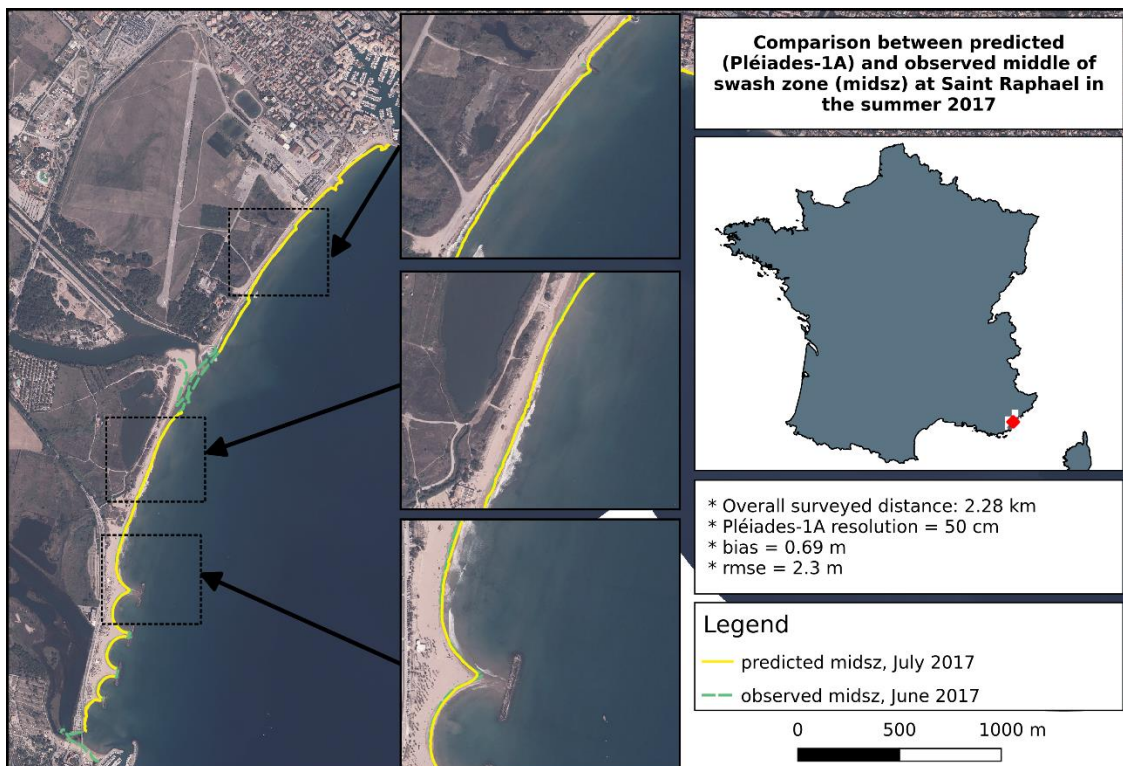


Figure 8 : Comparison between predicted (Pleiades-1A) and observed middle of swash zone at Saint Raphaël during summer 2017



4.1.1.3 Middle of swash zone detection based on SPOT-5 time series

4.1.1.3.1 Data

Several SPOT-5 images have been processed in order to predict the middle of swash zone of the Camargue POC site in 2008. The resulting indicator has been compared to a GPS survey carried out during summer 2008 over a distance of 21.7 km.

4.1.1.3.2 Results

Results are displayed in Figure 9. The bias is of 5 m and the RMSE is lower than 10 m. The main discrepancies between the GPS survey and the remotely sensed middle of swash zone are observed again in the vicinity of rocky longshore and cross-shore rocky protection structures.

Therefore, the uncertainty on the detected middle of swash zone based on SPOT-5 time-series is of the order of the pixel size, which demonstrates the good capacity of SPOT archives to contribute to the analyses of the erosion over the past 10 years. However, location error can reach 20 to 30 m at some location.

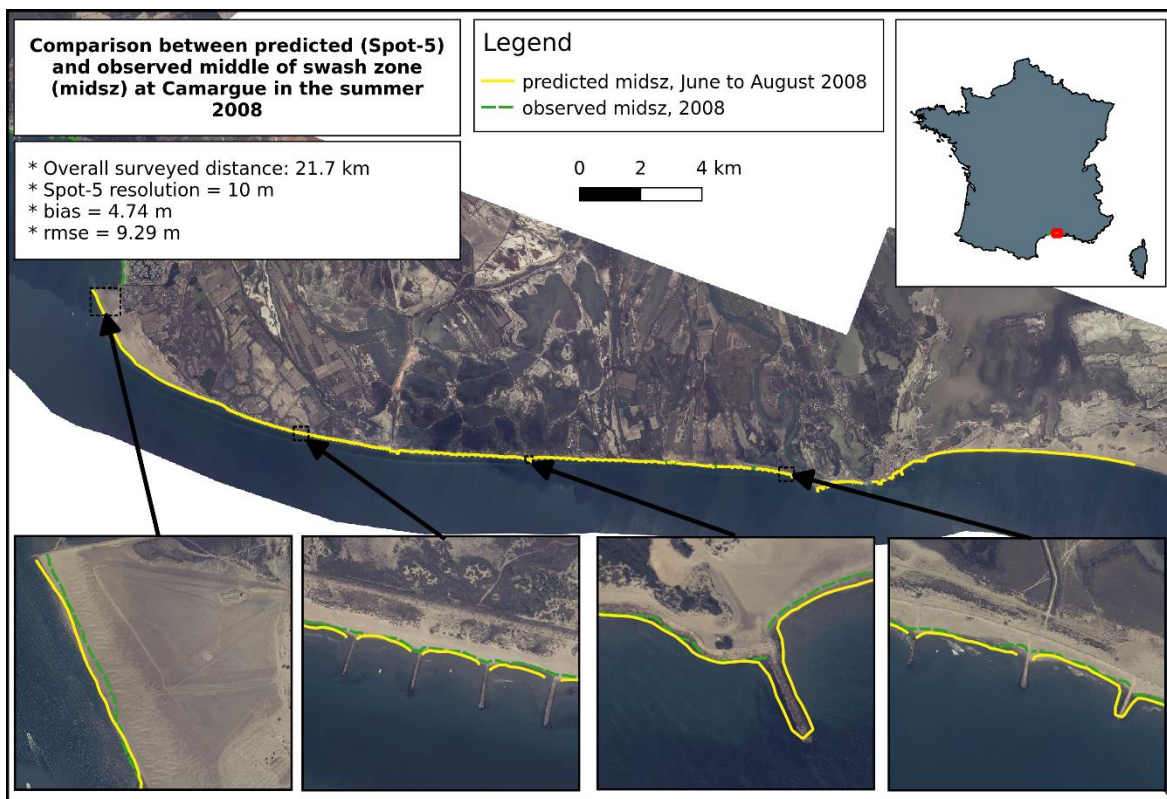


Figure 9 : Comparison between predicted (SPOT-5) and observed middle of swash zone along the Camargue during summer 2008

4.1.1.4 Middle of swash zone detection based on Sentinel-2 time-series

4.1.1.4.1 Data

Middle of swash zone based on Sentinel-2 imageries has been produced at Saint Raphaël in 2017 and 2019. In both cases, times-series of images acquired during summertime (June-August) have been processed and compared to GPS surveys carried out in June. The overall surveyed distance combining the field surveys is of 7.3 km.



4.1.1.4.2 Results

The RMSE obtained for the compilation of the comparisons performed in 2017 and 2019 is lower than 10 m. The bias ranges from 7 m in 2017 to 10 m in 2019. The result obtained in 2017 is shown in Figure 10 as an example. The location error rarely exceeds 15 m. The main detection difficulties are recorded in the vicinity of protection walls.

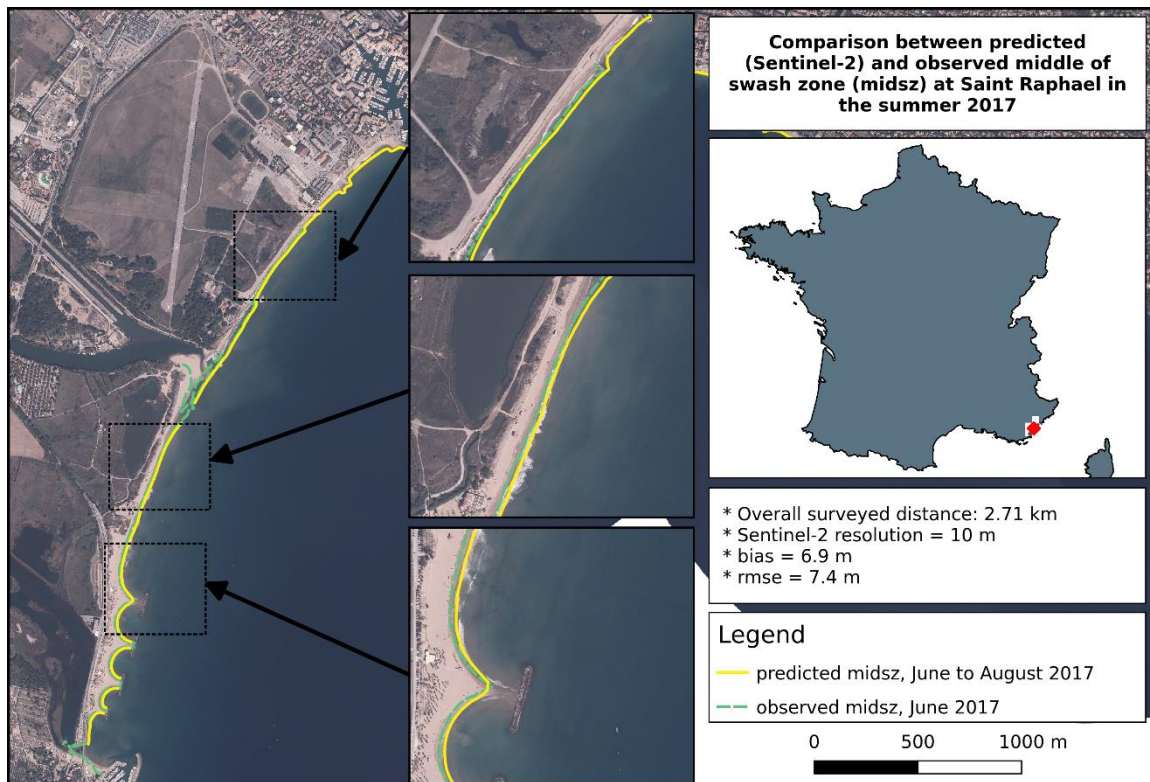


Figure 10 : Comparison between predicted (Sentinel-2) and observed middle of swash zone at Saint Raphaël during summer 2017

4.1.1.5 Middle of swash zone detection based on Landsat-8 time-series

4.1.1.5.1 Data

Middle of swash zone based on pansharpened Landsat-8 imageries has been produced at Saint Raphaël in 2013 and 2017. In both cases, times-series of images acquired during summertime (June-July 2013 and June-August 2017) have been processed and compared to GPS surveys carried out, respectively, in September 2013 and June 2017. The overall surveyed distance combining the field surveys is of 4.72 km.

4.1.1.5.2 Results

In both cases, the bias and the RMSE are lower than 10 m. The best performances are obtained for the indicator derived in 2017, as shows Figure 11 (bias and RMSE lower than 5 m). Maximum errors rarely exceed 10 to 15 m and they are in general located near the rocky defence structures.



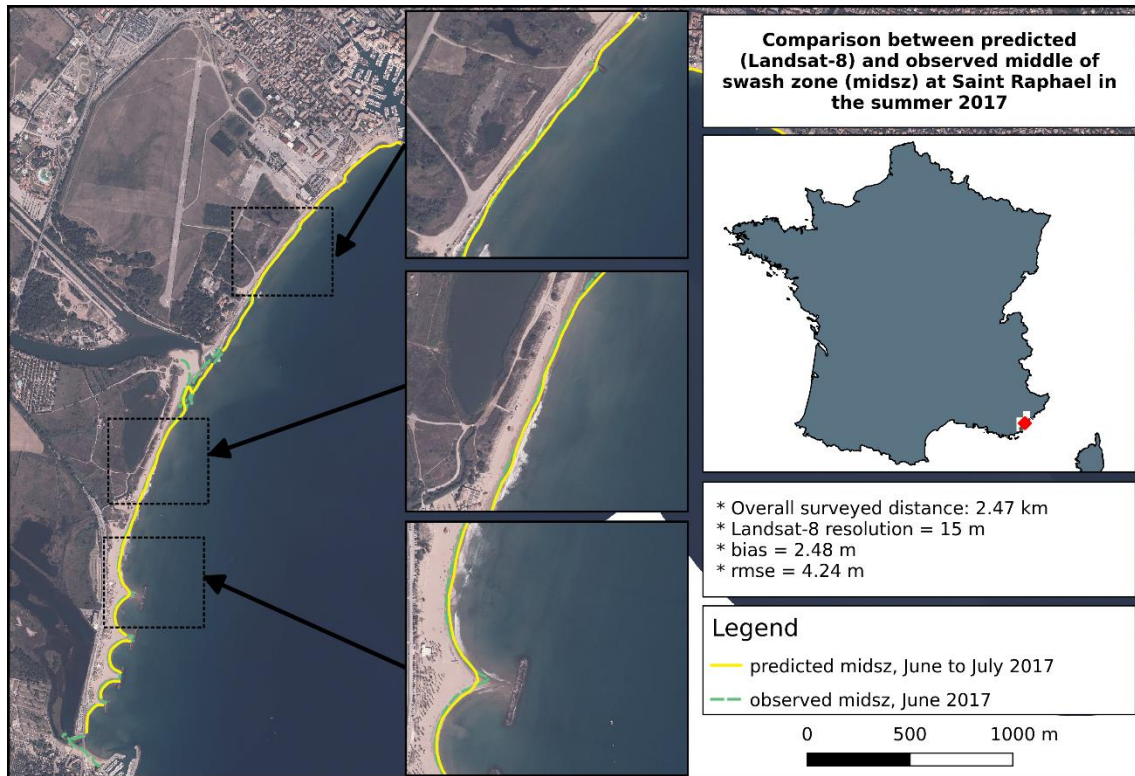


Figure 11 : Comparison between predicted (pansharpened Landsat-8) and observed middle of swash zone at Saint Raphaël during summer 2017

4.1.1.6 Discussion

The detection of the middle of swash zone based on algorithm 2b adapted from the recent work published by Vos et al. (2019) shows excellent result over the various validation experiments carried out during phase 1 and whatever the sensor considered for retrieving this indicator.

The good performance of the approach developed to extract the middle of swash zone in microtidal regions from optical image time-series is clearly demonstrated here. The performance of the approach is demonstrated over all sites that required this indicator and whatever the sensor used to retrieve the indicator. Also, validation encompasses major characteristics such as narrow beaches, presence of defence walls and groynes, urban and natural sandy shores where this indicator is usually requested. Finally, validation has been performed over a total distance of almost 38.5 km.

However, from these results, it seems that improvements could still be made is the vicinity of rocky defence structures where the middle of swash zone is not as accurate as on sandy locations. Therefore, during phase 2, it will be relevant to pursue the algorithm development of clarify its limitations and finalise the validation experiment.

4.1.2 Detection based on SAR data – algorithm 2d adapted

4.1.2.1 Background

Land and especially man-made objects have a strong back-scattering. Due to the instability of the water surface, SAR images have low amplitude and low coherence. Finding the perfect threshold will result a map which shows waterline detection. Single image or time-series have been tested to retrieve automatically the waterline. Due to the low performance of the algorithm, automatic threshold between water and land have been replace by man-made selection of the threshold.



Consequently, the water line derivation approach based on SAR data need to be improved and strengthened during phase 2. However, preliminary validation test of the SAR-retrieved middle of swash zone have been carried out, in order to show the potential of the method when the threshold between the water and land is defined manually.

4.1.2.1.1 Data

Two validation experiments have been carried out at Saint Raphaël during early and late summer 2017 and 2018, in order to benefit from various available GPS surveys.

4.1.2.1.2 Results

In all cases, the results seem rather promising (see example displayed on Figure 12). The bias and RMSE are reasonably low (lower of the order of the pixel size). However, location uncertainty of about 60 m are found at some locations.

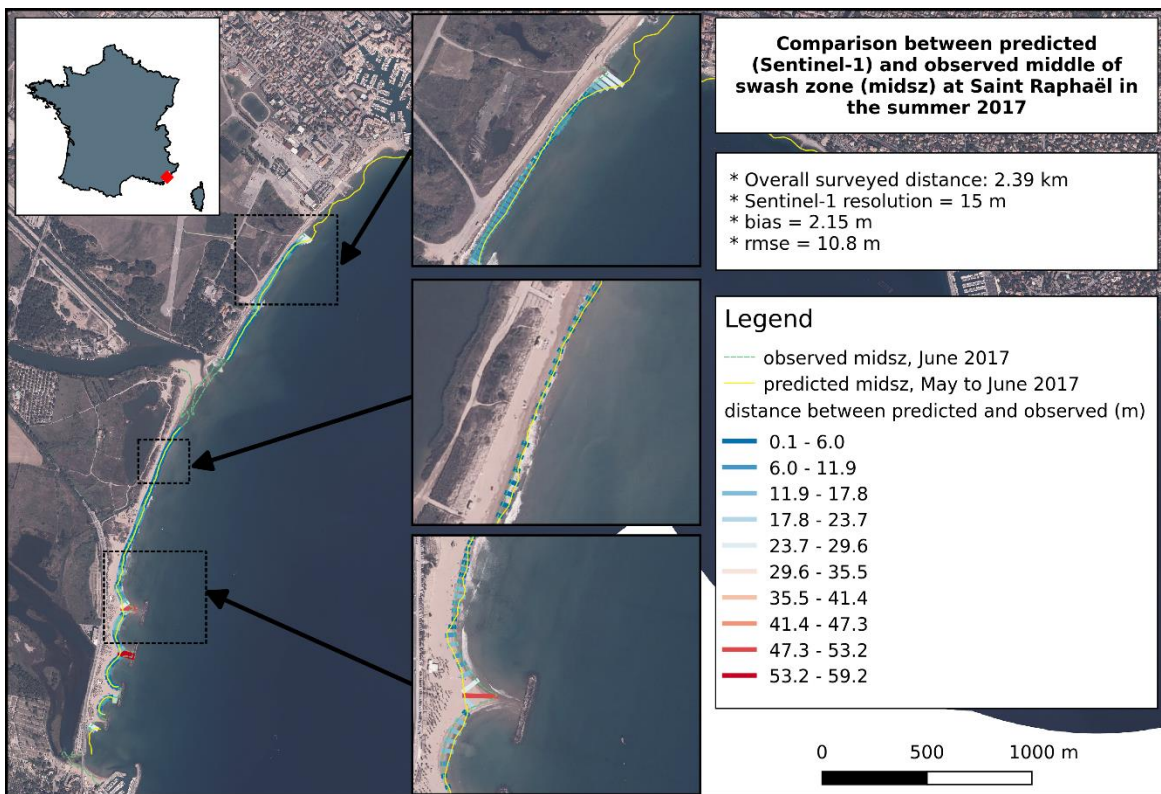


Figure 12. Comparison between predicted (Sentinel-1) and observed middle of swash zone at Saint Raphaël during early summer 2017

4.1.2.2 Discussion

Algorithm 2d will be improved and extensively validated over the Provence-Alpes-Côte d’Azur (PACA) region during year 2 for the retrieval of the middle of swash zone.

4.2 Waterline

4.2.1 Detection based on optical data – algorithm 2a



4.2.1.1 Background

The extraction of the coastline, defined as the line between water and land, is based on a spectral band ratio between the near Infrared and green bands. A threshold based on this ratio indicates the border between land and water and is defined based on the histogram of each image.

4.2.1.2 Sylt Odde

4.2.1.2.1 Data

For the detection of the coastline high resolution optical satellite data from Landsat (7 and 8) and Sentinel-2 have been used. The derived shorelines have been compared to historic very high-resolution images provided by Google Earth for verification. Another data source for verification are airborne images provided by the user (LKN SH). These orthorectified images are an absolute reference. The time difference between airborne and satellite images need to be considered.

4.2.1.2.2 Results

Coastline could be extracted from Landsat and Sentinel-2 images. When comparing the different years, the changes in the southern part of Sylt are clearly visible (Figure 13). These changes are related to the coastal protection measures that has been partly erased.

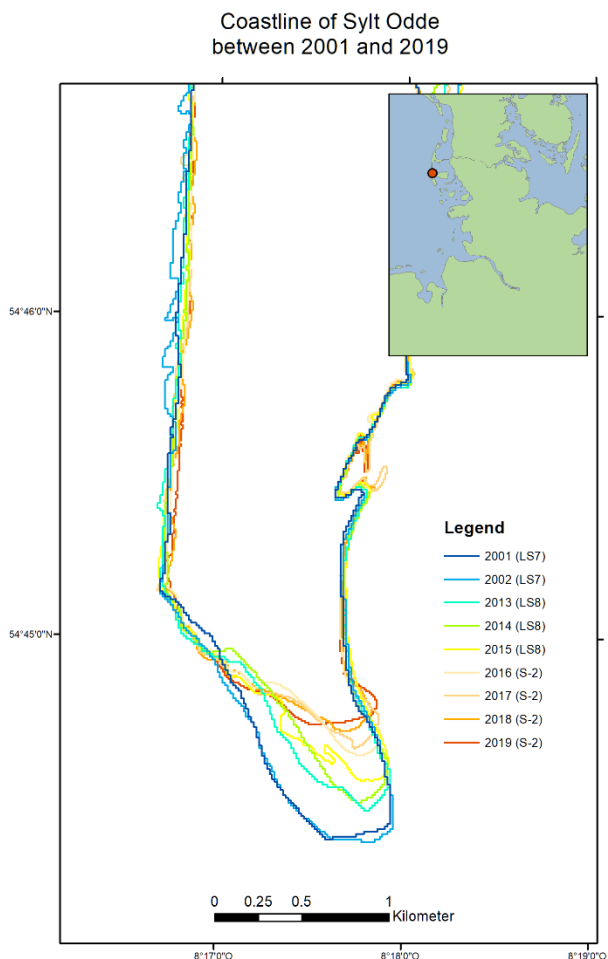


Figure 13 : Coastlines at Sylt Odde derived from Landsat-7 (LS7), Landsat-8 (LS8) and Sentinel-2 (S2) images showing the evolution of the southern part of Sylt after coastal protection has been partly erased.



The verification of the single coastlines with historic Google Earth imagery is shown in Figure 14 whereas the verification with airborne orthophotos is presented in Figure 15. The temporal difference between both data sources needs to be as small as possible in order to be a valid verification method.



Figure 14: Coastline Sylt Odde detected by satellites overlaid to VHR historic Google Earth (GE) images:
left: GE 10.07.2014/ Landsat-8 05.06.2014; middle: GE 24.07.2018/Sentinel-2 07.07.2018; right: GE 17.04.2019/Sentinel-2 06.07.2019

4.2.1.3 Discussion

The extraction of the land-water line is strongly influenced by the water level, which is influenced by tidal changes and/or wind vectors. Thus, the changes can be large between two images, but not indicating coastal erosion. In order to avoid an assessment of natural water level changes instead of coastal erosion, as many images as possible need to be considered. Time series can demonstrate trends in coastal erosion. For better assessments, the tidal status as well as the wind information should be reported in the metadata of the products. Further, the spatial resolution of the input images may differ, which influences the accuracy of the coastline position.



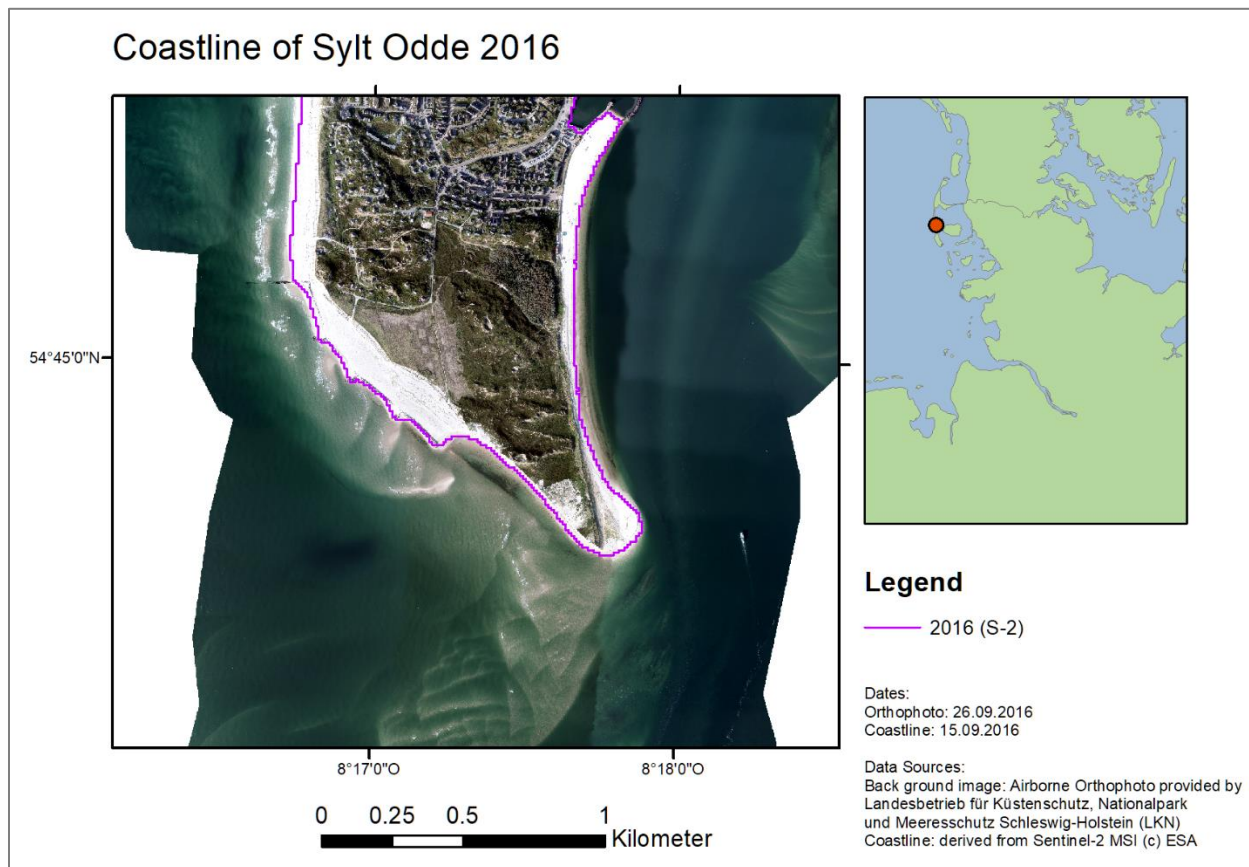


Figure 15 : Verification of coastline extraction with airborne orthophotos. Source of airborne data: Landesbetrieb für Küstenschutz, Nationalpark und Meeresschutz Schleswig-Holstein (LKN).

4.2.2 Detection based on optical data – algorithm 2b and 2c

4.2.2.1 Background

The algorithm 2b is based on the Normalized Difference Water Index (NDWI) whereas the algorithm 2c is based on supervised classification that differentiates water pixels from others located in the subaerial domain.

4.2.2.2 Gheorge Sf. Sulina

For the Romanian coastal area, both algorithm 2b and 2c were tested in order to inter-compare the results and draw conclusions on the accuracy of each of the methodology.

For the NDWI approach, a modified version of the index was computed, meaning that the SWIR band was used instead of the NIR one. This was chosen as the SWIR region of the electromagnetic spectrum is less prone to be affected by shallow or high turbidity waters.

4.2.2.2.1 Data

For the purpose of the validation exercises, the results obtained after processing a Sentinel-2 image, from 28th of April 2016 were used. *In-situ* measurements collected using a GPS on 13th of April 2016, covering a distance of approximately 27 km, were used as ground-truth information. Figure 16 shows the distribution of the extracted waterline, the baseline and the transects.



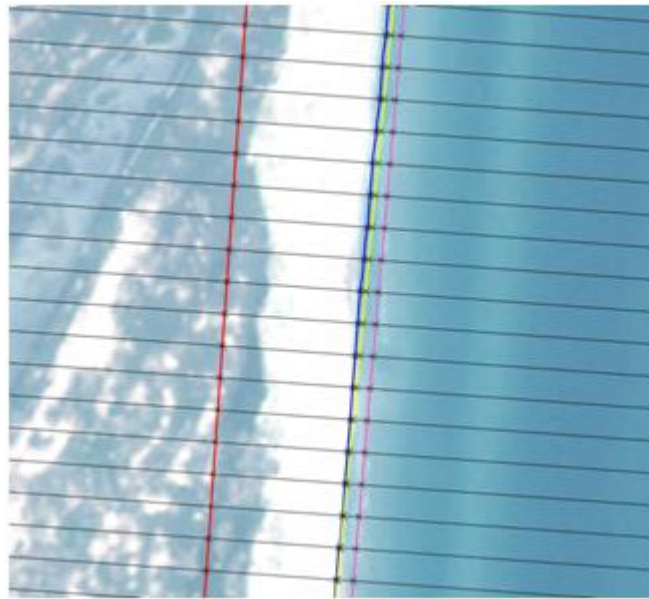


Figure 16 : Detail on the distribution of the baseline (red line), the in-situ GPS measurement (blue) and the satellite extracted waterline (2b - magenta; 2c - yellow).

4.2.2.2.2 Results

After computing the distance between the baseline and each of the waterline versions, the difference between in-situ and each algorithm result was determined. Figure 17 shows the overall distribution of these differences. It can be clearly observed that the supervised classification method performed better than the index-based approach. The negative values on the histogram denotes under-estimation of the water extent. The mean and median values of the distribution are -24.4 and -24.3, respectively for algorithm 2b and -5.7 and -5.5 for algorithm 2c.

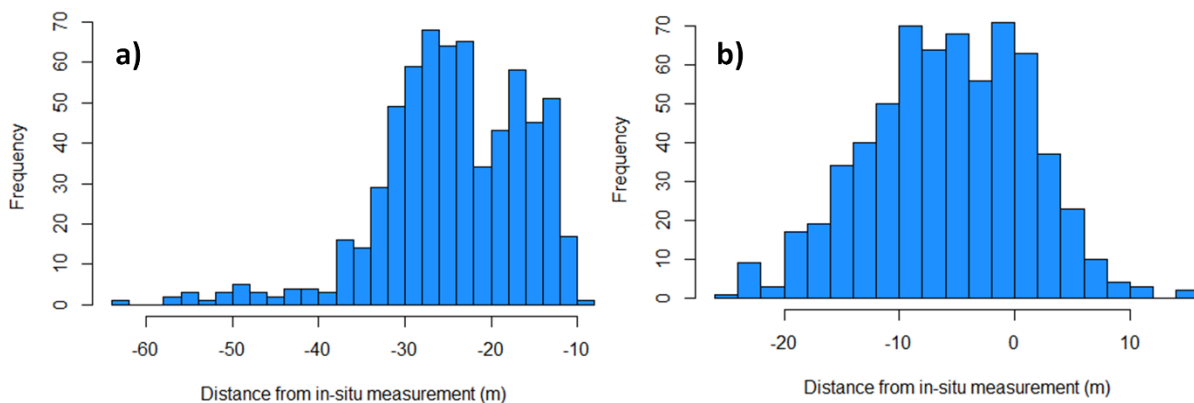


Figure 17: Distribution of the total number ($n=642$) of differences between the in-situ GPS measurements and satellite derived waterline; a) based on algorithm 2b; b) based on algorithm 2c

4.2.2.3 Discussion

The plan for next year is to improve the index-based approach (2b) in order to be able to use it as an automatic extraction method (which can be adapted more easily to big data processing schemes). While the classification methodology performs better (as a result of this first stage validation exercises), it is computational expensive and more difficult to apply it to long time series. Although the MNDWI algorithm yields not satisfactory results, it is expected that it can be improved,



since the errors are almost systematic (a shift towards the offshore sector is noticed). Therefore, a fine tuning of the methodology that is used to automatically detect the threshold (water-land) could diminish the current tendencies of under-estimation of water surface. *Validation activities will be performed for other periods and they will be repeated until an optimal threshold detection method is found.*

4.2.2.4 Vistonis Maroneia

The area is microtidal with mostly sandy beaches and some rocky cliff areas.

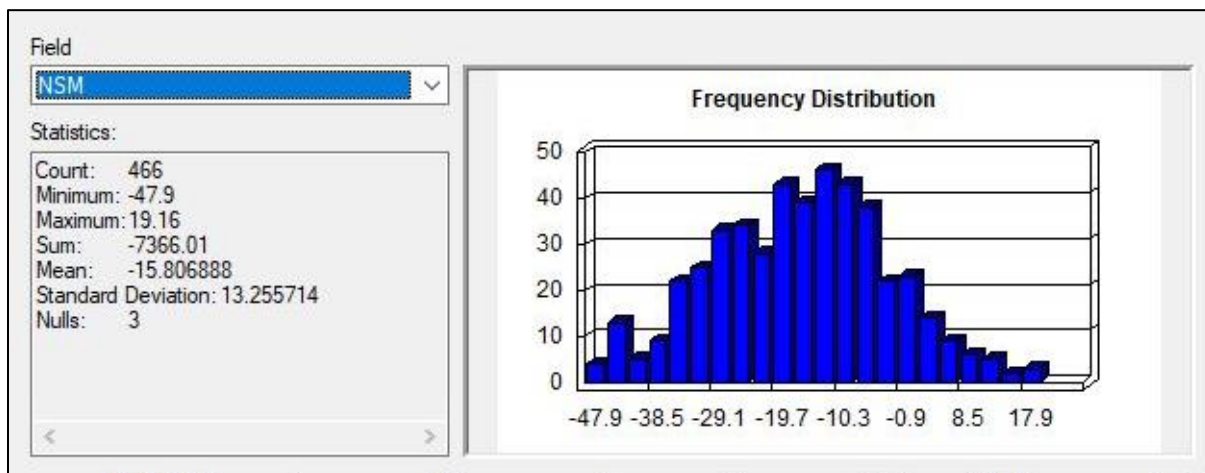
4.2.2.4.1 Waterline based on Landsat-8 imageries - Data

Waterline on Landsat-8 imageries, acquired on 20th of August 2019, has been produced over the POC site of Vistonis-Maroneia. For this specific POC site, a GPS survey took place from 30th of September to 1st of October 2019, with the use of RTK GPS techniques (Real Time Kinematic, L1/L2 frequencies) and therefore by achieving a mean horizontal accuracy of a 2-3 centimetres for the collected data. The overall surveyed distance combining the field surveys is of 14.50 km.

4.2.2.4.2 Results

The RMSE calculated is around 13 m, while the best performances (0.9 m) are obtained in sandy areas, whereas in few rocky areas and rocky defense areas maximum errors exceed 30 m (Figure 18).

The uncertainty on the predicted waterline from Landsat-8 imagery is of the order of the pixel size, which demonstrates the good capacity of this sensor to contribute to the analyses of the erosion over the past years. However, location error can reach to 30 m at some locations, where further investigation is needed in order to improve algorithm an action anticipated for the 2nd project phase.



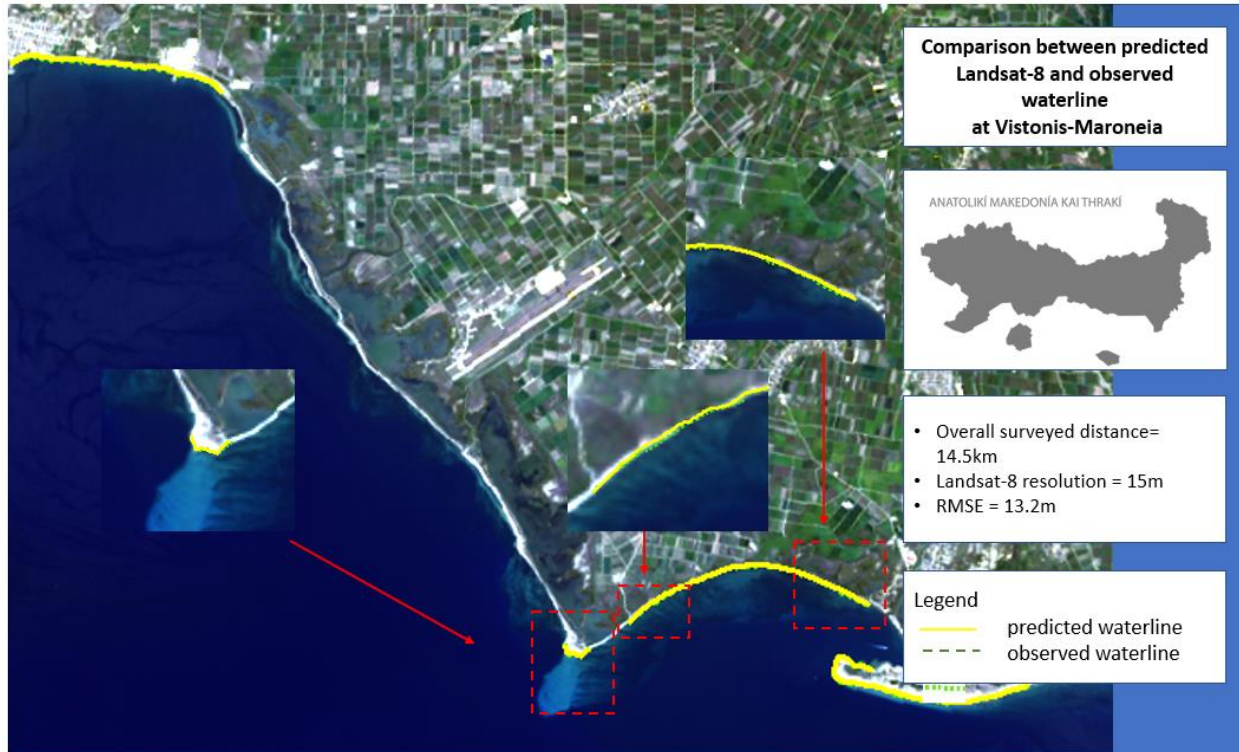


Figure 18 : Comparison between predicted (Landsat-8) 20th of August 2019 and observed waterline from 30th of September to 1st of October 2019 at Vistonis-Maroneia.

4.2.2.4.3 Waterline based on Sentinel-2 imageries - Data

Waterline on Sentinel-2 imageries, acquired on 24th of August 2019, has been produced over the POC site of Vistonis-Maroneia. For this specific POC site, a GPS survey took place from 30th of September to 2nd of October 2019, with the use of RTK GPS techniques (Real Time Kinematic, L1/L2 frequencies) and therefore by achieving a mean horizontal accuracy of a 2-3 centimetres for the collected data. The overall surveyed distance combining the field surveys is of 17.26 km.

4.2.2.4.4 Results

The RMSE calculated is around 7m, while best performances (1.2 m) are obtained in sandy areas, whereas in few rocky areas and rocky defense areas maximum errors exceed 30 m (Figure 19).

The uncertainty on the predicted waterline from Sentinel-2 imagery is of the order of the pixel size, which demonstrates the good capacity of Sentinel-2 to contribute to the analyses of the erosion over the past years. However, location error can reach to 30 m at some locations, where further investigation is needed in order to improve algorithm an action anticipated for the 2nd phase of the project.



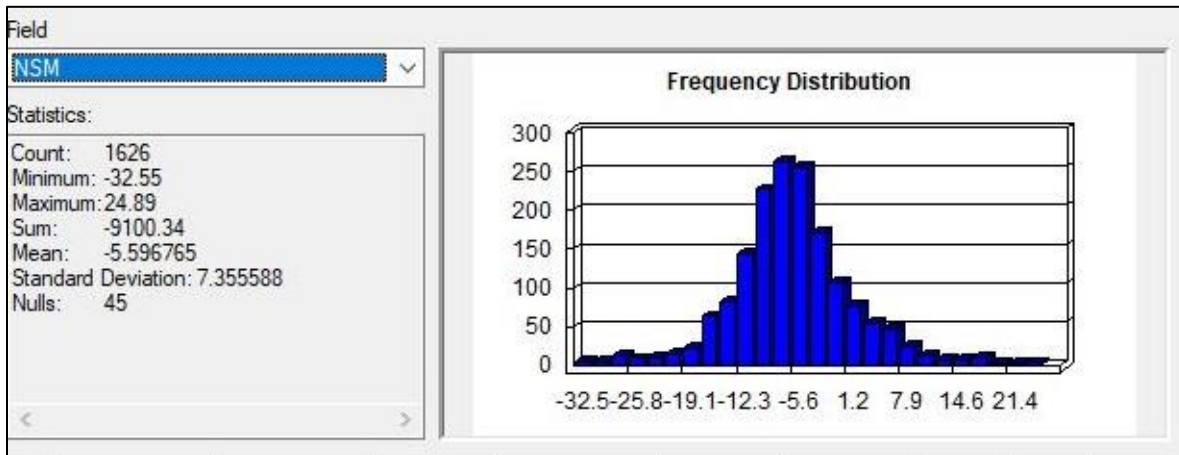


Figure 19 : Comparison between predicted (Sentinel-2) 24th August and observed waterline at Vistonis-Maroneia from 30th of September to 2nd of October 2019.

4.2.2.4.5 Waterline based on SPOT-7 imageries - Data

Waterline on SPOT-7 imageries, acquired on the 28th of August and 30th of September 2019 respectively, has been produced over the POC site of Vistonis-Maroneia. For this specific POC site, a GPS survey took place from 30th of September to 1st of October 2019, with the use of RTK GPS techniques (Real Time Kinematic, L1/L2 frequencies) and therefore by achieving a mean horizontal accuracy of a 2-3 centimetres for the collected data. The overall surveyed distance combining the field surveys is of 13.37 km.



4.2.2.4.6 Results

The RMSE calculated is around 4 m, while best performances (0.4 m) are obtained in sandy areas, whereas in few rocky areas and rocky defense areas maximum errors exceed 18 m (Figure 20). Therefore, the uncertainty on the predicted waterline from the SPOT-7 High Resolution imagery is of the order of the pixel size (taking into account the accuracy of ortho imagery).

Thus, it can be concluded that the detection of waterline based on HR imagery satisfies coastal managers monitoring needs in microtidal regions, even if one single image is used.

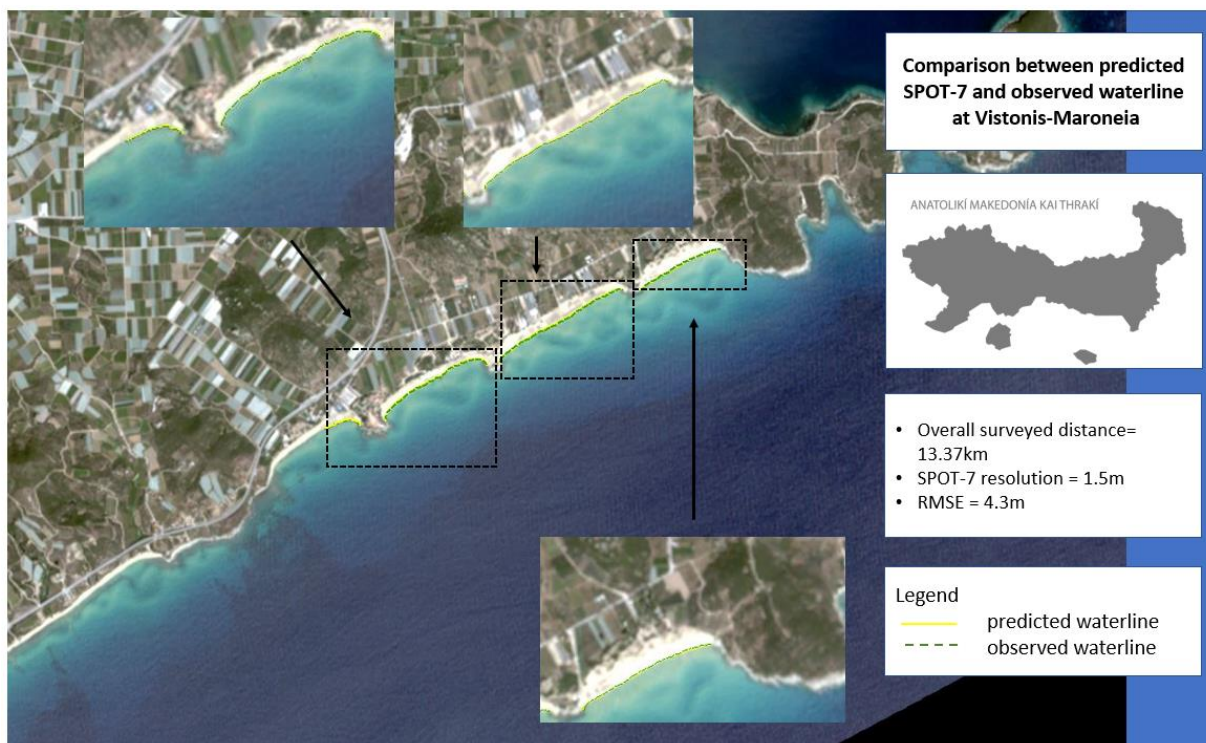
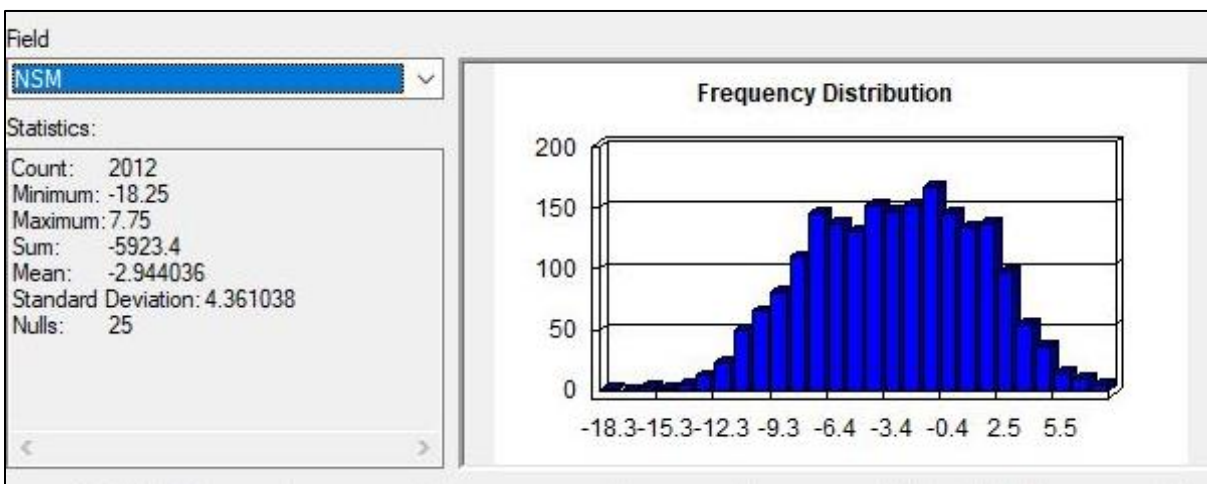


Figure 20 : Comparison between predicted (SPOT-7) 28th of August and 30th of September 2019 and observed waterline from 30th of September to 1st of October 2019 at Vistonis-Maroneia.



4.2.2.5 Discussion

The detection of the waterline based on algorithm 2b shows excellent results over the various validation experiments carried out during phase 1 and whatever the sensor considered for retrieving this indicator.

The good performance of the approach developed to extract the waterline in microtidal areas from optical image (high and very-high resolution) is clearly demonstrated here. The performance of the approach is demonstrated over the selected POC site, where validation data exist, and of course that was also required by the Greek end-users and whatever the sensor used to retrieve the indicator. Finally, validation has been performed over a total distance of almost 45.1 km. However, from these results, it seems that improvements could still be made in rocky defence structures and rocky areas in general where the predicted waterline is not as accurate as on sandy locations. Therefore, during phase 2, it will be relevant to pursue the algorithm development of clarify its limitations and finalise the validation experiment.

4.2.3 Detection based on SAR data (algorithm 2d)

4.2.3.1 Background

The waterline extraction from radar imagery was performed using a thresholding technique, based on the histogram distribution of the input imagery.

4.2.3.2 Gheorge Sf. Sulina

4.2.3.2.1 Data

For the purpose of the validation exercises, the results obtained after processing a Sentinel-1 image, from 25th of April 2016 were used. In-situ measurements collected using a GPS on 13th of April 2016 over a distance of 27 km were used as ground-truth information.

4.2.3.2.2 Results

Figure 21 shows the distribution of differences along transects between in-situ GPS measurements and Sentinel-1 extracted waterline. The negative values on the histogram denotes under-estimation of the water extent. The mean and median values of the distribution are 9.9 and -0.7, respectively, Maximum error reaches 50 to 100 m.



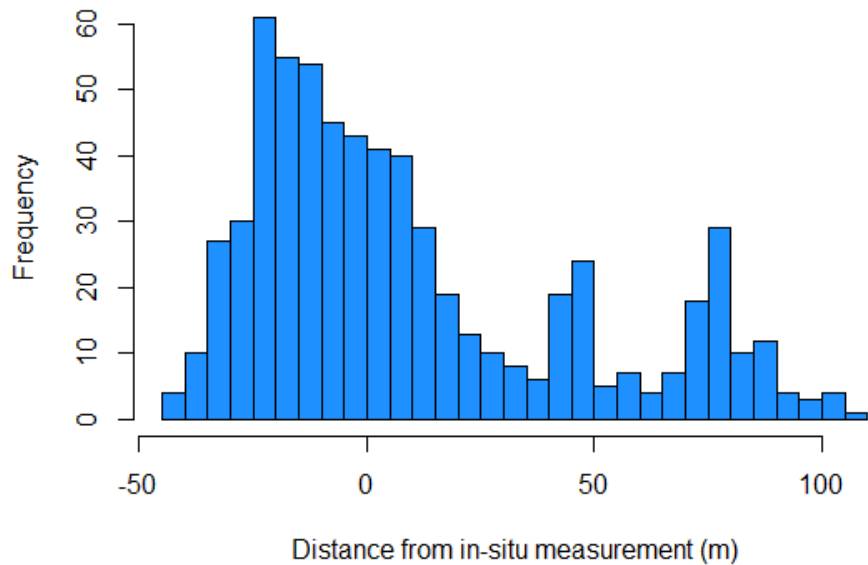


Figure 21: Distribution of the total number ($n=642$) of differences between the in-situ GPS measurements and satellite (Sentinel-1) derived waterline.

4.2.3.3 Discussion

Along with the outcome of validation tasks performed for the middle of swash zone in France, new developments are needed to reduce maximum errors that are observed at some location.

4.3 Dune foot

4.3.1 Detection based on optical data – algorithm 3a

4.3.1.1 Background

The algorithm 3a consists in dune foot extraction using the cross-shore variation of first-order texture metrics from VHR optical data. The detection approach is based on successive processing steps:

- A classification to filter out woods and water surfaces;
- Texture analysis is applied to sand pixels (first order (occurrence) metrics are calculated);
- Discontinuities are looked for in the masked data range image, they are iteratively searched for in a 6x3 moving window. The first discontinuity has been defined as the upper limit of the landward excursion of tide. Once the threshold is reached the interface location (point) is stored vector file. Then, the window continues moving landward and mean and standard deviation of the data range in the window are calculated. Two thresholds are defined to determine the location of a second discontinuity characterizing the foot dune. The location of the second discontinuity is stored.

Algorithm 3a has been tested in Aveiro and Biscarrosse. Worldview and Pleiades imageries have been processed since this algorithm is relevant for VHR images only. A validation exercise has been performed in Aveiro (Aveiro South POC site).

4.3.1.2 Data

Pleiades multispectral images (2 m) have been processed. Data were acquired the 12th of March 2014. Validation data were acquired the 14th of April 2014 during a field survey at the low tide with the INSHORE system (Baptista et al., 2011).



Field collected data were processed following the procedure described in Baptista et al. (2011).

The comparison is made over a global length of 10.19 km.

4.3.1.3 Results

Results are shown on Figure 22. The bias is lower than 0.4 m, which is really good. However, the RMSE is about 10 m, which is too high for short term dune foot monitoring. Uncertainty lower than 5 m would be acceptable. However, the scatter plot shows that errors are generally lower than 10 m, with the exception of reduced sections of the coastline.

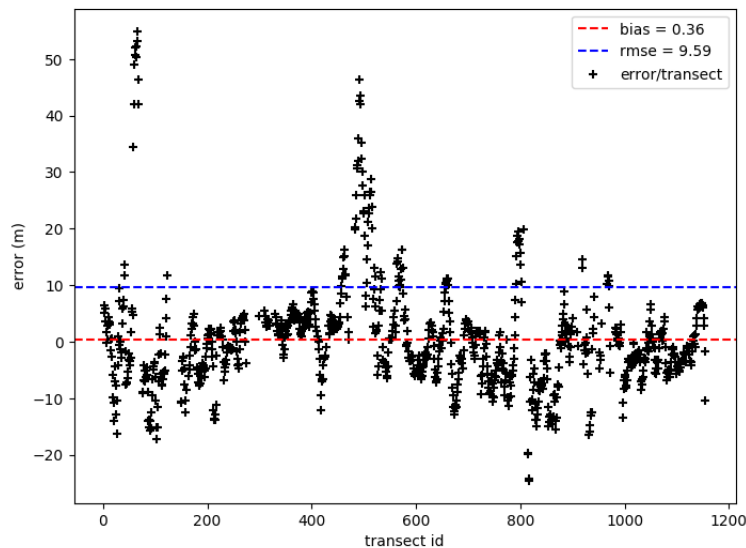


Figure 22 : Difference between estimated (12th of March 2014) and measured (14th of April 2014) dune foot location at South Aveiro.

4.3.1.4 Discussion

This single validation exercise is not enough to control this detection approach properly. Although promising these preliminary results show that:

- Algorithm 3a elaborated along the French New Aquitaine Coast could be improved for the Portuguese Atlantic coast and certainly better calibrated;
- The comparison between field-measured and remotely sensed dune foot should be carefully analyzed to understand the main discrepancies observed: they can either derive from poor calibration of the algorithm or algorithm limitation that were not envisaged so far;
- **Validation must be performed several times and at several places to strengthen these preliminary results.**

4.3.2 Detection based on optical data – algorithm 3h

4.3.2.1 Background

The algorithm 3h is based on a mono-date or a multi-date supervised classification process using training polygons and a Random Forest model. In addition to spectral bands, texture features are computed to feed the model in order to enhance its capacity to differentiate smooth beach sand from the more textured vegetated dune sand. A single image can be used but multiple images acquired during the same stormless period usually increase the accuracy of the dune foot detection. In the case of multi-date approach, all images and their texture features are stacked in a single dataset to train and apply the classification model. The classification result is then post-processed with a marching square algorithm to retrieve the dune foot line.



4.3.2.2 Biscarrosse

4.3.2.2.1 Data

To derive the dune foot of summer 2019, six cloudless Sentinel-2 images acquired between May and August 2019 were collected. For the validation, a field data acquired in June 2019 with a GPS device was used (vertical accuracy of about 5 m).

4.3.2.2.2 Results

As shown in Figure 23, satellite derived dune foot is mostly consistent with the field data given the 10 m spatial resolution of Sentinel-2 (RMSE = 15.49 m). Significant differences up to 35 m are nevertheless locally observed as shown in the smaller zoomed-in areas in Figure 23- top, with the detected line either more seaward or more landward than the field data.

4.3.2.3 South Aveiro

4.3.2.3.1 Data

One cloudless Sentinel-2 image (21st of March 2018) is exploited here to derive a single-date dune foot line. The result is validated with a field data acquired between 13th of March 2018 and 20th of March 2018 during low tide with the INSHORE system (Baptista et al., 2011).

4.3.2.3.2 Results

The detected dune foot is here less consistent with the observed data (Figure 24) with an overall bias showing a more landward detection of one Sentinel-2 pixel on average (bias = -10.31 m). Significant differences of up to 40 m are observed locally. The result oscillates widely around the field data.

4.3.2.4 Discussion

The observed differences, whether in Biscarrosse or Aveiro, are mainly due to local radiometric particularities such as darker sand close to the dune foot causing the detected line to go seaward or lighter sand on dune slopes causing the detected line to go landward. In the case of Aveiro's dune, the presence of vegetation patches close to the dune footstep has probably introduced confusions in the classifier. Also, Aveiro's longer AOI is characterized by a larger heterogeneity in the radiometry and the texture associated either with beach sand or with the dune top and slopes. This could partially explain the less accurate results for this POC site. All in all, these inaccuracies are mainly imputable to the classification approach known to be sensitive to such variabilities.

The less accurate result of Aveiro could also be due to the fact that only one image has been used for this site, whereas 6 Sentinel-2 images have been exploited in Biscarrosse. This shows that multi-date dataset can significantly increase the accuracy of the detection.

A possible alternative classification approach consisting in averaging single-date detected dune foot lines rather than merging features prior to the classification could help in improving the results and reduce such inaccuracies. Also, clipping the AOI into multiple smaller AOIs to train locally specific classification models could help in taking into account the sand radiometric heterogeneities along the shoreline.

Additional results are needed to strengthen these preliminary results.



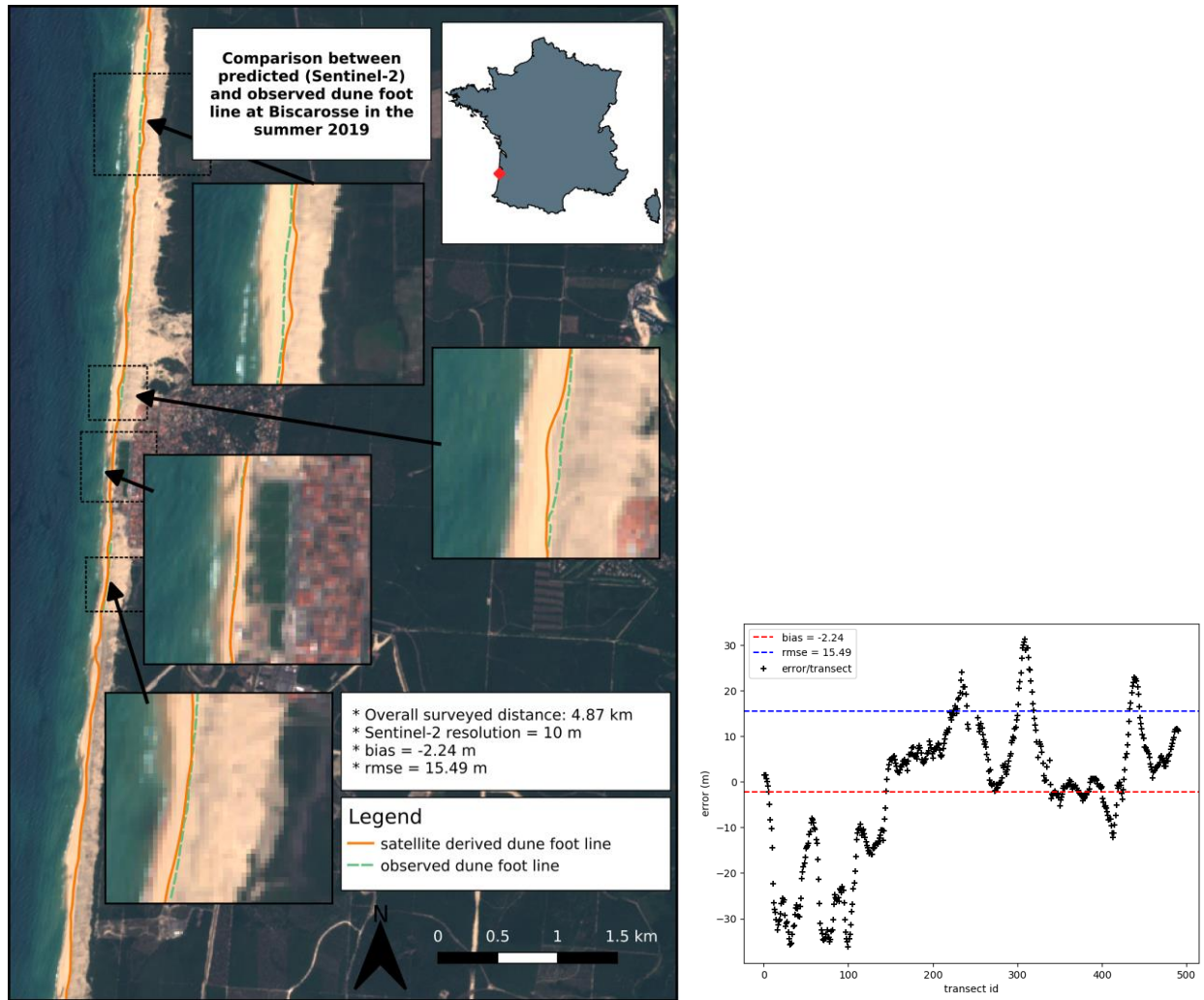


Figure 23 : Comparison between a Sentinel-2 derived dune foot line and an observed dune foot line at Biscarosse in summer 2019 - (top) comparison map - (bottom) validation plot representing the distance between the observed dune foot line and the Sentinel-2 derived dune foot line by transects perpendicular to the coastline.



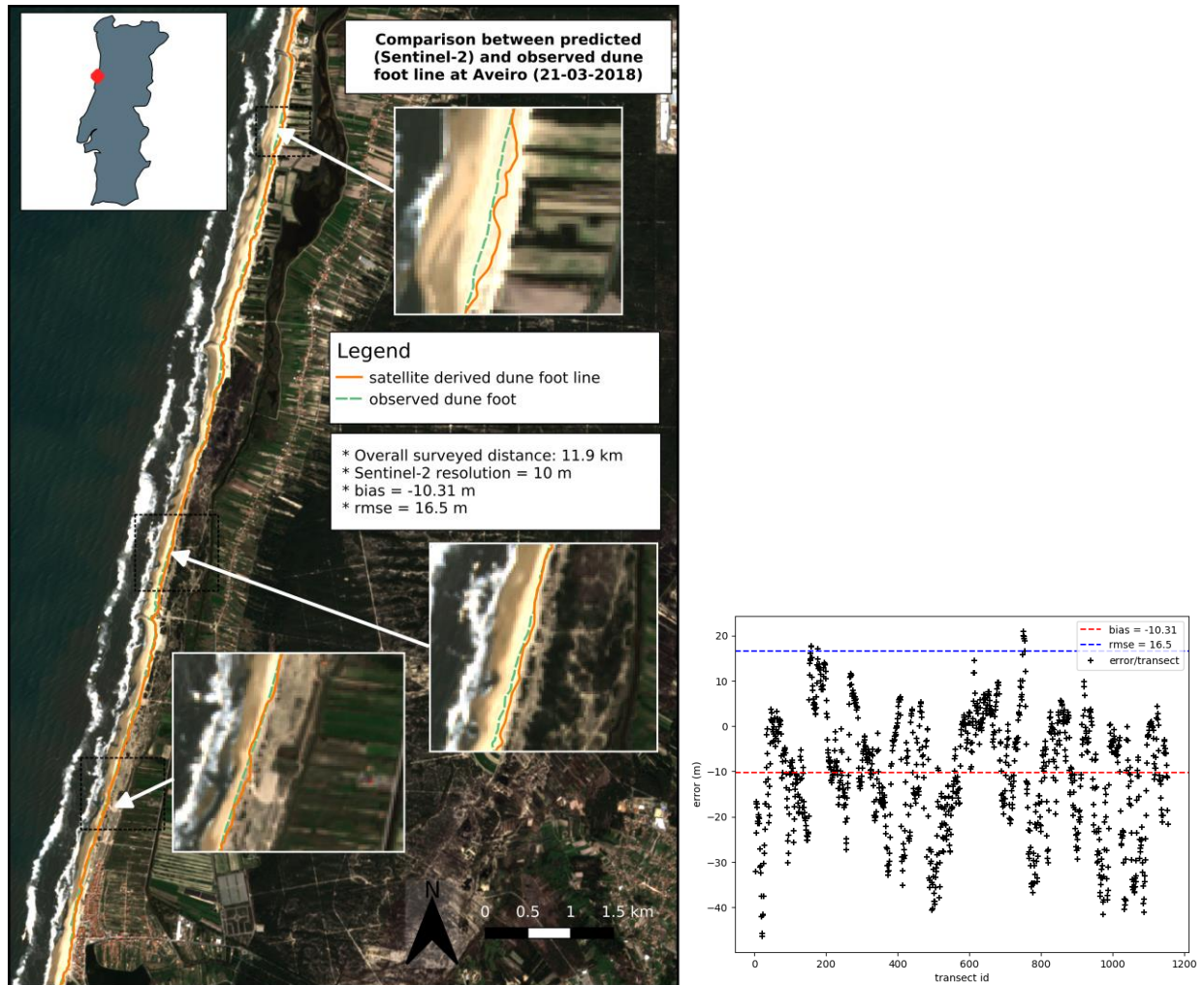


Figure 24 : Comparison between a Sentinel-2 derived dune foot line and an observed dune foot line at South Aveiro (21st of March 2018) - (top) comparison map - (bottom) validation plot representing the distance between the observed dune foot line and the Sentinel-2 derived dune foot line by transects perpendicular to the coastline.

4.4 Cliff lines (cliff apex, cliff foot)

4.4.1 Detection based on optical data – algorithm 3i

4.4.1.1 Cliff apex detection at Quiberville

4.4.1.1.1 Background

The satellite data used to produce this cliff apex have been processed using a processing chain (algorithm 3i) with the following steps: (1) supervised classification approach to detect cliff shadows and others (rock, vegetation,...), (2) water index computation, (3) Otsu (1979) thresholding on the water index value between a set of shadow and other pixels, (4) contours finding using a marching square algorithm with the previously obtained threshold and (5) cliff line extraction from the contours.



4.4.1.1.2 Data

Tests have been performed on Sentinel-2 and Landsat-8 images acquired in August and July 2015, respectively, at Quiberville. Validation data used have been extracted from a Lidar acquired in June 2015. Extraction consists in the manual digitalization of the cliff apex based on the slope raster calculated from the Lidar using the `r.slope` tool of GRASS. The validation method implemented here is the baseline approach.

4.4.1.1.3 Results

Results for Sentinel-2 and Landsat 8 are displayed in Figure 25 and Figure 26), respectively. Overall results are rather promising since the bias and RMSE are lower than the pixel size, in both cases. However, the scatter plot of the uncertainty measured along each of the transect use to compare the observation with the prediction (bottom plots on Figure 25 and Figure 26) shows that the error exceeds regularly 10 m and that can reach at some locations 40 to 60 m.

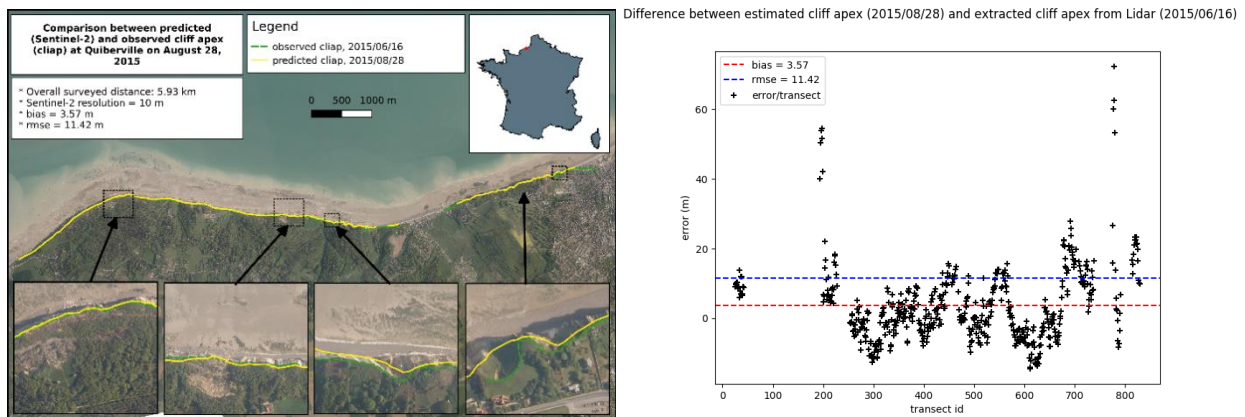


Figure 25 : Comparison between predicted (Sentinel-2) and observed cliff apex at Quiberville in 2015 - (top) detailed map of the detection - (bottom) scatter plot derived from the baseline approach.

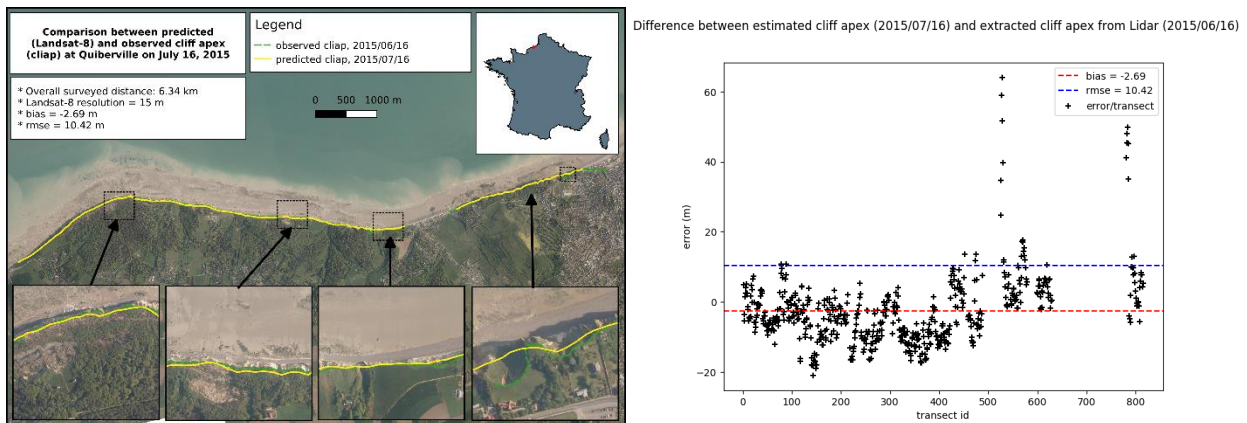


Figure 26 : Comparison between predicted (Landsat-8) and observed cliff apex at Quiberville in 2015- (top) detailed map of the detection - (bottom) scatter plot derived from the baseline approach.

4.4.1.2 Cliff foot at Erretega

4.4.1.2.1 Background

The satellite data used to produce this cliff foot have been processed using a processing chain (3i) with the following steps: (1) supervised multitemporal classification approach to detect rock, water, sand,... based on all images spectral bands and



some statistical features (water index, soil index,...) stacked in a single matrix (2) retrieval of the cliff foot line using a marching square algorithm and (3) post-processing by smoothing the retrieved line.

4.4.1.2.2 Data

The cliff foot has been derived from Sentinel-2 data acquired between June and August 2018 (23rd of June 2018, 23rd of July 2018 and 22nd of August) and compared with GPS surveys (point coordinates). In order to validate the cliff foot, the GPS coordinates have been automatically linked, without any Lidar or photo support. Then, the baseline approach was used to compute the distance between the field observations and the apex location derived from satellite imagery.

4.4.1.2.3 Results

Results are displayed in Figure 27. Although the bias and RMSE appear rather small in comparison to the image resolution, the distance measured between the observation and the prediction strongly varies from about -20 m to + 20 m apart (bottom plot on Figure 27). The zooms on Figure 27 underlines these discrepancies that appear all along the cliff line.

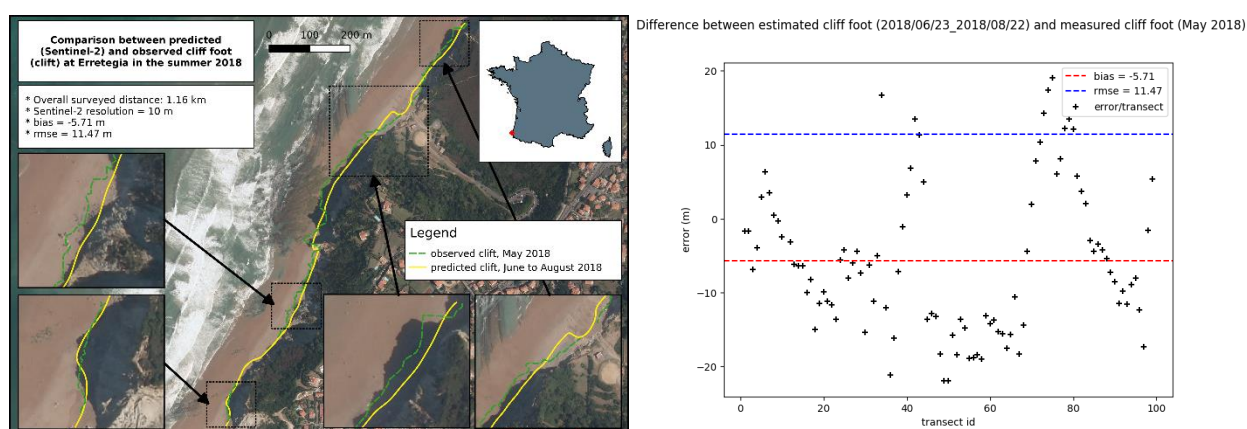


Figure 27 : Comparison between predicted (Sentinel-2) and observed cliff foot at Erretega in 2018 - (top) detailed map of the detection - (bottom) scatter plot derived from the baseline approach.

4.4.1.3 Discussion

The results although promising show rather important discrepancies between observations and detection. **The algorithms and retrieved indicators must be improved during phase 2 and extensively validated. Also, it appears necessary to better control the use of Lidar survey and to improve the used of the GPS coordinates to validate our predictions and, more generally, to strengthen the validation approach.**

4.5 Bathymetry

4.5.1 Detection based on optical data – algorithm 4a

4.5.1.1 Background

This algorithm requires bathymetric field data, even if it covers only partially the area of interest. Once the satellite data has been preprocessed (atmospheric correction, mask creation and glint correction), an empirical model can be fitted between *in-situ* depths and reflectance value of all visible spectral bands according to the Lyzenga method. The calibrated model is then applied on the image of reflectance values where land, cloud, shadow, turbid water, deep water and other outlier pixels have been previously masked. If water bottom types vary within the area of interest, a water bottom map can be used as input in order to calibrate a specific empirical model for each bottom type. Depth field data are preprocessed to resample the data at the resolution of the image and further split in two separate datasets, one for the calibration and the other for validation.



4.5.1.2 Saint Raphaël

4.5.1.2.1 Data

A Sentinel-2 data acquired on 6th of July 2017 has been processed and the result compared with *in-situ* data acquired on the area of interest in July 2017 during a field survey. The collected depths were further interpolated using a TIN interpolator to cover the whole area.

4.5.1.2.2 Results

The Figure 28-left shows the bathymetry results with retrieved depth up to 12 m. The regression diagram (Figure 28-right) displays high consistency between satellite derived and field depths with only a few pixels showing differences higher than 1 m. We can also see that very shallow pixels ($z < 1$ m) are not retrieved here. Masks created during the preprocessing steps tend to discard pixels in such areas since, as they are mostly located close to beach sand pixels, they tend to be saturated because of adjacency effects.

The difference map for this result (Figure 29) shows disparities in terms of spatial distribution of the absolute errors. In shallow waters ($z < \sim 6$ m), derived depths are slightly overestimated while in deeper waters ($z > \sim 6$ m), depths tend to be more underestimated. All in all, differences stay lower than 1 m in the entire depth range.

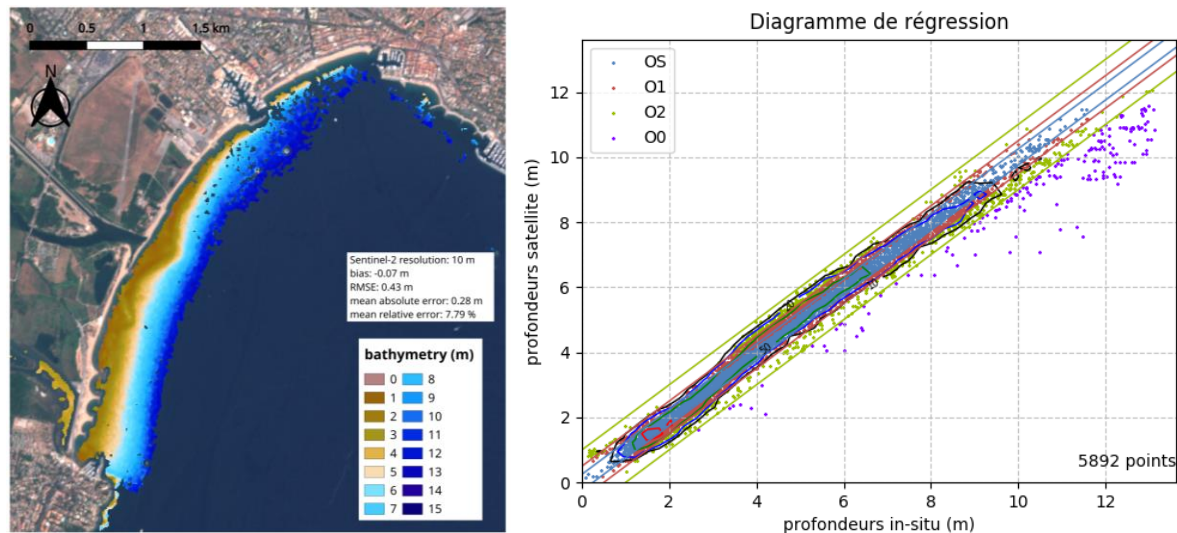


Figure 28 : (left) Bathymetry map obtained with Lyzenga empirical model on a Sentinel-2 data acquired in Saint-Raphaël (6th of July 2017) – (right) Regression diagram between field data and satellite derived bathymetry with isolines and dots corresponding to OHI orders (blue line and dots: ± 0.25 m – Special Order, red line and dots – Order 1: ± 0.5 m, green line and dots – Order 2: ± 1 m, purple dots – Order 0: $> \pm 1$ m). Iso-contours represent point density.

4.5.1.3 Discussion

When *in-situ* data are available, the Lyzenga empirical model enables to retrieve highly consistent bathymetric data with a RMSE usually close or inferior to 0.5 m. When bottom types and water optical properties are homogeneous, the calibrated model can be applied on larger areas than the one covered by *in-situ* data and increasing thereby the geographic extent of the bathymetry map. Besides, underwater sandbars and other features are realistically represented, and their evolution can be monitored using time-series of images. Nevertheless, the presence of any features disturbing locally the water pixel radiometry (changes in bottom types, turbid plumes, sunlight, etc.) will invariably decrease the result's accuracy. The main drawback of this approach is that it depends on the availability of *in-situ* data close to the area of interest but also close to the acquisition date of a fully exploitable satellite data. These conditions are not often met.



Lyzenga's algorithm performance has been demonstrated quite often, it doesn't need any more experiment during phase 2.

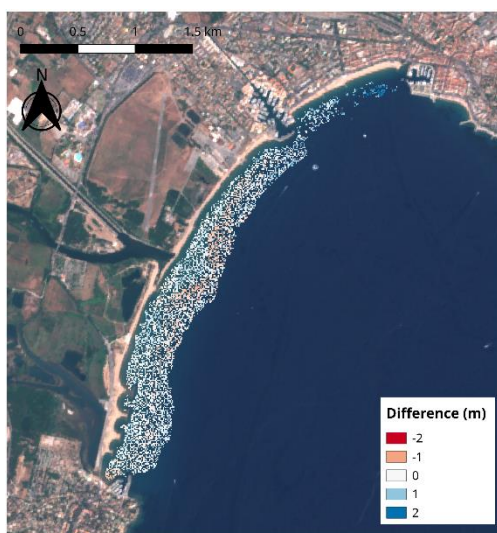


Figure 29: Difference map between satellite derived bathymetry (Lyzenga - Sentinel-2 data acquired in Saint-Raphaël on 6th of July 2017) and field data.

4.5.2 Detection based on optical data – algorithm 4b

4.5.2.1 Background

This algorithm is based on a semi-analytical approach (QAB or Quasi-Analytical Bathymetry) to estimate water depth by using a radiative transfer model derived from Lee's Quasi-Analytical Algorithm equations. This model estimates optical properties of water (absorption and back-scattering coefficients) in optically deep-water pixels. These parameters along with satellite reflectance values and the bottom albedo are further used in shallow water pixels to derive water depths. This approach relies entirely on physical phenomenon occurring within the water column and does not require the use of any *in-situ* data. Two main hypotheses are made. First, the input reflectance values are assumed to be reliable and as close as possible to ground measured reflectance. This means that atmospheric correction is mandatory and that effects such as sunlight or adjacency effects are considered as low. Second, water optical properties are considered as homogeneous in the area. Any turbid plumes or beach sand resuspension will cause errors.

As in Lyzenga approach (algorithm 4a), the calibrated model is applied on the image of reflectance values where land, cloud, shadow, turbid water, deep water and other outlier pixels have been previously masked. If water bottom types vary within the area of interest, a water bottom map can be used as input in order to take this heterogeneity into account and adapt the bottom albedo accordingly.

4.5.2.2 Saint Raphaël

4.5.2.2.1 Data

Satellite data acquired with three different sensors have been selected to apply the QAB approach in Saint-Raphaël:

- Sentinel-2A data (10 m – 6th of July 2017)
- Pleiades-1A (2 m – 6th of July 2017)
- Landsat-8 pansharpener (15 m – 4th of September 2017)

Both Sentinel-2 and Pleiades data were acquired on the same day. The Landsat-8 image has been pre-processed to produce a pansharpener image enhancing the spatial resolution from 30 to 15 m.



To evaluate their respective accuracy, we used a field dataset acquired on the area of interest in July 2017 during a field survey. The collected depths were interpolated using a TIN interpolation method to cover the whole area.

4.5.2.2.2 Results

Bathymetric maps produced with Sentinel-2, Pleiades and Landsat-8 images are respectively displayed in Figure 30, Figure 31 and Figure 33. In all three results, the satellite derived bathymetry is highly consistent with the *in-situ* data even though none of these *in-situ* data has been used to calibrate the model. Mean absolute error and RMSE are close or inferior to 0.5 m which is usually the highest expected level of accuracy for this approach.

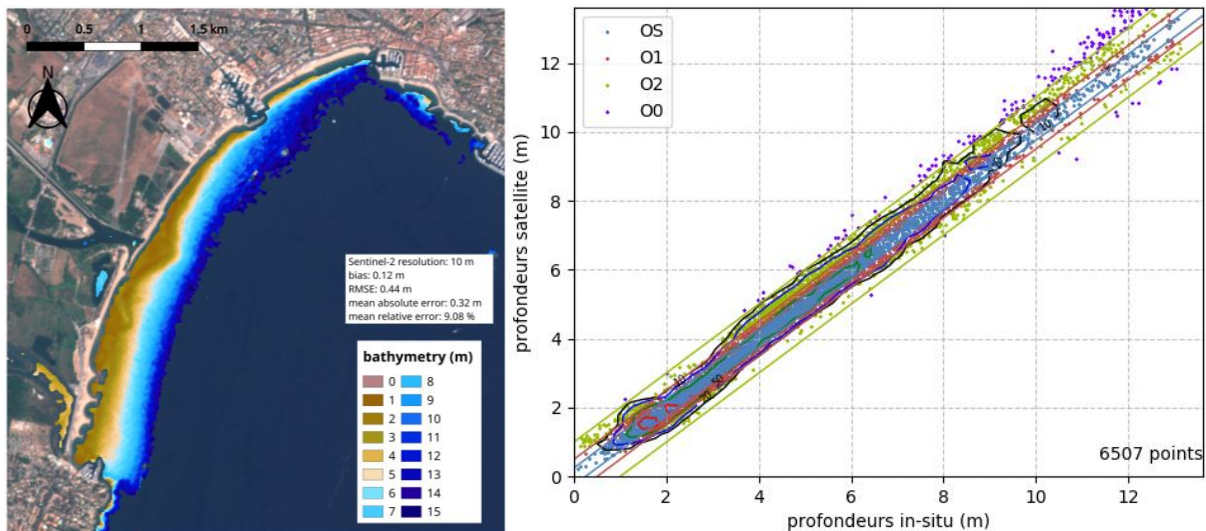


Figure 30 : (left) Bathymetry map obtained with QAB model on a Sentinel-2 data acquired in Saint-Raphaël (6th of July 2017) – (right) Regression diagram between field data and satellite derived bathymetry with isolines and dots corresponding to OHI orders (blue line and dots: +/- 0.25 m – Special Order, red line and dots – Order 1: +/- 0.5 m, green line and dots – Order 2: +/- 1 m, purple dots – Order 0: > +/- 1 m). Iso-contours represent point density.

A few differences can however be highlighted between the three sensors. First, high resolution sensors (Sentinel-2 and Landsat-8) provide more accurate bathymetry data with significantly lower errors on average than very high-resolution sensor (Pleiades). This is mainly due to the fact that very high-resolution images are generally associated with higher noise content. This is clearly shown in the regression diagram of the Pleiades result (Figure 31 – right) where the cloud point is much more spread out around the 1:1 line. Landsat-8 and Sentinel-2 data, because of their coarser resolution and their significantly lower signal to noise ratio, enable to produce smoother and hence more consistent bathymetric models. On the other hand, smaller or thinner immersed structures are not captured by high resolution sensors and do not appear in the model. Such structures can be seen in the north-east of the Pleiades data in Saint-Raphaël.

Second, the very shallow pixels ($z < 1$ m) have been retrieved in the Pleiades result. The masks created during the pre-processing steps tend to include more of these pixels. Nevertheless, even though they are not excluded, the accuracy of retrieval in this area is often not satisfactory, as it is shown in the regression diagram in and in the difference map in Figure 32. Again, this probably due to a combination of adjacency effects, resuspended beach sand or a small change in albedo in this area. Regardless of the sensor, this very shallow area is often less accurate and should be considered accordingly.

Finally, the Landsat-8 bathymetric model reaches higher depths than both other sensors. The maxima depth for Pleiades and Sentinel-2 is around 8 and 10 m respectively while the maxima depth for Landsat-8 is around 15 m. The higher radiometric sensitivity and higher signal to noise ratio of Landsat-8 explains probably this ability. Unfortunately, the maxima depth of the available field data (10 m) does not allow to validate this result.



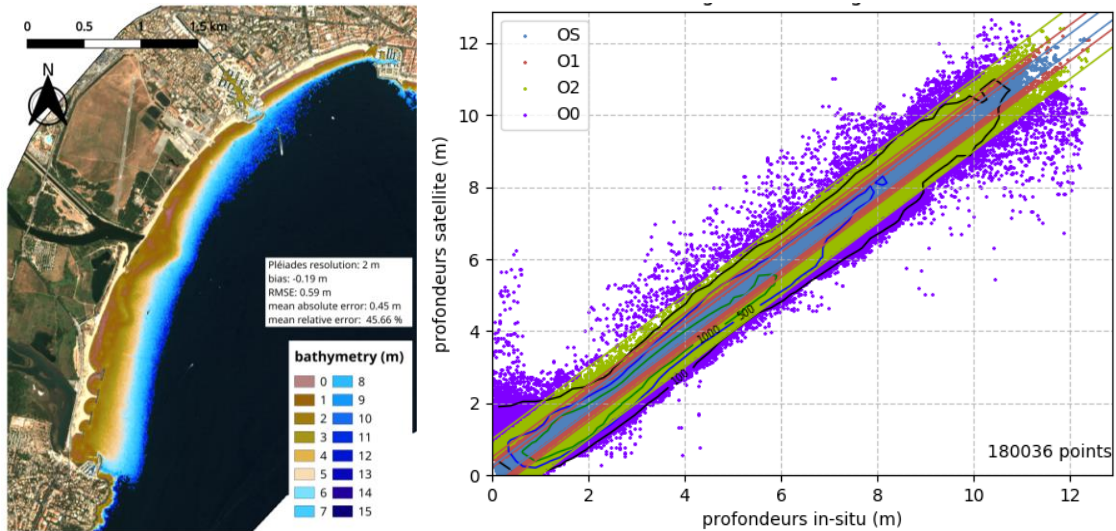


Figure 31 : (left) Bathymetry map obtained with QAB model on a Pleiades data acquired in Saint-Raphaël (6th of July 2017) – (right) Regression diagram between field data and satellite derived bathymetry with isolines and dots corresponding to OHI orders (blue line and dots: +/- 0.25 m – Special Order, red line and dots – Order 1: +/- 0.5 m, green line and dots – Order 2: +/- 1 m, purple dots – Order 0: > +/- 1 m). Iso-contours represent point density.

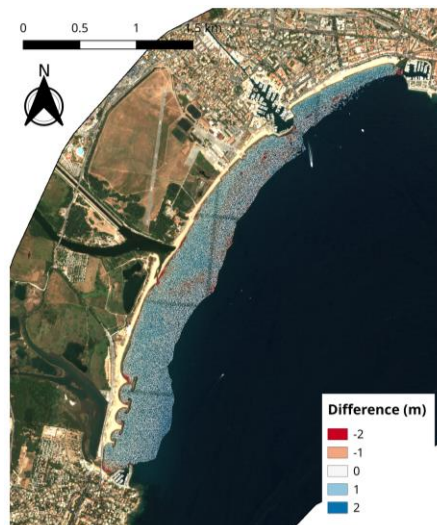


Figure 32 : Difference map between satellite derived bathymetry (QAB - Pleiades data acquired in Saint-Raphaël on 6th of July 2017) and field data.



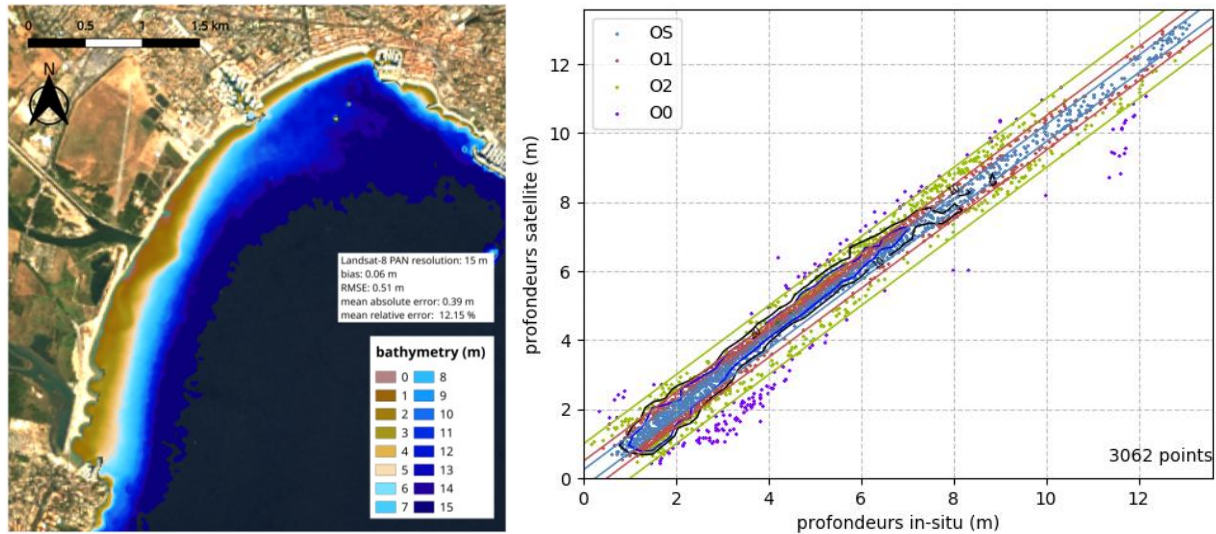


Figure 33 : (left) Bathymetry map obtained with QAB model on a Landsat-8 pansharpened data acquired in Saint-Raphaël (4th of September 2017) – (right) Regression diagram between field data and satellite derived bathymetry with isolines and dots corresponding to OHI orders (blue line and dots: +/- 0.25 m – Special Order, red line and dots – Order 1: +/- 0.5 m, green line and dots – Order 2: +/- 1 m, purple dots – Order 0: > +/- 1 m). Iso-contours represent point density.

4.5.2.3 Camargue

4.5.2.3.1 Data

One cloudless Sentinel-2 image (29th of July 2018) is exploited here to retrieve a bathymetry map using the semi-analytic QAB approach. The result is validated with a field data acquired around the beach of Saintes-Marie-de-la-Mer in July 2018.

4.5.2.3.2 Results

The bathymetry map has been produced on the coastal area of Camargue from Grau-du-Roi to Fos-sur-Mer (~100 km of coastline). In order to account for the presence of several river outlets along the shore and the variability of turbidity it provokes, the Sentinel-2 image has been partitioned into several sub-sectors to refine the estimation of water properties. Bathymetry derived from each sector has been further merged to produce one single output.

The result presented in Figure 34 shows a good consistency between the result and the field data collected around the beach of Saintes-Marie-de-la-Mer with most of the validation points located between -1 and 1 m error. The validation statistics are slightly lower in comparison to QAB results obtained with Sentinel-2 in Saint-Raphaël, with a mean absolute error of 0.5 m and a RMSE of 0.8 m. This is mostly due to the higher heterogeneity of turbidity in the Camargue area. The error diagram as well as the difference map show that the highest overestimation errors are mostly found in very shallow waters in small beaches surrounded by artificial breakwaters. Organic and anthropogenic matters tend to accumulate in these enclosed areas which changes locally the albedo. Inversely, the highest underestimation errors are found close to the river outlet on the western side of the area. Higher turbidity found in these river plumes are the main source of error. These plumes should be properly masked out to avoid such errors.



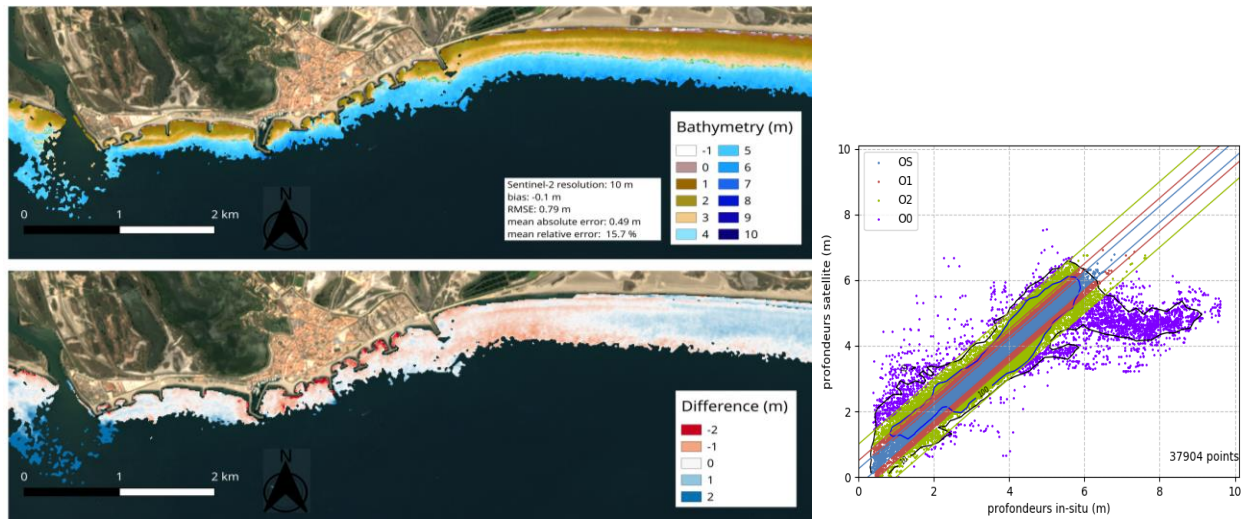


Figure 34 : (top) Bathymetry map obtained with QAB model on a Sentinel-2 data acquired in Saintes-Marie-de-la-Mer (29/07/2018) – (middle) Difference map between satellite derived bathymetry and field data - (bottom) Regression diagram between field data and satellite derived bathymetry with isolines and dots corresponding to OHI orders (blue line and dots: +/- 0.25 m – Special Order, red line and dots – Order 1: +/- 0.5 m, green line and dots – Order 2: +/- 1 m, purple dots – Order 0: > +/- 1 m). Iso-contours represent point density.

4.5.2.4 Discussion

The QAB semi-analytical approach enables to provide realistic bathymetric model without the use of *in-situ* data. The overall accuracy of this approach is generally lower than the Lyzenga empirical approach with a RMSE usually between 0.5 and 1 m. The overall accuracy depends also on the considered sensor. High resolution images (Landsat-8 and Sentinel-2) are generally associated with a higher signal to noise ratio and provide smoother models than very high-resolution data (Pleiades).

The application of the semi-analytical approach relies on a few important prerequisites. First, as it is based on a radiative transfer model, preprocessing steps such atmospheric correction and sun glint correction have to be carried out very carefully so that retrieved water surface reflectances are as realistic as possible. Second, it is assumed that water optical properties are homogeneous in the data. Any disturbances such as turbid waters or chlorophyll organisms within the water column will invariably cause errors. This means that the selection of the image data has to be very thorough and not all images, even cloudless, can be used with such approach. As it was chosen in Camargue, the strategy of cutting the main area of interest into several subsectors can be efficient to reduce the effects on the model due to the heterogeneity of water optical properties.

In comparison, Lyzenga models are not as much concerned by such prerequisites since this approach is purely empirical. It can directly be applied on raw data without applying any atmospheric correction.

The performance of the QAB algorithm, whatever the optical image used, is clearly demonstrated here. It does not seem relevant to develop an extensive and expensive validation plan for phase 2, since most of the already existing validation data were already used during phase 1.



4.5.3 Detection based on SAR data – algorithm 4c

4.5.3.1 Background

The bathymetry estimated with the algorithm 4c-swell inversion is generated through the application of the Fast Fourier Transform (FFT) over Synthetic-Aperture Radar (SAR) image to obtain a directional spectrum and then, to calculate the wavelength and wave direction. After that, the water depth is estimated from linear wave theory.

This algorithm has been tested at Aveiro, Bidart and Erretegia. It had been previously validated at Aveiro by Pereira et al. (2019) and here it is presented the validation for Bidart and Erretegia.

4.5.3.2 Bidart/ Erretegia

4.5.3.2.1 Data

The satellite derived bathymetries of Bidart and Erretegia French POC sites (coastal indicators products named as SFS-FR-BID-BATHY-4C-SINGL-20180325-S1B-UTM30 and SFS-FR-ERRE-BATHY-4C-SINGL-20180325-S1B-UTM30, respectively) were obtained after processing the Sentinel 1-B image called S1B-IW-GRDH-1SDV-20180325T060804-20180325T060829-010184-01280D-19A9 (Figure 35) following the methodology described in the Technical Specification Report.

The satellite derived bathymetry of 25th of March 2018 referred to NGF-IGN69 is represented in Figure 36 (see SDB).

The coastal field bathymetry was provided by the CAPB (Communauté d'Agglomération Pays Basque) in France. The measures were carried out on 2nd of March 2018 using a single beam echo sounder and the recorded data were processed with Hypack software. The processed data (X and Y coordinates and Z depth values referred to NGF-IGN69) were used to create the digital elevation model (see FMB in Figure 36).

The satellite derived and coastal field bathymetry has in common a small area at Bidart POC site (Figure 36). Therefore, the validation can only be performed at Bidart along the isobath of 20 m.

4.5.3.2.2 Results

The depth differences between the observed isobath of 20 m and the satellite derived depths at the location of this isobath are plotted in the Figure 37. The minimum depth difference is of 4.3 m and the maximum one is of 9.9 m with a mean value of 5.2 ± 0.5 m for the north section and of 8.3 ± 1.0 m for the south section. Therefore, the mean value of the relative error is of 0.26 in the north section and 0.42 in the south section.

4.5.3.3 Discussion

The differences between measured and satellite derived bathymetry obtained for the French coast were slightly higher than the obtained ones by Pereira et al. (2019) for the Portuguese coast (the mean value of difference for isobath $z=20$ m equals to 1.5 ± 0.7 m).

Additional results would be needed to strengthen these preliminary results.



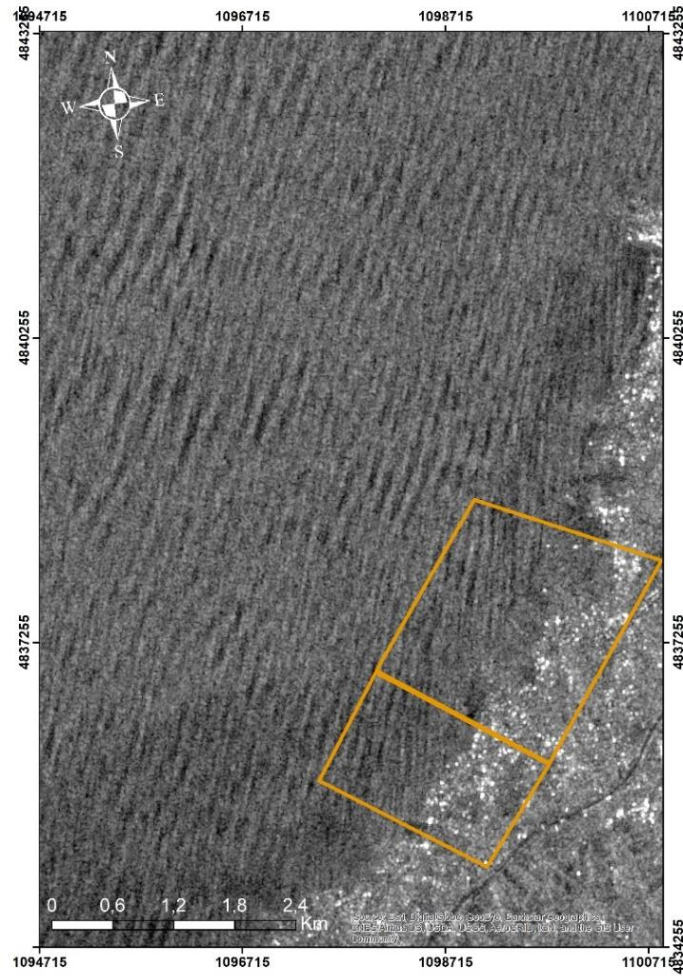


Figure 35: Sentinel 1-B satellite image acquired on 25th March 2018 at France POC sites of Bidart and Erretegia (orange polygons).



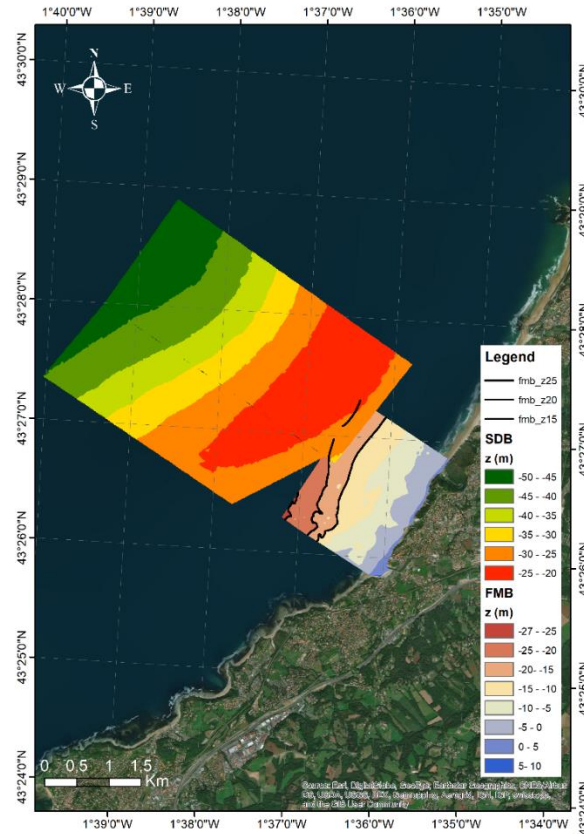


Figure 36 : Satellite derived (SDB) and field measured (FMB) bathymetry with the observed isobaths (black lines).

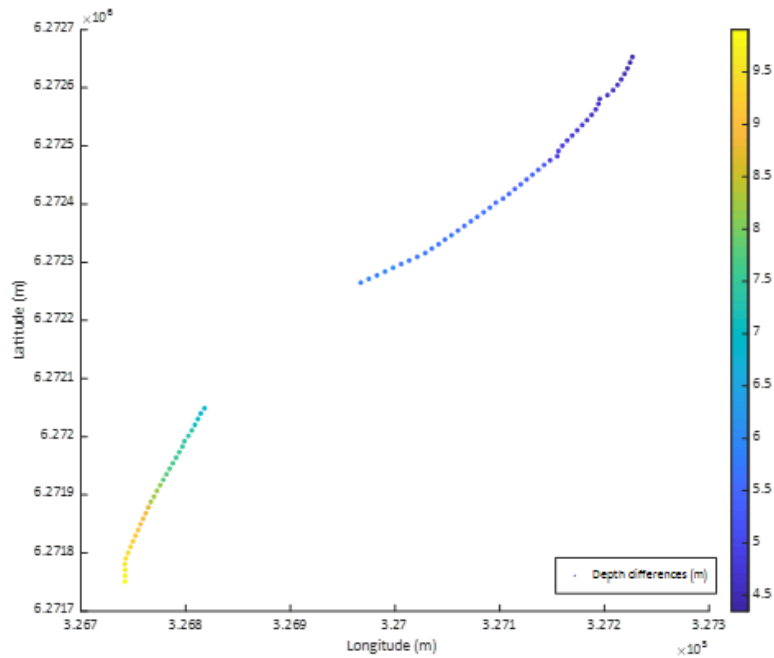


Figure 37: Depth differences in meters between observed isobath (20 m) and satellite derived depths at isobath location.



4.6 Submerged sandbars

4.6.1 Detection based on optical data – algorithm 6a

4.6.1.1 Background

The algorithm used to detect the submerged sandbars positions takes advantage of the increase of the reflectance values, in the visible part of the electromagnetic spectrum, in the proximity of the sandbars. The methodology is completely automatic and can be used to process large amounts of satellite data, thus being suited for time series analysis.

4.6.1.2 Gheorge Sf. Sulina

4.6.1.2.1 Data

For validation purposes, the sandbars positions were extracted from four different Sentinel-2 images and using two higher resolution inputs - one Spot 7 and one Pleiades 1B image. The extracted values were then compared with *in-situ* measurements, consisting of sandbars crest positions determined based on bathymetric measurements performed by the Sfantu Gheorge Marine and Fluvial Research Station (SCMF). More than 140 individual pairs of satellite – *in-situ* match-up pairs were used in order to quantify the accuracy of the algorithm and the capabilities offered by different Earth Observation data sources to extract the sandbars.

4.6.1.2.2 Results

The sandbars locations detected from satellite imagery and surveys are in very good agreement (Figure 38). The correlation between the two datasets is very good, expressed in high coefficients of determination for both all data ($R^2 = 0.9761$) and for individual pairs of data (R^2 is ranging from 0.9848 to 0.9941).

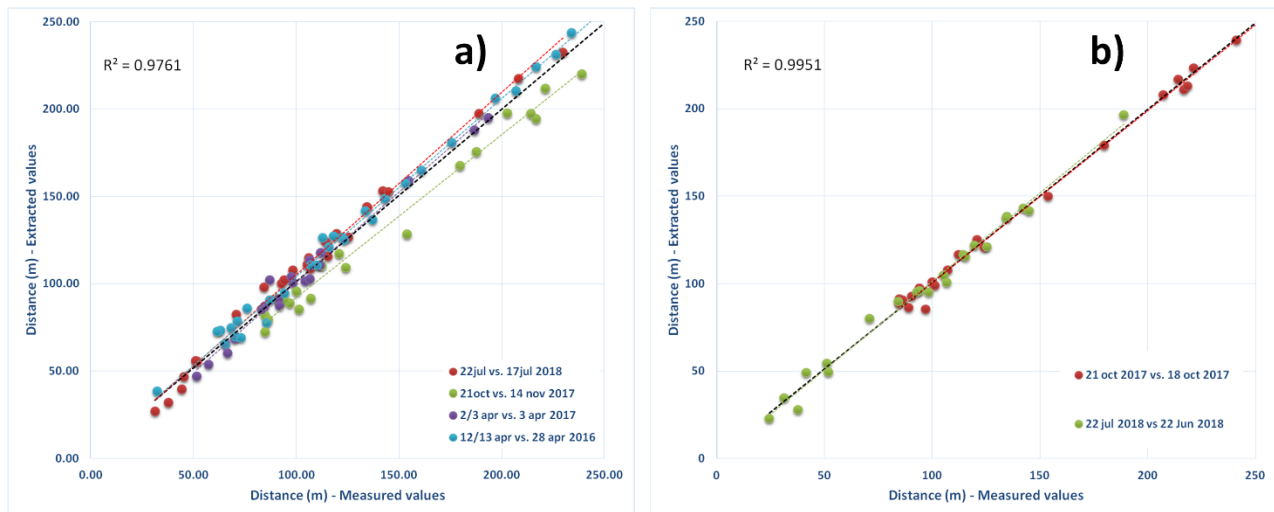


Figure 38: Match-ups between satellite extracted and *in-situ* measured sandbars locations; a) results based on Sentinel-2 data; b) results based on Spot 7 (red points) and Pleiades (green points); the determination coefficients shown on graphics refer to the entire set of points

The mean average percentage difference (MAPD) was equal to 6.2 % for all 96 Sentinel-2 match-ups and equal to 4.2% for the high-resolution datasets. The highest value for MAPD (7.75%) (Table 1) was recorded for the October - November 2017 match-ups, the pair of *in-situ* and satellite estimations with the largest time gap between them, of 25 days. Given the fact



that this corresponds to a high wave energy situation, the higher difference could be determined by sandbars migration, rather than algorithm accuracy itself. This hypothesis is sustained also by the fact that for the April 2017 scenario, when the in-situ measurements and satellite pass are on the same day, the MAPD has the lowest value, of only 4.36%. This provides high confidence in the extraction algorithm and the accuracy of the detected sandbars positions.

Table 1: Statistics associated with the match-ups between satellite and in-situ derived sandbars locations; n denotes the number of match-ups, ΔT - the time difference between the satellite pass and the in-situ field survey, MAPD - Mean Absolute Percentage Difference, MB - Mean Bias (mean of the absolute differences between satellite and in-situ estimations)

Period	Satellite	n	ΔT (days)	R ²	MAPD (%)	MB (m)
22 Jul vs 17 Jul 2018	Sentinel-2	25	5	0.9921	7.41	6.64
21 oct vs 14 nov 2017	Sentinel-2	20	24	0.9848	7.75	10.79
3 Apr vs 3 Apr 2017	Sentinel-2	20	0	0.9849	4.36	3.82
13 Apr vs 28 Apr 2016	Sentinel-2	31	15	0.9941	5.64	5.64
21 Oct 2017 vs 18 Oct 2017	SPOT 7	23	3	0.9962	2.84	3.35
22 Jul 2018 vs 22 Jun 2018	Pleiades 1B	22	30	0.9888	5.73	3.87

4.6.1.3 Discussion

While slight improvements are to be observed when using higher resolution satellite data, the accuracy of Sentinel-2 based results are high enough in order to qualify these images as suitable for long-term analysis of sandbars dynamics. Moreover, the lack of high-resolution images availability with a good revisit time makes the Sentinel-2 products the only valid option for such applications.

During Phase 2, the validation actions will focus on Landsat data since the good performance of the algorithm for SPOT, Pleiades and Sentinel-2 has been clearly demonstrated during phase 1.

4.7 Summary: validation actions performed during year 1 and planned for the year 2

All in all, validation actions performed during phase 1 concerned 11 of the algorithms described in the Technical Specifications (TS), and 2 additional algorithms adapted from TS. The total number of products evaluated during phase one was of 35, about 15% of the total number of products carried out (Table 2).

An evaluation of the performances achieved with regards to end-users' requirements is presented in Figure 39. This figure shows an assessment for the coastal erosion indicators for which quantitative validation has been performed: depth retrieval (bathymetry based on SAR and optical data) and submerged sandbars, middle of swash zone, waterline, dune foot, cliff foot and cliff apex location. Result are represented by box plot. Blue box plot specifies the accuracy ranges requested by the end users. For the dune foot, the uncertainty on GPS surveys, that was derived in the field based on surveys carried by 8 individual operators, is also indicated. Then, vertical or horizontal accuracies achieved are highlighted by quantitative values and, also, by a colour code. Large boxes show the range of root mean square errors achieved, considering each validated product one by one. On each side of these large boxes, minimum and maximum errors observed



on all validation scatter plots (e.g. Figure 33 - right) are reported. Green colour underlines the accuracy ranges that fulfil end-users' specification. Yellow, orange and red colours underline main discrepancies between remotely-sensed an observed indicator. Firstly, the Figure 39 demonstrates that, for these 7 indicators, at least one of the detection approaches developed allows satisfying the expected observation accuracy for one or several coastal regions. From the detailed analysis developed in the previous sections, we can add valuable expertise to this diagram. For instance, in case of optical bathymetry, it was shown that maximum errors occur for Pleiades processing (Figure 31 - right). For the middle of swash zones, major location errors are observed when the indicators are derived from SAR imagery, but also, from optical data, in more rare cases. We can also observe in Figure 39 that the accuracy range achieved for the dune foot and cliff lines are commonly of the order of maximum acceptable accuracy. These considerations shall strengthen our validation plan for next year.

To conclude, this comparison clearly shows that EO data, including past images, allows to derive indicator with accuracy convenient for coastal erosion monitoring. For operational monitoring purposes, this result is fundamental and really encouraging. However, even small error bars shall be carefully considered for operational monitoring purposes, since coastal changes can be of the order of the accuracy cumulated to image space resolution. Monitoring solution shall be always adapted to the expected trend in coastline position, for short term as well as for long-term monitoring perspectives.

Table 2. Number of products evaluated per algorithm family

Algorithm code and description	Number of products evaluated during phase 1
2a – Optical Waterline	4
2b – Optical Waterline	4
2b – adapted - Optical Middle of swash zone	5
2c – Optical Waterline	1
2d – SAR Waterline	1
2d – adapted – SAR Middle of swash zone	2
3a – Optical Dune foot	1
3h – Optical Dune foot	2
3i – Optical Cliff apex	3
4a – Optical Bathymetry with Ground control point	1
4b – Optical Bathymetry without Ground control point	4
4c - SAR Bathymetry without Ground control point	1
6a – Optical Submerged sandbars	6

Finally, a global summary of the validation actions that were performed during phase one and that are planned for year 2 are displayed in Table 3. The details of the validation plan are documented in the section 5 - Validation Plan for Phase 2, beginning on page 50. Table 3 includes the page number of the section detailing the validation plan for each algorithm, individually.



Figure 39. Comparison between vertical and horizontal accuracies specified by the end-users and the accuracies achieved by Space for Shore products

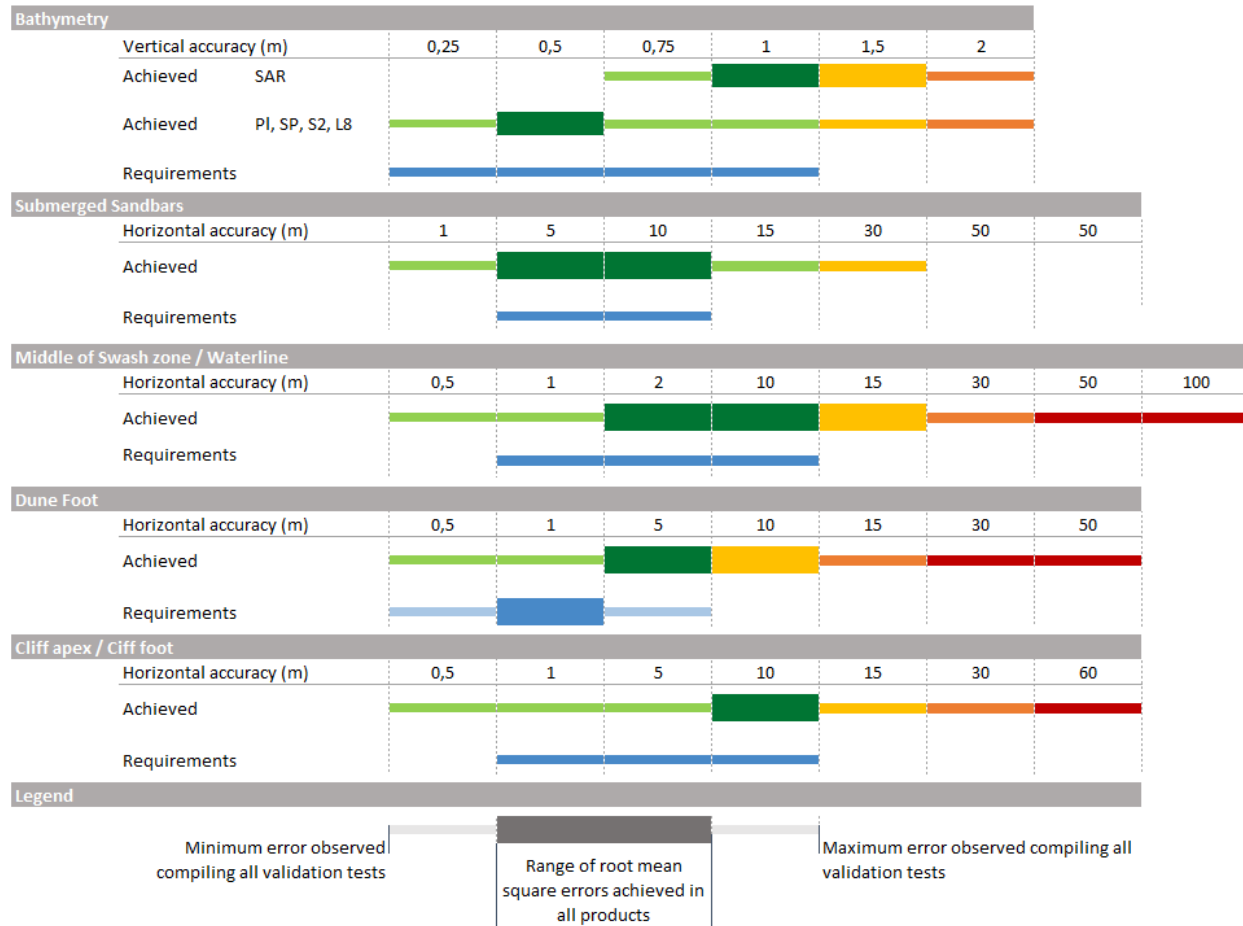


Table 3: Overview of the algorithm groups and algorithms tested, to be tested, and validation status

Algorithm Group	Algorithm	Status	Validation status	Page number
DEMs	Algorithm 1a DEM generation from optical data	Tested	To be performed during phase 2	57
	Algorithm 1b DEM generation from SAR data	Tested	To be performed during phase 2	54
Water Line and Creek	Algorithm 2a Water line detection using band ratios	Tested	To be continued during phase 2	50
Edge Detection	Algorithm 2b and 2b - adapted Water line detection using NDWI	Tested	Almost completed	51, 52
	Algorithm 2c Water line detection using a supervised classification process	Tested	Completed with the exceptions of tests that will be performed for beach width retrieval (algorithm 3e)	60
	Algorithm 2d and 2b - adapted Water line detection using binary products from SAR amplitude data	Tested, low performance achieved	Extensive validation ins needed during phase 2	55, 53



	Algorithm 2e Edge detection tidal creeks using SAR	Tested	To be performed during phase 2	64
Extraction of subaerial morphological structures and changes	Algorithm 3a Dune foot extraction using the cross-shore variation of first-order texture metrics from VHR optical data	Tested	Partly completed	55
	Algorithm 3b Dune foot extraction based on beach/dune slope from DEM	Tested	To be performed during phase 2	57
	Algorithm 3c Cliff line extraction using the cross-shore variation of the beach/cliff slope from DEM	Tested	To be performed during phase 2	57, 59
	Algorithm 3d Manual linear feature extraction from DEMs (3D digitization)	Tested	To be performed during phase 2	59
	Algorithm 3e Beach width computation	Tested	To be performed during phase 2	60
	Algorithm 3f Top-of-the-cliff vertical movement monitoring using PSI	Tested	To be performed during phase 2	61
	Algorithm 3g Intertidal creek morphological characteristics	To be tested during phase 2	To be performed during phase 2	64
	Algorithm 3h Dune foot extraction using supervised classification	Tested	Partly completed	65
	Algorithm 3i Cliff line extraction using supervised classification	Tested	Partly completed	67
	Bathymetry	Algorithm 4a Empirical model to retrieve bathymetry from HR/VHR optical data	Tested	Completed
Algorithm 4b Quasi-analytical model to retrieve bathymetry from HR/VHR optical data		Tested	Completed	-
Algorithm 4c Bathymetry swell inversion		Tested	Partly completed	69
Classification methods	Algorithm 5a Supervised classification approaches based on optical data	Used for dune and cliff line extraction	No need for validation	
	Algorithm 5b Classification based on texture information derived from SAR amplitude data	Unused	To be performed during phase 2 if required by end-users	-
	Algorithm 5c Decision tree classification based on band ratios and LSU	Used for land-water separation in intertidal flats	To be validated with sediment information from publications in phase 2.	64
Extraction of submerged morphological structures and changes	Algorithm 6a Submerged sand banks	Tested	Almost completed (to be tested only for Landsat in phase 2)	70
	Algorithm 6b Mapping change of sandbars	No information for validation available	Looking for data in phase 2	70



5 VALIDATION PLAN FOR PHASE 2

5.1 Current products

5.1.1 Water line detection using band ratios (algorithm 2a)

5.1.1.1 Overall strategy and objective

The waterline indicator based on band ratios has been derived for two German test sites: Sylt Odde and Kiel Probstei. While Sylt Odde is located in the North Sea, Kiel Probstei is a test site at Baltic Sea Coast. During phase 1, the end users provided existing orthophotos from different years and Laserscan data for the two test sites which have been used for a visual assessment with the extracted coastlines. The comparison showed satisfactory results but also that the time difference between the data set is very relevant, especially for fast changing coastlines. Furthermore, the tidal range and information about weather (wind) conditions during the acquisition needs to be included in the analysis. In phase 2, the assessment with the existing data and with additional data provided by the users will be performed as well as dedicated field measurements are foreseen for 2020. Both, qualitative and quantitative comparisons will be performed.

5.1.1.2 Method

The extracted water lines will be validated against different data sources, mainly airborne derived orthophotos, Laserscan data and GPS survey data. The comparison will be performed on a qualitative basis, comparing the data provided by the users with the satellite derived land-water line (orthophotos and indicator). The comparison with extracted linear data (i.e. extracted from Laserscan data) will be used to calculate the spatial difference between both lines in regular distances. GPS measurements will be used to determine the the closest distance to the water line indicator and the mean of all distances will provide a quantitative number that can be compared for all years.

The results will be discussed taking into account the conditions of the acquisitions (both for ground based, orthophotos and satellite data) in order to show the influence of water level and wind conditions for the quality of the indicators.

5.1.1.3 Data

5.1.1.3.1 Airborne data

Orthophotos

- Kiel Probstei: 2010, 2013, 2016, 2019
- Sylt Odde: 2003, 2009, 2010, 2013, 2014, 2016, 2017, 2018, 2019

Laserscan data

- Kiel Probstei: 2016 (raster & point data) plus coastline derived from Laserscan data
- Sylt Odde: 2018

5.1.1.3.2 Field / environmental data

- Sylt Odde: yearly measurements beginning of each year and after sand nourishments
- Dedicated GPS surveys in 2020
- Gauge data for water level for acquisition dates
- Wind data for acquisition dates

5.1.1.3.3 Satellite data

- Landsat-8 and Sentinel-2 from all suitable acquisitions (cloud free over test area) (both test sites)
- For 2020, 4-10 suitable images are expected per test site, depending on weather conditions



5.1.1.4 Expected results

The first validation results have been assessed by the users and were positively received. The outcome of the phase 2 validation will further demonstrate the agreement between the satellite-based indicators and the existing data the users. The data provided by the users are currently used for assessing all topics related to coastal erosion and coastal protection. Therefore, it is most relevant to demonstrate the agreement and limitations along those reference data. This approach will enable the user to assess the potential of the satellite data and to provide a good ground to develop an integrated monitoring concept.

5.1.1.5 Team involved in the product validation plan

- LLUR (end user, product design, in-situ data, assessment)
- LKN (end user, in-situ data)
- BC (producer optical data)

5.1.2 Waterline detection based on optical imagery (algorithm 2b)

5.1.2.1 Overall strategy and objective

During the 1st phase of the project all involved Greek end-users stressed out their need to receive from Sfs consortium waterlines over different POC sites and in specific years. Indeed, as such Terra Spatium produced waterline indicator (for a total of 1.8km) for years 2013, 2015, 2017 and 2019. Meantime, the validation results achieved so far revealed that the uncertainty on the predicted waterlines is of the order of the pixel size, which is beyond doubt a satisfying outcome.

Validation activities carried out in Romania led to close conclusions.

Nevertheless, the following tasks are anticipated for 2nd phase of the project, that aim to improve the algorithm results in weak areas and explore algorithms constraints. In particular, it is envisaged to:

- Proceed on the validation of the performance of the algorithm, once the necessary improvement will be applied, in rocky areas and rocky defense structures, where the tested algorithm still fails to give satisfactory results,
- Benchmark the validation of the performance of the algorithm once applied to non-pansharpened and pansharpened Landsat imagery,

5.1.2.2 Method

The baseline method (cf. section 3.1.1, p.9 and Figure 1) will be used to achieve the aforementioned validation tasks.

The available GPS survey data (collection date from 30th September to 2nd October 2019), with the use of Real Time Kinematic GPS techniques will be used for the POC site of:

- Vistonis-Maroneia,
- Gheorge Sf. Sulina.

For the phase 2 some of the existing data will be exploited to improve the detection algorithm, while a different and independent dataset will be used for validation purposes.

5.1.2.3 Data

5.1.2.3.1 Field data

The GPS survey (45,1 km) took place from 30th September to 2nd October 2019, with the use of RTK GPS techniques (Real Time Kinematic, L1/L2 frequencies) and therefore by achieving a mean horizontal accuracy of a 2-3 centimetres for the collected data.

GPSs survey collected over a distance of 27 km will be used to evaluate products in Romania.

Therefore, all the data that will be used for product validation, are archived by the consortium. No additional field survey or data collection are needed.



5.1.2.3.2 Imagery

30-m resolution Landsat images acquired between 1998 and 2020, along with commercial high-resolution SPOT1-5 legacy archive imagery, will be processed to obtain results over the POC sites.

5.1.2.4 Expected results

Two main results are expected from this validation plan:

- The calculation of the uncertainty of waterlines detection based on 30-m resolution Landsat data, taking into account the error introduced by the field survey,
- The calculation of the uncertainty of waterlines detection based on high-resolution SPOT1-5 legacy archive, taking into account the error introduced by the field survey.

5.1.2.5 Team involved in the product validation plan

The team involved in this validation action is composed of:

- Terra Spatium,
- Terrasigna,
- University of Bucharest,
- End-user enrolled for the POC site of Vistonis-Maroneia.

5.1.3 Middle of swash zone based on optical imagery (algorithm 2b – adapted)

5.1.3.1 Overall strategy and objective

The middle of the swash zone is the main shoreline indicator for French sandy Mediterranean shores. An extensive indicator production accompanied by a robust validation experience has been already achieved over all POC sites where the indicator was requested by the coastal managers.

The remaining tasks concern:

- The validation of the performance of the algorithm, once the necessary improvement will have been made, in the vicinity of rocky longshore and cross-shore defense structures, where the tested algorithm still fails to give satisfactory results,
- The validation of the performance of the algorithm once applied to non-pansharpended Landsat imagery,
- The estimation of the field survey uncertainty.

5.1.3.2 Method

The baseline method (cf. section 3.1.1, p.9 and Figure 1) will be used to achieve the validation tasks that have been defined. We have an extensive database of GPS surveys to proceed with the validation plan, split between Saint Raphaël, Hyères and Camargue. A fraction of surveys (about 38.5 km) was used for validation purposes during phase 1. For phase 2, we will upgrade the validation effort by including all relevant data already recorded in order to demonstrate the validation over 50 km of coast in total.

Since some of the field data will be exploited to improve the detection algorithm, we will use an independent dataset for validation purposes.

During phase 2, field and image matchups will be obtained considering Sentinel-2 and 30-m resolution Landsat imagery only.

In order to estimate the uncertainty of the GPS field survey, the middle of swash zone will be monitored at the same location by 4 different operators over a total distance of 5 km. A global accuracy range will be obtained from the statistical analysis of the 4 field reconnaissance missions.



5.1.3.3 Data

5.1.3.3.1 Field data

In order to reach our objective (overall validation distance of 50 km), GPS surveys will be acquired from May to July 2020 (1) to complete the existing dataset and (2) to estimate the uncertainty of the field operator. The sectors of Hyères and Camargue will be investigated, since we obtained rare or old surveys, respectively, over these two POC sites. A 3-day field survey will be organized to collect complementary surveys. Usual GPS material deployed by the CEREGE / Aix Marseille University will be used to ensure the coherence of the most recent surveys with the ones carried out by this operator at Saint Raphaël and Camargue POC sites previously.

The middle of swash zone will be monitored by the expert of Aix Marseille University involved in the project, supported by I-SEA's team. The middle of the swash zone will be surveyed long a total section of shore of about 10-15 km approximately, focusing sectors exhibiting rocky defense structures.

All surveys carried until 2019 that will be used for product validation, are archived by the consortium. An additional field survey planned in 2020 will complete the necessary validation data.

5.1.3.3.2 Imagery

Sentinel-2 data from May to August 2020 will be used to produce the indicator along the shores surveyed in 2020.

Then, 30-m resolution Landsat images acquired between 1998 and 2020 will be processed to obtain relevant matchups over the 3 POC sites. The image time-series will be chosen within the 2 months preceding or following the surveys.

5.1.3.4 Expected results

Three main results are expected from this validation plan:

- The calculation of the error bar on the GPS field survey,
- The calculation of the uncertainty of the middle of swash zone detection based on 30-m resolution Landsat data, taking into account the error introduced by the field survey,
- The calculation of the uncertainty of the middle of swash zone detection based on 2-m to 10-m resolution optical imagery based on a 50 km matchup database, taking into account the error introduced by the field survey.

5.1.3.5 Team involved in the product validation plan

The team involved in this validation action is composed of:

- I-SEA,
- Aix Marseille University (CEREGE),
- End-user enrolled in PACA region.

5.1.4 Middle of swash zone based on SAR imagery (algorithm 2d - adapted)

5.1.4.1 Overall strategy and objective

As underlined in the previous section, the middle of the swash zone is the main indicator used for shoreline monitoring purposes over the French sandy Mediterranean POC sites. An extensive production of this indicator based on Sentinel-1 and ERS data has been achieved during phase 1. The results of the validation experiment completed were only partially satisfactory. They clearly demonstrated that the indicator is visible and could be extracted on the mean backscatter coefficient on VV polarization from input products, however developments are needed to strengthen and automate the detection method.

Therefore, an extensive validation of the indicator derived from Sentinel-1 and ERS must be completed during phase 2.



5.1.4.2 Method

The baseline method (cf. section 3.1.1, p.9 and Figure 1) will be used to achieve the validation tasks that have been defined. We have an extensive database of GPS surveys to proceed with the validation plan, split between Saint Raphaël, Hyères and Camargue. In addition to the data already at our disposal, a field survey will be carried out between May and July 2020 in PACA region. The global dataset will represent 70 to 80 km of field surveys recorded between 1998 and 2020. It is expected that a significant fraction of the surveys will be used for algorithm improvement. We will use an independent dataset for validation purposes and expect to compare field surveys with SAR-derived indicator over 10 km to 30 km for each sensor.

5.1.4.3 Data

All the data that will be used for product validation, are archived by the consortium. No additional field survey or data collection are needed.

5.1.4.3.1 Field data

5.1.4.3.1.1 ERS product validation

All GPS surveys recorded before 2011 will be used for algorithm improvement and validation:

- Camargue: 2002, 2004, 2005, 2006, 2008,
- Hyères: 2011,
- Saint Raphaël: September 2011, December 2011.

5.1.4.3.1.2 Sentinel-1 product validation

All GPS surveys recorded from 2014 will be used for algorithm improvement and validation:

- Camargue: June-August 2020,
- Hyères: 2015, June-August 2020,
- Saint Raphaël: June, September and December 2014-2019, June and September 2020.

5.1.4.3.2 Imagery

The image time-series used to retrieve the indicator will be chosen within the 2 months preceding or following the surveys.

5.1.4.4 Expected results

Two main results are expected from this validation plan:

- The calculation of the uncertainty of the middle of swash zone detection based on 10-m resolution Sentinel-1 data, taking into account the error introduced by the field survey,
- The calculation of the uncertainty of the middle of swash zone detection based on ERS imagery, taking into account the error introduced by the field survey.

5.1.4.5 Team involved in the product validation plan

The team involved in this validation action is composed of:

- I-SEA,
- Aix Marseille University (CEREGE),
- End-user enrolled in PACA region.



5.1.5 Waterline detection based on SAR imagery (algorithm 2d)

5.1.5.1 Overall strategy and objective

An extensive validation effort is required to assess the accuracy of waterlines obtained by processing SAR data. This action is crucial for 2 main reasons: firstly, because this indicator is primordial and secondly because SAR imagery is of high interest to get past information through long Earth observation archives and to collect data at all time.

Validation will be carried out in Greece and Romania. Indeed, these validation results will enhance the outcomes of the validation plan defined to determine the middle of swash zone (section 5.1.4, p. 53 and following).

5.1.5.2 Method

The baseline method (cf. section 3.1.1, p.9 and Figure 1) will be used to achieve the validation tasks that have been defined. For the phase 2 some of the existing data will be exploited to improve the detection algorithm, while a different and independent dataset will be used for validation purposes.

5.1.5.3 Data

5.1.5.3.1 Field data

In Greece, the GPS survey took place from 30th September to 2nd October 2019, with the use of RTK GPS techniques (Real Time Kinematic, L1/L2 frequencies) and therefore by achieving a mean horizontal accuracy of a 2-3 centimetres for the collected data. GPS survey operation was performed over a total distance of almost 45,1 km.

In Romania, *in-situ* measurements collected using a GPS on 13th of April 2016 were used as ground-truth information. The distance covered by the survey was of 27 km.

5.1.5.3.2 Images

Sentinel-1 images recorded in the days following or preceding the field reconnaissance will be processed.

5.1.5.4 Expected results

The main result expected from this validation plan is to obtain the uncertainty of the waterline detection based on 10-m resolution Sentinel-1 data. Average and maximum detection error will be calculated. Individual calculation will be performed in Greece and Romania. Also, if it appears relevant, global uncertainty will be also calculated merging all the validation experiments.

5.1.5.5 Team involved in the product validation plan

The team involved in this validation action is composed of:

- Terra Spatium,
- Terrasigna,
- University of Bucharest,
- End-user enrolled for the POC site of Vistonis-Maroneia.

5.1.6 Dune foot based on textural analysis of VHR optical data (algorithm 3a)

5.1.6.1 Strategy

Dune foot extraction using the cross-shore variation of first-order texture metrics from VHR optical data based tested on South Aveiro and Biscarrosse POC sites. For both these sandy macrotidal areas, the dune foot is the main 2D shoreline indicator. First results are promising. However, the detection method must be upgraded and automated.



Therefore, the extensive validation of the final results obtained will be achieved during phase 2. A global validation will be calculated integrating all the available matchups and all the sensors used to derive the dune foot.

The estimation of the field survey uncertainty will be also estimated.

5.1.6.2 Method

The baseline method (cf. section 3.1.1, p.9 and Figure 1) will be used to validate the dune foot derived from textural analysis of VHR optical imagery. Validation effort will focus on 2 image datasets acquired during phase 1 for South Aveiro and Biscarrosse (Pleiades and WorldView imageries, respectively). It will be consolidated by results obtained at Cap Ferret and La Salie during a previous project led by I-SEA (Lafon et al., 2014).

5.1.6.3 Data

5.1.6.3.1 Field data

For the Aveiro POC site, the GPS survey (polyline) realised the 14th of April 2014 during a field survey at the low tide with the INSHORE system (Baptista et al., 2011) and carried out over a 10.19 km shoreline will be exploited for the dune foot validation.

At Cap Ferret and La Salie the GPS survey (polyline) covers a total distance of about 6.5 km and have been collected in April 2013.

At Biscarrosse, MNT derived from DGPS measurement carried out in April 2014 will be used to validate the dune foot. The dune foot will be first extracted from the MNT using the r.slope tool of GRASS.

Finally, GPS data obtained in 2019 at Biscarrosse along the dune foot will be used to estimate the uncertainty of the GPS survey. This uncertainty is due to GPS accuracy and operator choices. During the experiment carried out at Biscarrosse the dune foot had been collected with GPSs by 8 different operators during a 2-days field survey. A total distance of 2 kms has been covered by the field teams. The results will be processed in order to estimate average and maximum uncertainty on the field monitoring.

All the data that will be used for product validation, are archived by the consortium. No additional field survey or data collection are needed.

5.1.6.3.2 Imagery

At South Aveiro, the processed Pleiades image has been acquired on the 12th of March 2014.

At Cap Ferret and La Salie, we will use a Pleiades image recorded on the 13th of April 2013.

Finally, at Biscarrosse a WorldView-2 image recorded on the 5th of August 2014 will be processed.

5.1.6.4 Expected results

This experiment will allow us to derive an overall uncertainty value of the method together with evaluation of the average and maximum expected error bar on the derived dune foot location, taking into account the error introduced by the field survey.

5.1.6.5 Team involved in the product validation plan

The team involved in this validation action is composed of:

- I-SEA,
- Aveiro University,
- End-used enrolled in Nouvelle Aquitaine and Aveiro region.



5.1.7 Dune foot extraction based on VHR imagery-derived DEM (algorithms 1a + 3b)

5.1.7.1 Strategy

This detection approach, highly prospective, has been applied to South Aveiro only. Therefore, the validation will be restricted to this POC site. The dune foot is derived from a DEM built using Pleiades stereo imagery. Since the available validation data are restricted to GPS dune foot survey, then the final derived product, that is the dune foot, will be validated. Due to missing data, the DEM derived from Pleiades stereo data will not be controlled.

The estimation of the field survey uncertainty will be also estimated, following the method detailed in section 5.1.6 (p. 55 and following).

5.1.7.2 Method

The baseline method (cf. section 3.1.1, p.9 and Figure 1) will be used to validate the dune foot derived from textural analysis of VHR optical imagery.

5.1.7.3 Data

5.1.7.3.1 Field data collection

The GPS survey (polyline) realised the 14th of April 2014 during a field survey at the low tide with the INSHORE system (Baptista et al., 2011) and carried out over a 10.19 km shoreline will be exploited for the dune foot validation.

All the data that will be used for product validation, are archived by the consortium. No additional field survey or data collection are needed.

5.1.7.3.2 Imagery

The processed Pleiades stereo images have been acquired on the 12th of March 2014.

5.1.7.4 Expected results

This experiment will allow us to derive a first evaluation of the uncertainty value of the average error bar on the derived dune foot location, taking into account the error introduced by the field survey.

5.1.7.5 Team involved in the product validation plan

The team involved in this validation action is composed of:

- I-SEA,
- Aveiro University,
- End-used enrolled in Nouvelle Aquitaine and Aveiro region.

5.1.8 Cliff lines extraction based on VHR imagery-derived DEM (algorithm 1a + 3c)

5.1.8.1 Overall strategy and objective

DEM generation and cliff indicator extraction, based on VHR imagery can be evaluated for 3 different areas: Erretegia, Vaches Noires and Corniche Basque. If the final objective of this validation action focusses the validation of the cliff apex and cliff foot locations, we will also evaluate the difference between the satellite-derived DEM and reference existing data.

5.1.8.2 Method

5.1.8.2.1 DEM evaluation

Digital Surface Model validation is often achieved using ground control points acquired with a GNSS device or an airborne LIDAR DSM (eg., Poli et al. 2015).



5.1.8.2.2 Indicator extraction

The cliff foot and cliff apex can be derived from:

- Automated thresholding of the MNT at a given altitude (Plat et al., 2013; Baudouin et al., 2015)
- Manual extraction based on the slope field derived from the MNT (see algorithm 3d, section 5.1.10, p. 59 and following)
- CliffMetrics (Automatic Cliff Metrics delineation) delineates the location of the coastline, coastline normals, and cliff metrics along these normal (Payo et al., 2018),
- The transect-based approach of Le Mauff et al. (2018).

These various methods will be tested and the derived indicators will be compared with ground-truth or Lidar data. Comparison between satellite-derived and reference data shall be made between indicators obtained with the same method.

5.1.8.2.3 Indicator 2D location assessment

The comparison between satellite-derived cliff lines and reference data will be carried using two different approaches:

- The baseline method (cf. section 3.1.1, p.9 and Figure 1),
- The method based on area (Costa, 2000; Ali, 2003) developed hereafter.

The approach based on areas has been early developed by Robin (2002a, 2002b) and is found particularly adapted to evaluate the coastline erosion in the case of the Vaches Noires POC site (Letortu, 2013). Therefore, following the same concept has the one used to control the shoreline location with the baseline approach, the model based on area model will be adapted to assess the 2D accuracy of the cliff foot and apex location.

This method considers the surfaces between two coastlines and not the distances along transects perpendicular to the coastline. Conceptually, the coastlines are intersected at a same level and, if needed, close at their extremity. Polygons are created between the intersections and the coastlines. A careful and manual verification of the topology must be considered before measuring the surface of the polygon. Then this surface is weighted by the average coastline length characterising each polygon. This approach presents the interests (1) to adapted to complex coastline morphologies, (2) to highlight the detection errors (onshore / offshore) and (3) to enable an easy focus on main difficulties linked with the detection of cliff lines.

5.1.8.3 Data

5.1.8.3.1 Reference data

In Normandie, in particular for Vaches Noires POC site, field data are acquired regularly to monitor cliff erosion (Table 4). They are completed by remotely sensed surveys like lidar or drone photogrammetry. For the Basque country, we had also access to the field and lidar surveys detailed in Table 5.

All the data listed in Table 4 and Table 5, that will be used for product validation, are archived by the consortium. No additional field survey or data collection are needed.

Table 4. Data available for Vaches Noires POC site valuable to validate VHR imagery-derived cliff lines

Data type	Date
Terrestrial laser scanning survey of the cliff front	Every 3 months since 2014
3D SFM photogrammetry	12th of June 2019



Table 5. Data available for Erretegia POC site valuable to validate VHR imagery-derived cliff lines

Data type	Date
Field surveys of cliff apex and cliff bottom	2014, 2017
Airborne lidar surveys (IGN)	7th of October 2017

5.1.8.3.2 Imagery

Three stereo acquisitions will be processed for this validation action:

- Vaches Noires: WorldView images acquired the 29th of July 2019,
- Erretegia and Corniches Basques: Pleiades images acquired the 27th of July 2017.

5.1.8.4 Expected results

From this validation experiment we expect:

- Obtain soundful uncertainty assessment of the for the cliff apex and cliff foot indicators extracted from satellite-derived DEMs in various geomorphological conditions,
- Evaluate the impact of the accuracy of the DEM on the cliff line uncertainty.

5.1.8.5 Team involved in the product validation plan

The team involved in this validation action is composed of:

- I-SEA,
- Terra Spatium,
- End-used enrolled in Nouvelle Aquitaine and Normandie regions.

5.1.9 Cliff lines extraction based on VHR/HR imagery-derived DEM (algorithm 1b + 3c)

We will apply exactly the same strategy as the one detailed in the previous section. The only difference between the section is the image used that will be involved in the production process. Images that will be used are:

- One CosmoSkyMed image recorded in September 2014 (TPM image already ordered and stored by the consortium),
- All available Sentinel-1 images recorded 4 to 6 months before or after the reference data acquisition.

5.1.10 Manual linear feature extraction from DEMs (algorithm 3d)

5.1.10.1 Overall strategy and objective

The validation will be restricted to areas were stereo high-resolution imagery over POC sites exist. Therefore, cliff lines (foot and apex) will derive manually from a DEM built by using SPOT-7 stereo imagery with stereo-vision. Since the available validation data are restricted to GPS survey, then the final derived product, that is the foot and apex, will be validated.

5.1.10.2 Method

The baseline method (cf. section 3.1.1, p.9 and Figure 1) will be used to validate the foot and apex derived manually from a DEM built by using SPOT-7 stereo imagery with stereo-vision.



5.1.10.3 Data

5.1.10.3.1 Field data

The GPS survey took place from 30th September to 2nd October 2019, with the use of RTK GPS techniques (Real Time Kinematic, L1/L2 frequencies) and therefore by achieving a mean horizontal accuracy of a 2-3 centimetres for the collected data.

All the data that will be used for product validation, are archived by the consortium. No additional field survey or data collection are needed.

5.1.10.3.2 Imagery

The processed Spot-7 stereo images have been acquired on the 28th of August 2019.

5.1.10.4 Expected results

This experiment will allow us to derive a first evaluation of the uncertainty value of the average error on the derived cliff lines (foot and apex), taking into account the error introduced by the field survey.

5.1.10.5 Team involved in the product validation plan

The team involved in this validation action is composed of:

- Terra Spatium,
- End-user enrolled for the POC site of Vistonis-Maroneia

5.1.11 Beach width (algorithm 3e)

5.1.11.1 Strategy

Beach width has been assessed in microtidal and macrotidal POC sites (Saint Raphaël and Biscarrosse, respectively).

In Mediterranean low tide range regions, the beach width is the distance between the middle of swash zone and the upper beach limit. In that specific case, the validation issue concerns exclusively the middle of swash zone. An important effort is being deployed to validate this indicator crucial for coastal erosion monitoring. Therefore, the uncertainty derived from the validation experiments described in sections 5.1.3 (p. 52 and following), and 5.1.4 (p. 53 and following) will be

Most important here is the evaluation of the uncertainty achievable in macrotidal regions. At such location, the beach width is the distance between the upper limit reached by the tides and the dune foot. The dune foot location can be obtained by various approaches. Validation experiments for each of them are described in sections 5.1.6 (p. 55), 5.1.7 (p. 57) and 5.1.14 (p. 65).

Therefore, the validation experiment detailed in this section will here concern the location of the upper limit reached by the tides but the global uncertainty measured on beach width will be obtained by combining the uncertainty of the dune foot location and the upper limit reached by the tide.

5.1.11.2 Method

The uncertainty on beach width indicator derived from satellite data will be obtained by comparing:

- Average and maximum error on dune foot location (using the baseline method (cf. section 3.1.1, p.9 and Figure 1) to compare field and remotely-sensed data,
- Average and maximum error on the location of the upper limit reached by the tide (using the baseline method (cf. section 3.1.1, p.9 and Figure 1) to compare field and remotely-sensed data,
- Field and satellite measured beach width, using the area-based approach (Costa, 2000; Ali, 2003).

Waterline based on optical and SAR data will be extracted using algorithm 2c and 2d, respectively.



5.1.11.3 Data

5.1.11.3.1 Field data

Field data obtained during a field experiment carried out at Biscarrosse in 2019 will be valorized for this validation action. During this field survey, the dune foot and the waterlines have been collected by field operators during a 2-day experiment for 2 different tide coefficients around 12 am UTC. A total distance of 2 km has been covered by the field teams.

A field survey will be organized in 2020, with particular focus on the water line at the time of Sentinel-1 and -2 overpasses. About 10 field teams will be deployed simultaneously in the vicinity of Biscarrosse to follow the waterline at high tide for medium tide range. We expect to obtain validation along about 4 km of shore. A 2-day field survey will be carried out allowing to walk along the waterline at about 6 am and 12 am UTC to correspond to Sentinel sensors acquisition time.

All surveys carried until 2019, that will be used for product validation, are archived by the consortium. An additional field survey planned in 2020 will complete the necessary validation data.

5.1.11.3.2 Imagery

Sentinel-2 images recorded at the date of the missions carried out in 2019 will be download and processed. Clear sky was observed during the field survey. In 2020, Sentinel-1 images at the date of the field survey will be download and processed. Additionally, Sentinel-2 images at the date of the field survey will be download and processed too. In case of cloud cover during the field surveys, Sentinel-2 images recorded for equivalent tidal range and meteorological conditions will be download and processed to extract waterlines that should be close to the ones observed during the field surveys.

5.1.11.4 Expected results

This experiment will allow us to derive a first evaluation of the uncertainty value of the average error bar on the derived beach width location, taking into account the error introduced by the field survey.

Also, the results obtained to qualify the waterline with Sentinel-1 will also contribute to validation of the algorithm 2d already developed in sections 5.1.4 (p. 53 and followings) and 5.1.555 (p. 55 and following).

5.1.11.5 Team involved in the product validation plan

The team involved in this validation action is composed of:

- I-SEA,
- End-used enrolled in Nouvelle Aquitaine region.

5.1.12 Top-of-the cliff vertical movements (algorithm 3f)

5.1.12.1 Overall strategy and objective

For monitoring the test sites along French coast where cliffs are present the Interferometric Point Target Analysis (IPTA) algorithm (Werner et al., 2003) has been used based on Sentinel 1 A & B SLC SAR images with a high temporal resolution. Each site has been monitored by one geometry and the rates concern deformation in LOS (Line Of Sight) that means movement towards or away the satellite. Also, in principle, this method is based on the existence of scatterers on the ground. So, it is possible to have measurements only in areas where scatterers are presented. In our case, there are gaps in scatterers and therefore, it is not possible to measure possible instability along the coast as shown in Figure 40. Our proposal, for phase 2, concerns the application of like-SBAS algorithms (Neokosmidis et al., 2016) that are more suitable to measure potential instability in areas where scatters do not exist using Sentinel data from ascending and descending geometry. Both approaches will be combined to derive exhaustive maps of the cliff vertical movements. In second phase our strategy will be focused on apply interferometric processing using data from both geometry acquisitions (descending and ascending) follow by the decomposition of the interferometric phase in up -down and east -west and not along the LOS (line of sight). After producing the maps in terms of the processing steps the results will be validated by other inputs (Table 6 and Table 7).



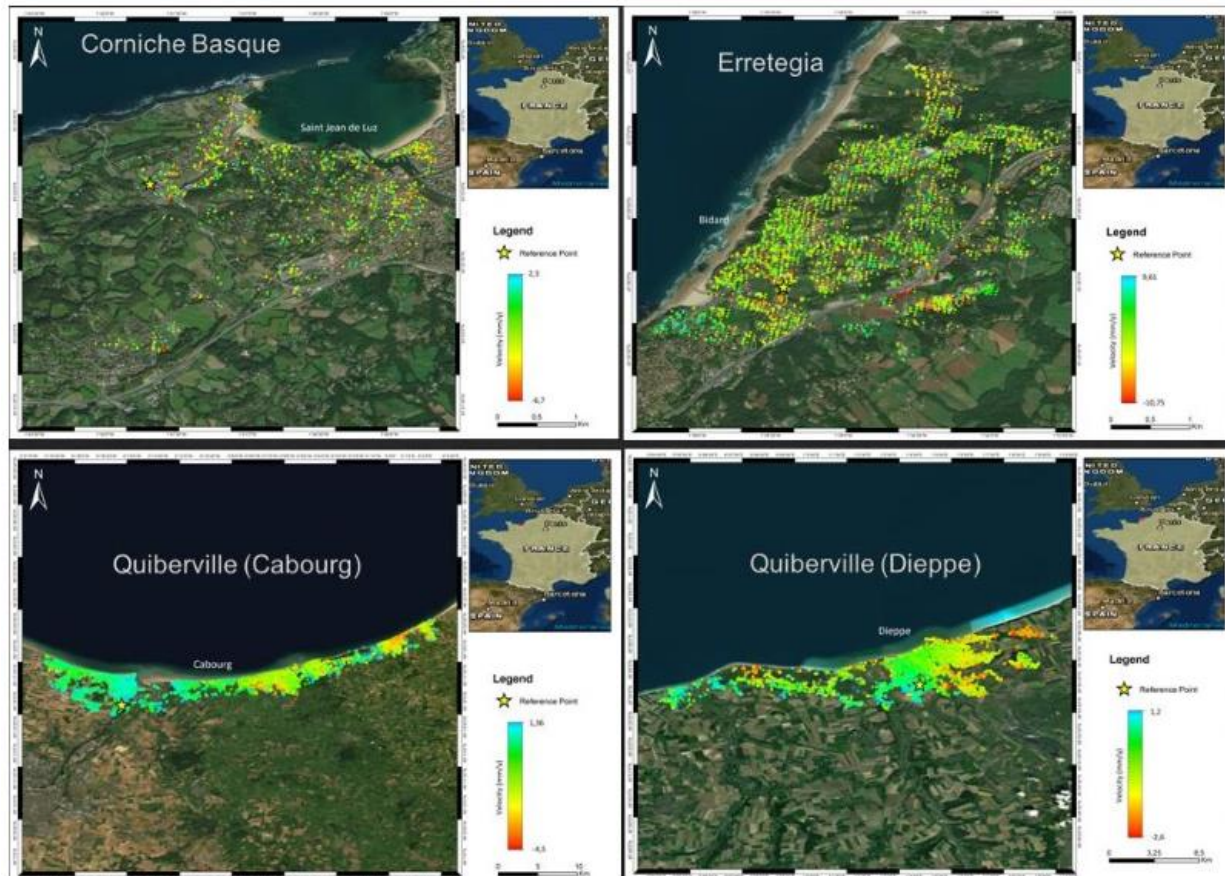


Figure 40. Result of the application of the IPTA algorithm to calculate cliff vertical movement for 4 of the French POC sites

5.1.12.2 Method

The validation of cliff vertical movements will be performed over a maximum of two different sites.

With regards to Persistent Scatterer InSAR (PSI), five complementary aspects of the PSI measurements should be considered in the validation:

- The intrinsic quality of the PSI measurements, taking into account that PSI basically provides “relative measurements” that includes the verification of:
 - WGS84 Geographic coordinates (geolocation of points),
 - Mean PS annual velocity over the observed period, measured in the radar Line-of-Sight (LOS),
 - The PS phase coherence, with values between 0 and 1 (optimal) which indicates the quality of the PS measurements, quality of scatterers,
 - Ps time series analysis,
- The quality of the deformation velocity and time series estimated by PSI, which will be assessed by direct comparison with the reference data coming from levelling, local GPS network or field work,
- The comparison of DEMs or DTMs (produced from airborne laser scanning) covering the same time span period that SAR data cover,
- The comparison of optical high-resolution images or airborne pictures for the same period as PSI,
- Terrestrial laser scanning.



5.1.12.3 Available reference data

In Normandie (ex. Quiberville, cf. Figure 40), the existing data that can contribute to PSI and SBAS-like validation are listed in Table 6. Available data are exhaustive cover a long time-range. Therefore, the POC sites in Normandie are particularly suited to the evaluation of the quality of the result obtained for the proposed indicator. Available data for the Côte Basque are less numerous. They are detailed in Table 7.

Table 6. Data available in Normandie valuable to validate Interferometric measurement of the cliff vertical movement

Data type	date	Location
Airborne lidar surveys	2012 (litto3D), 2016	Normandie
Airborne lidar surveys	23 rd of June 2009, 13 th of March 2016	Les Vaches Noires
Terrestrial laser scanning survey of the cliff front	Every 3 months since 2010	Ailly / Puy
Terrestrial laser scanning survey of the cliff front	Every 3 months since 2014	Les Vaches Noires
3D SFM photogrammetry	Twice a month since 2014	Les Vaches Noires
Tacheometer topography	Since 1992	Various sites
Ortho-littorale	2000-2002 ; 2011-2014	Normandie

Table 7. Data available for the Côte Basque valuable to validate Interferometric measurement of the cliff vertical movement

Data type	date	Location
Airborne lidar surveys	2012, 2016, 2017, 2018	Corniche Basque, Erretegia
Drone photogrammetry	2017	Erretegia
Ortho-littorale	2000-2002 ; 2011-2014	Basque Country

All the data that will be used for product validation, are archived by the consortium. No additional field survey or data collection are needed.

5.1.12.4 Expected results

In the first phase, the interferometric results produced with data that based on one geometry so they provide information for the land movement in LOS (line of sight) also, the study areas without scatterers cannot provide useful data for the movement. So, in the second phase, would be used the technique of DS (distributed scatterers) including like SBAS methods (Neokosmidis et al., 2016). A DS object reflects lower radar energy compared to PSs and it usually covers several pixels in high resolution SAR images. These pixels exhibit similar scattering properties and can be used together for deformation estimation. As was mentioned before the validation will be performed using the data sources as was mentioned in Table 2 and 3. Moreover, validation will follow both the quality and the quantity (accuracy) aspect so will be confirmed the movement of the study area and the type of movement.

5.1.12.5 Team involved in the product validation plan

The team involved in this validation action is composed of:

- Harokopio University;
- I-SEA,
- End-used enrolled in Nouvelle Aquitaine and Normandie regions.



5.1.13 Intertidal creek morphological characteristics (algorithm 2e, 3g and 5c)

5.1.13.1 Overall strategy and objective

The indicators on tidal creek morphology have been produced for parts of the German Wadden Sea positioned in Schleswig-Holstein (Wesselburener Watt; Blauort). This area was selected because measurements of morphological changes and sediment types exist for past years. In general, ground based measurements in intertidal flat areas are difficult to perform due to the limitation to low tide and the accessibility of remote areas. Therefore, ground based measurements are limited. Airborne data are available for 2-3 years and will be used accordingly.

Information about intertidal changes and erosion indicators are formed from different methods. The validation of these intertidal related products is based on the same in-situ information and therefore is described here in common. We will perform a combination of comparison with sparse data available, methodological comparison (SAR, optic) and dedicated ground-based measurements performed in 2020. Further, Drone overflights are planned, which needs to be further elaborated.

5.1.13.2 Method

A methodological comparison between SAR and optically derived products will be performed for tidal creek positions and changes. This has been started in phase 1 but will be intensified in phase 2. As the tidal creek positions have been derived completely independent for SAR and optical data (different acquisitions & different techniques), a comparison allows at least a relative assessment. It will be performed by visual inspection. The existing airborne data from 2012, 2017 and 2018 will be used for qualitative comparison by overlaying the satellite derived creek positions.

For morphological changes and sediment type changes, different data sets are available, but information is still very sparse. The plan for phase 2 is to perform validation based on the existing data and literature review (*e.g.*, sediment analyses performed by Reimers, 2003). Field measurements of the position of one dedicated creek (Ossengoot) are available for the past years and will be used for a detailed validation of this sub-region of Blauort. Here, quantitative analyses will be performed providing the distances between field GPS surveys and the derived indicators.

Finally, the plan for phase 2 is to perform dedicated data sampling on ground in 2020. Here a transect from the coast to the Blauort Sandbank will be used to perform sediment samples and to derive the exact GPS position of the creeks that are crossed. Some parts of the creeks will be mapped.

5.1.13.3 Data

5.1.13.3.1 Airborne data

Orthophotos

- 2012, 2017, (2020/21)
- 2018 Orthophotos of outer tidal areas

Laserscan data

- 2016 (incl. Orthophotos)

Drone overflights

- Planned for 2020 (needs confirmation)

5.1.13.3.2 Field data

- Sediment data from Transects (2009, 2012, 2017, 2020)
- Creek position from Transect (2020)
- GPS positions of Ossengot creek for the past years
- Dedicated GPS measurements in 2020



5.1.13.3.3 Satellite data

- Optical Data: suitable low tide images from Sentinel-2 and Landsat-8 (expected: 2-4 during 2020)
- SAR Data: suitable low tide data from Sentinel-1 (10-20 expected)

5.1.13.4 Expected results

We will provide several qualitative assessments:

- comparison between SAR (yearly aggregated products) with single image products derived from optical data. One assessment for each year.
- airborne orthophotos overlaid with satellite based indicators (optic and SAR)
- Laserscan topography overlaid with satellite based indicators (optic and SAR)

For these indicators, it is important to work with the time series of products in order to detect real trends in the creek movements. This reduces the influence of the water level for single images.

Comparison of sediment types will be demonstrated for the closest acquisition compared to the ground truth measurements. It will be presented in confusion matrices.

The mean distance of creeks between ground-based position and image position will be provided in meters.

5.1.13.5 Team involved in the product validation plan

- LLUR (end user, product design, in-situ data, assessment)
- LKN (end user, in-situ data)
- BC (producer optical data)
- UHH (producer SAR data)

5.1.14 Dune foot extraction using supervised classification (algorithm 3h)

5.1.14.1 Strategy

Dune foot extraction using supervised classification of optical imagery has been tested on South Aveiro and Biscarrosse POC sites. For both these sandy macrotidal areas, the dune foot is the main 2D shoreline indicator. First results are promising. However, this detection method needs to be upgraded. Also, it needs to be tested and evaluated on Landsat data.

Therefore, the identified 2 main validation tasks:

- validation of the final results obtained once the processing method will have been successfully improved, based on SPOT and Sentinel-2 imagery, completed, if appears valuable, by Sentinel-1 data,
- validation of dune foot derived from Landsat image classification, in synergy, if it appears valuable, with ERS or Sentinel-1 data.

The estimation of the field survey uncertainty will be also estimated.

5.1.14.2 Method

The baseline method (cf. section 3.1.1, p.9 and Figure 1) will be used to validate the dune foot derived from supervised classification of HR imager.

5.1.14.3 Data

5.1.14.3.1 Field data

For the Aveiro POC site, the GPS surveys (polyline) realised the 14th of April 2014 and the 20th of March of 2018 at the low tide with the INSHORE system (Baptista et al., 2011) together with a new field survey that will be performed at 2020 will be exploited for the dune foot validation. Also, a GPS survey exists that was carried out in 2002.



At Biscarrosse, MNTs derived from DGPS measurement carried out in:

- April 2014,
- February, May, September and November 2016,
- February, April, June, July, August and November 2017,
- February 2018

will be used to validate the produced dune foots. From each MNT, the dune foot will be first extracted using the r.slope tool of GRASS.

The GPS survey carried in 2019 at Biscarrosse along the dune foot will be used to estimate the uncertainty of the GPS survey and also to validate dune foot extracted in 2019. Finally, a GPS dune foot survey will be carried out at Biscarrosse in 2020, during the same field survey as the one defined to monitor the waterline (see section 5.1.11.3.1, p.61).

All surveys carried until 2019, that will be used for product validation, are archived by the consortium. Additional field surveys planned in 2020 will complete the necessary validation data.

5.1.14.3.2 Imagery

In South Aveiro, we will process:

- All Landsat relevant images (possibility in combination with ERS / Sentinel-1 data) for the years 2002, 2014, 2018 and 2020,
- One Spot image acquired the 26th of June 2014,
- All Sentinel-2 relevant images (possibility in combination with Sentinel-1 data) for the years 2014, 2018 and 2020.

At Biscarrosse, we will use:

- All Landsat relevant images (possibility in combination with Sentinel-1 data) for the years 2014 and 2016 to 2020,
- A Spot time series acquired in 2014,
- All Sentinel-2 relevant images (possibility in combination with Sentinel-1 data) for the years 2014 and 2016 to 2020.

5.1.14.4 Expected results

This experiment will allow us to derive an overall uncertainty value of the method together with evaluation of the average and maximum expected error bar on the derived dune foot location, taking into account the error introduced by the field survey.

Individual uncertainties obtained when exploiting Sentinel-1, SPOT and Landsat will be calculated. These uncertainties will take into account the error introduced by the field survey.

Our database allows us to derive the quantitative uncertainty of results if ERS data are introduced in the production process for Aveiro. Unfortunately, our database does not allow us to provide such results at Biscarrosse. For this POC site, as an alternative, qualitative assessment using airborne or satellite high resolution images may be proposed, if it appears soundful (ortho-littorales V1 and V2 and Formosat images acquired in 2009, 2010 and 2011 by the Aquitaine Coast Observatory).

5.1.14.5 Team involved in the product validation plan

The team involved in this validation action is composed of:

- I-SEA,
- Aveiro University,
- End-used enrolled in Nouvelle Aquitaine and Aveiro region.



5.1.15 Cliff line extraction using supervised classification (algorithm 3i)

5.1.15.1 Overall strategy and objective

The algorithm performance will assess for 3 different POC sites: Quiberville and Vaches Noires in Normandie and Erretegia in the Basque Country. Our main objective is to assess the potential of HR imagery, in particular of HR times series to derive cliff apex and/or cliff foot according to the location. Up to now, algorithm 3i only uses Landsat and Sentinel-2 optical data, the additional exploitation of SAR imagery (ERS and Sentinel-1) will be evaluated during phase 2.

The Table 8 summarizes the different validation tasks that will be undertaken during phase 2.

Table 8. Validations actions planned during phase 2 to assess cliff line obtained for HR imagery classification

Site	Indicator name	Indicator date	Sensor
Erretegia	Cliff foot	2017	S2, L8-P, L8 S2 + S1, L8-P + S1, L8 + S1
Erretegia	Cliff foot	2018	S2, L8-P, L8 S2 + S1, L8-P + S1, L8 + S1
Quiberville	Cliff apex	2013	L5, L8-P, L8 L5 + S1
Quiberville	Cliff apex	2015	S2, L8-P, L8 S2 + S1, L8-P + S1, L8 + S1
Quiberville	Cliff apex	2017	S2, L8-P, L8 S2 + S1, L8-P + S1, L8 + S1
Vaches Noires	Cliff foot	2009	L5 ERS
Vaches Noires	Cliff foot	2016	S2, L8-P, L8 S2 + S1, L8-P + S1, L8 + S1
Vaches Noires	Cliff foot	2019	S2, L8-P, L8 S2 + S1, L8-P + S1, L8 + S1

5.1.15.2 Method

The comparison between the cliff lines extracted from image classification and the reference data will be carried using two different approaches:

- The baseline method (cf. section 3.1.1, p.9 and Figure 1),
- The method based on area (Costa, 2000; Ali, 2003) developed in section 5.1.8 (p. 57 and followings).

When they are not monitored in the field with ground GPS devices, the cliff foot and cliff apex can be derived from:

- Automated thresholding of the MNT at a given altitude (Plat et al., 2013; Baudouin et al., 2015),
- Manual extraction based on the slope field derived from the MNT (see algorithm 3d, section 5.1.10, p. 59 and following)
- CliffMetrics (Automatic Cliff Metrics delineation) delineates the location of the coastline, coastline normals, and cliff metrics along these normal (Payo et al., 2018),
- The transect-based approach of Le Mauff et al. (2018).



Cliff line and cliff apex will be output based on these various approaches forming a set of reference data. All these reference cliff lines will be compared with the satellite-derived ones in order to potentially identify the best reference data for our indicator.

5.1.15.3 Data

5.1.15.3.1 Reference data

Available reference data are listed in Table 9. **All the data that will be used for product validation, are archived by the consortium. No additional field survey or data collection are needed.**

Table 9. Available reference data to evaluation cliff line location

Data type	date	Location
Airborne lidar surveys	23rd of June 2009, 13th of March 2016	Les Vaches Noires
Terrestrial laser scanning survey of the cliff front	Every 3 months since 2014	Les Vaches Noires
3D SFM photogrammetry	Twice a month since 2014	Les Vaches Noires
Airborne lidar surveys	2017, 2018	Erretegia
DGPS surveys	2017, 2018	Erretegia
Airborne lidar surveys	2013, 2015, 2017	Quiberville

5.1.15.3.2 Imagery

Archived imagery acquired 4 to 6 months before or after the available reference data will be downloaded and processed.

5.1.15.4 Expected results

An extensive validation plan is established for this indicator with main aim to:

- Identify the best production process based either on optical imagery only or by using optical and SAR imagery in synergy,
- Calculate the uncertainty of the most appropriate input datasets:
 - Sentinel-2 or Sentinel-2 + Sentinel-1,
 - Landsat-Pansharpened or Landsat-Pansharpened + Sentinel-1 or Landsat-Pansharpened + ERS, or Landsat + ERS,
 - Landsat or Landsat + Sentinel-1 or Landsat + ERS.

Average and maximum uncertainties will be derived from this validation plan: for each site and compiling the different site if we demonstrate that this final compilation is scientifically relevant.

5.1.15.5 Team involved in the product validation plan

The team involved in this validation action is composed of:

- I-SEA,
- Terra Spatium,
- End-users enrolled in Nouvelle Aquitaine and Normandie regions.



5.1.16 Bathymetry (algorithm 4c)

5.1.16.1 Overall strategy

The bathymetry is an important indicator requested by end-users. The indicator production in high energetic environments (French and Portuguese Atlantic shores) is a challenge because of the turbidity of the water and for that reason, new methodologies have been explored.

The indicator production accompanied by validation has been already achieved where field data were available (*i.e.* French POC site: Bidart).

The current algorithm 4c-Bathymetry Swell Inversion, that uses the Fourier Fast Transform, generates realistic bathymetries for depths higher than 15-20 m. Nevertheless, our end-users are also interested in shallower waters (*i.e.* depths lower than 15 m). Therefore, a new algorithm that uses the Wavelet Transform is being developed to try overcoming the depth limitation of the previous one (*i.e.* to produce bathymetries at shallower waters).

Remaining tasks concern:

- The application of the new algorithm (Bathymetry Swell Inversion – Wavelet Transform)
- The validation of the performance of this new algorithm

5.1.16.2 Method

The baseline method (cf. section 3.2.1.2, p.10 and Figure 5) will be used to achieve the validation tasks that have been defined.

5.1.16.3 Data

5.1.16.3.1 Field data collection

Field data collected both French and Portuguese POC sites cover shallower waters. Field data for French POC sites are available for validation purposes (cf. section 4.5.3.2.1) whereas field data for Portuguese POC site are being acquired biannually in the framework of COSMO project (<https://cosmo.apambiente.pt/>) led by Portuguese Environment Agency (end-user of the Space For Shore Project).

All the data that will be used for product validation, are archived by the consortium. No additional field survey or data collection are needed.

5.1.16.3.2 Imagery

Sentinel –1 data described in section 4.5.3.2.1 for French POC sites will be used again.

Sentinel –1 data close to the date of field surveys carried out in Portuguese POC site will be analysed to check if a well-defined swell is presented. If the imagery, that matches with observations, accomplishes this requirement, bathymetry will be derived using Bathymetry Swell Inversion-Wavelet Transform. Therefore, the validation of this new algorithm can be performed at this POC site too.

5.1.16.4 Expected results

The main result expected from this validation plan is:

- The suitability of the new algorithm to derive bathymetries at shallower waters in high energetic environments.

5.1.16.5 Team involved in the product validation plan

The team involved in this validation action is composed of:

- I-SEA,
- Aveiro University,
- End-user enrolled in Nouvelle Aquitaine and Aveiro region.



5.1.17 Submerged sand banks (algorithm 6a)

5.1.17.1 *Method and objective*

The main objective of the validation exercises for phase 2 will be to assess if Landsat imagery can be used to detect sandbars positions and how this can be performed as well as with what accuracy. If the results are satisfactory, a combination with Sentinel-2 data, which performs well (according to the already performed validation) would guarantee a denser time series to be used for such applications.

5.1.17.2 *Data*

Landsat 8 images will be used. Scenes will be selected as to be as close as possible from the date of the bathymetric survey used as in-situ reference data (September 2015, April 2016, April and October 2017, July 2018)

5.1.17.3 *Expected results*

The statistics associated with the accuracy of Landsat based extractions will be compared to the ones derived for Sentinel-2 and high-resolution data. Conclusions regarding the suitability of Landsat data for sandbars monitoring will be drawn.

5.1.17.4 *Team involved in the product validation plan*

The team involved in this validation action is composed of:

- Terrasigna,
 - University of Bucharest.
-
-

5.1.18 Mapping change of sandbars (algorithm 6b)

5.1.18.1 *Overall strategy and objective*

The indicator for underwater sandbars (sand riffs) that are derived for 2 German test sites (Sylt Odde and Kiel Probstei) have not yet been validated in phase 1. The products derived from optical data are currently based on RGB or single band brightness. The users are interested in the movement of the sand riffs therefore movies have been produced from subsequent images. Validation data is sparse for the North Sea test site (Sylt Odde), but measurements are available for Baltic Sea (Probstei).

The indicator has experimental status and will be further developed in close cooperation with the users during phase 2.

5.1.18.2 *Method*

Movies of subsequent images show consistency or movement of sand bars. Derived transects provide the positions of sand bar riffs over time. For Kiel Probstei in the Baltic Sea, transects are available showing the underwater habitats (not available yet to the team). The transects will be qualitatively compared to the RGB images. It will be tested if also a quantitative assessment of sand bar positions will be possible with the transect data.

5.1.18.3 *Data*

5.1.18.3.1 **Field data**

- Underwater transects of habitats of past years (to be confirmed)

5.1.18.3.2 **Satellite data**

- Sentinel-2 data



5.1.18.4 *Expected results*

As this indicator is an experimental indicator, we will investigate during phase 2 how to generate and validate the products. First discussions with the users have shown great interest in these products, especially because only very little information is available.

5.1.18.5 *Team involved in the product validation plan*

- LLUR (end user, product requirements and design, in-situ data, assessment)
- LKN (end user, product requirements and design, in-situ data)
- BC (producer optical data)

5.2 New products

5.2.1 Dune foot extraction using SAR data (3j)

5.2.1.1 *Overall strategy and method*

The dune foot is the main indicator of the shoreline in macrotidal sandy areas. The literature does not reveal any method adapted to the detection of the dune foot based on SAR imagery. However, backscattering observed by SAR is expected to change with changing surface property in the vicinity of the dune foot (*e.g.*, drastically varying vegetation cover, sediment roughness and texture ...).

Our strategy here is to superpose ground truth observations of the dune foot with SAR imagery in order to identify which property can be used in the SAR signature to extract the dune foot based on Sentinel-1 or ERS imageries. The capacities of all possible polarization and incidences configurations will be evaluated.

The detection process will be calibrated using a fraction of the GPS observations carried out for South Aveiro and Biscarrosse POC sites. Remaining data will be used for validation purposes.

5.2.1.2 *Data*

5.2.1.2.1 *Reference data*

Available filed data for both sites are reassembled in the Table 10. ***All surveys carried until 2019, that will be used for product validation, are archived by the consortium. Additional field surveys planned in 2020 will complete the necessary validation data (see details of the planned field survey at Biscarrosse in section 5.1.9.3.1, p.45).***

Unfortunately, our database does not allow us to assess the usefulness and the capacity of ERS data to retrieve the dune foot at Biscarrosse. As an alternative, airborne or satellite high resolution image may be proposed, if it appears relevant.

5.2.1.2.2 *Imagery*

All Sentinel-1 and ERS imageries recorded from 2 to 3 months before or after available field surveys will be download and processed.

5.2.1.3 *Expected results*

This experiment is figured out to demonstrate the potential of SAR imagery to allow detecting the dune foot along macrotidal sandy coasts.

If the conclusion is positive, then we will also derive an overall uncertainty value of the method together with evaluation of the average and maximum expected error bar on the derived dune foot location, taking into account the error introduced by the field survey (as already explained in previous sections dedicated to dune foot detection).



Table 10. Data available to calibrate and validate an algorithm based on SAR imagery dedicated to dune foot detection

Data type	date	Location
GPS surveys (INSHORE system)	2002, 14 th of April 2014, 20 th of March 2018, 2020	Aveiro
MNT derived from DGPS surveys	<ul style="list-style-type: none"> • April 2014, • February, May, September and November 2016, • February, April, June, July, August and November 2017, • February 2018 	Biscarrosse
GPS surveys of the dune foot	June 2019	Biscarrosse
Ortho-littorale	2000-2002 ; 2011-2014	Biscarrosse
Formosat imagery	2009, 2010, 2011	Biscarrosse

5.2.1.4 Team involved in the product validation plan

The team involved in this action is composed of:

- I-SEA,
- Aveiro University,
- Hamburg and Harokopio Universities,
- End-used enrolled in Nouvelle Aquitaine and Aveiro region.

5.2.2 Maximum swash zone excursion (run-up)

5.2.2.1 Overall strategy method and data

This last indicator is particularly challenging. It would be useful to assess the impact of onshore run-up incursion during major storm. The detection method must be established first, then validated.

As recommended in the literature, field surveys might be performed after major storm conditions to measure the line of the maximum swash (run-up) excursion with a DGPS-RTK. This first option is opportunistic and may be activated during phase 2 in case of major storm. In such a case, we will simultaneously order images with the emergency service offered by Airbus and organise a field survey in any of the site covered by our consortium.

Another option that might be considered is the utilization of a high frequency video camera (Almar et al., 2012; Andriolo, 2019; López-Olmédilla et al., 2019). This option offers excellent opportunities to analyse the capacity of optical and SAR imagery to record various water level whatever the prevailing wave-surge conditions. In order to propose soundful evaluation of both imageries, we will use video record performed at Biscarrosse for several years.

5.2.2.2 Expected results

This experiment is figured out to demonstrate the potential of optical and/or SAR imagery to allow detecting the run-up during severe storm conditions.

Although it is possible to easily derive waterlines from SAR and optical data, the image time-revisit may not be adapted to retrieve this indicator. The comparison between Biscarrosse video records and images series during storms will enable us to verify the exact capacity of space data to capture almost instantaneous features. If possible, realistic observation and validation of the concepts and hypothesis formulated at Biscarrosse will be evaluated during real storm conditions.

5.2.2.3 Team involved in this action

The team involved in this action is composed of:



- I-SEA (coordination),
 - All regional coordinators,
 - End-used enrolled in Nouvelle Aquitaine region.
-

5.3 Synthesis of the planned validation actions

An overall synthesis of all the validation actions planned is given in the Table 11. Table 11 includes detailed information about the algorithms and image families involved in the validation plan. Table 12 summarizes the number and type of reference data that will be used for product validation purposes. Data to be acquired in 2020 are clearly highlighted in the Table 12.



Table 11. Synthesis of the planned validation action, sensor names in bold and algorithm codes in italics are included

	BATHY.	BEACH WIDTH	CLIFF APEX	CLIFF FOOT	DUNE FOOT	MAXIMUM SWASH ZONE	SUBMERGED SANDBARS	TIDAL FLAT / TIDAL CREEK MORPH.	TOP-OF-THE-CLIFF VERTICAL MOVEMENT	WATERLINE AND MIDDLE OF SWAH ZONE
FR - ST RAPHAËL						Sentinel-1 Sentinel-2 <i>(2c, 2d, 3e)</i>				ERS Sentinel-1 Sentinel-2 Landsat <i>(2b, 2d)</i>
FR - HYERES						Sentinel-1 Sentinel-2 <i>(2c, 2d, 3e)</i>				ERS Sentinel-1 Sentinel-2 Landsat <i>(2b, 2d)</i>
FR - CAMARGUE						Sentinel-1 Sentinel-2 <i>(2c, 2d, 3e)</i>				Sentinel-2 Landsat <i>(2b, 2d)</i>
FR - CORNICHE BASQUE			Sentinel-1 CosmoSkyMed Pleiades <i>(1a, 1b + 3c, 3d)</i>	Sentinel-1 CosmoSkyMed Pleiades <i>(1a, 1b + 3c, 3d)</i>					Sentinel-1 <i>(3f)</i>	
FR - ERRETEGIA	Sentinel-1 <i>(4c)</i>		Sentinel-1 CosmoSkyMed Pleiades <i>(1a, 1b + 3c)</i> , Sentinel-1 Sentinel-2 Landsat-8 <i>(3i)</i>	Sentinel-1 CosmoSkyMed Pleiades <i>(1a, 1b + 3c)</i> , Sentinel-1 Sentinel-2 Landsat-8 <i>(3i)</i>					Sentinel-1 <i>(3f)</i>	
FR - BISCARROSSE		Sentinel-1 Sentinel-2 <i>(3e)</i>			WorldView-2 <i>(3a)</i> , Landsat combined with ERS/Sentinel-1 SPOT Sentinel-2 combined with Sentinel-1 <i>(3h, 3j)</i>	Sentinel-1 Sentinel-2 <i>(2c, 2d, 3e)</i>				Sentinel-1 Sentinel-2 <i>(2b, 2d)</i>
FR - VACHES NOIRES			WorldView CosmoSkyMed <i>(1a + 3c)</i> , Sentinel-1 ERS Landsat-5	Sentinel-1 WorldView CosmoSkyMed <i>(1b, 1a + 3c)</i> , Sentinel-1 ERS					Sentinel-1 <i>(3f)</i>	



		Landsat-8 Sentinel-2 (3i)	Landsat-5 Landsat-8 Sentinel-2 (3i)	
FR - QUIBERVILLE		Sentinel-1 Landsat-5 Landsat-8 Sentinel-2 (3i)		Sentinel-1 (3f)
GE - KIEL PROBSTEI				Sentinel-2 (6b) Landsat-8 Sentinel-2 (2a)
GE - NS BLAUORT				Sentinel-1 Sentinel-2 Landsat-8 (2e, 3g, 5c)
GE - NS SYLT ODDE				Sentinel-2 (6b) Landsat-8 Sentinel-2(2a)
RO - SULINA-SF. GHEORGHE			Sentinel-1 Landsat SPOT 1-5 (2c, 2d)	Sentinel-1 Landsat SPOT 1- 5 (2b, 2c, 2d)
GR - VISTONIS- MARONEIA		SPOT-7 (3d)	SPOT-7 (3d)	Sentinel-1 Landsat (2b)
PT -AVEIRO SOUTH	Sentine l-1 (4c)		Pleiades (1a, 3b), Pleiades (3a), Landsat combined with ERS/Sentinel-1 SPOT Sentinel-2 combined with Sentinel-1 (3h, 3j)	



Table 12. Synthesis of the number of available validation data. Note: Data to be collected during 2020 have been indicated in red after the symbol plus

	BATHY.	BEACH WIDTH	CLIFF APEX	CLIFF FOOT	DUNE FOOT	MAXIMUM SWASH ZONE	SUBMERGED SANDBARS	TIDAL FLAT / TIDAL CREEK MORPH.	TOP-OF-THE-CLIFF VERTICAL MOVEMENT	WATERLINE AND MIDDLE OF SWAH ZONE
FR - ST RAPHAËL						GPS (+1)				GPS (15+1)
FR - HYERES						GPS (+1)				GPS (2+1)
FR - CAMARGUE						GPS (+1)				GPS (5+1)
FR - CORNICHE BASQUE			GPS (2) Airborne (2)	GPS (2) Airborne (2)					Airborne (4) Ortho-littoral (6)	
FR - ERRETEGIA	Multibeam echosounder (1)		GPS (2) Airborne (2)	GPS (2) Airborne (2)					Airborne (4) Drone (1) Ortho-littoral (7)	
FR - BISCARROSSE		GPS (2)			GPS (13+1), Orthophoto (6)	Video system				
FR - VACHES NOIRES			TLS (20) SFM photogrammetry (1)	TLS (20) SFM photogrammetry (1)					Airborne (4) TLS (20) SFM photogrammetry (30) Ortho-littoral (7) Tacheometer topography (since 1992)	
FR - QUIBERVILLE			Airborne (3)						Airborne (2) Ortho-littoral (7) Tacheometer topography (since 1992)	
GE - KIEL PROBSTEI										Orthophotos (4) LaserScan (1) GPS (+1)
GE - NS BLAUORT								Orthophotos (3+1) LaserScan (1)		



				Drone (+1) GPS (+1)	
GE - NS SYLT ODDE					To be confirmed (6b) Orthophotos (9) LaserScan (1) GPS (1/year and after sand nourishments +1)
RO - SULINA- SF. GHEORGHE					Bathymetric surveys (4) GPS (1)
GR - VISTONIS- MARONEIA		GPS (1)	GPS (1)		GPS (1)
PT -AVEIRO SOUTH	Multibeam/ monobeam echosounder (1)			GPS (2+1)	



6 REFERENCES

- Ali T.A. 2003. New Methods for Positional Quality Assessment and Change Analysis of Shoreline Features. 156 p. Thèse : Géodésie : Columbus.
- Almar, R., Bergsmaa, E.W. J., Maisongrande, P., Almeida, L.P.M. 2019. Wave-derived coastal bathymetry from satellite video imagery: A show case with Pleiades persistent mode. *Remote Sensing of Environment*, 231, 111263. doi: 10.1016/j.rse.2019.111263
- Almar, R., Ranasinghe, R., Senechal, N., Bonneton, P., Roelvink, D., Bryan, K.R., Marieu, V., Parisot, J.-P. 2012. Video-based detection of shorelines at complex meso–macro tidal beaches. *Journal of Coastal Research*, 28, 1040. doi: 10.2112/jcoastres-d-10-00149.1
- Andriolo, U. 2019. Nearshore Wave Transformation Domains from Video Imagery. *Journal of Marine Science and Engineering*, 7 (6), 186. doi:10.3390/jmse706086
- Athanasidou, P., de Boer, W., Yoo, J., Ranasinghe, R., Reniers, A., 2018. Analysing decadal-scale crescentic bar dynamics using satellite imagery: A case study at Anmok beach, South Korea. *Marine Geology* 405. doi: [10.1016/j.margeo.2018.07.013](https://doi.org/10.1016/j.margeo.2018.07.013)
- Baptista, P., Cunha, T.R., Matias, A., Gama, C., Bernardes, C., Ferreira, O. 2011. New land-based method for surveying sandy shores and extracting DEMs: the INSHORE system. *Environmental Monitoring and Assessment*, 182 (1-4), 243-257.
- Baudouin, V. avec la collaboration de Plat, E., Bouchez, M., Sauvaget, B., Loquet, M., 2015. Identification et cartographie des aléas liés aux talus et falaises du littoral de Vendée, rapport BRGM/RP- 64271-FR, 151 p, 92 illustrations, 2 annexes.
- Caballero, I., Stumpf, R.P. 2019. Retrieval of nearshore bathymetry from Sentinel-2A and 2B satellites in South Florida coastal waters. *Estuarine, Coastal and Shelf Science*, 226, 106227. doi: 10.1016/j.ecss.2019.106277
- Cabezas-Ramadán, C., Pardo-Pascual, J.E., Palomar-Vázquez, J., Fernández-Sarría, A. 2019 Characterizing beach changes using high-frequency Sentinel-2 derived shorelines on the Valencian coast (Spanish Mediterranean). *Science of Total Environment*, 691, 216-231. doi:10.1016/j.scitotenv.2019.07.084
- Casal, G., Harris, P., Monteys, X., Hedley, J., Cahalane, C., McCarthy, T. 2019. Understanding satellite-derived bathymetry using Sentinel 2 imagery and spatial prediction models. *GIScience & Remote Sensing*. doi: 10.1080/15481603.2019.1685198
- Cenci, L., Disperati, L., Persichillo, M.G., Oliveira, E.R., Alves, F.L., Phillips, M. 2017. Integrating remote sensing and GIS techniques for monitoring and modeling shoreline evolution to support coastal risk management. *GIS & Remote Sensing*. doi: 10.1080/15481603.2017.1376370
- Chénier, R., Ahola, R., Sagram, M., Faucher, M.-A., Shelat, Y. 2019. Consideration of Level of Confidence within Multi-Approach Satellite-Derived Bathymetry. *International Journal of Geo-Information*, 8, 48, doi:10.3390/ijgi8010048
- Costa S., 2000. Réactualisation des connaissances et mise en place d'une méthode de suivi de la dynamique du littoral haut normand et picard. Rapport final, Préfecture de Picardie, Contrat de Plan Interrégional du Bassin de Paris (CPIBP), 103 p.
- Dehouck, A., Martiny, N., Froudefond, J.M., Sénéchal, N., Bujan, S., 2009. New outcomes from spatial remote sensing during the ECROS experiment: towards validation of ocean color products and large-scale bathymetry mapping in a coastal zone. *Journal of Coastal Research* SI56, 1756–1760.
- Di Luccio, D., Benassai, G., Di Paola, G., Mucerino, L., Buono, A., Roskopf, M., Nunziata, F., Migliaccio, M., Urciuoli, A., Montella, R. 2019. Shoreline Rotation Analysis of Embayed Beaches by Means of In-situ and Remote Surveys. *Sustainability*, 11(3), 725. doi: 10.3390/su11030725



- Dolan R., Hayden B.P., Hejrwood J. A, 1978. New photogrammetric method for determining shoreline erosion. *Coastal Engineering*, 2, 21-39.
- Esmail, M., Elham-Mahmod, E., Fath, H. 2019. Assessment and prediction of shoreline change using multi-temporal satellite images and statistics: Case study of Damietta coast, Egypt. *Applied Ocean Research*, 82, 274-282. doi: 10.1016/j.apor.2018.11.009.
- Evagorou, E., Mettas, C., Agapiou, A., Themistocleous, K., Hadjimitsis, D. 2019. Bathymetric maps from multi-temporal analysis of Sentinel-2 data: the case study of Limassol, Cyprus. *Advances in Geosciences*, 45, 397-409. doi: 10.5194/adgeo-45-397-2019
- Frodella, W., Ciampalini, A., Gigli, G., Lombardi, L., Raspini, F., Nocentini, M., Scardigli, C., Casagli, N. 2016. Synergic use of satellite and ground based remote sensing methods for monitoring the San Leo rock cliff (Northern Italy), *Geomorphology*, 264, 80-94.
- García-Rubio, G., Huntley, D., Russell, P. 2015. Evaluating shoreline identification using optical satellite images. *Marine Geology*, 359 (1), 96-105. doi: 10.1016/j.margeo.2014.11.002
- Hamylton, S.M., Hedley, J.D., Beaman, R.J. 2015. Derivation of high-resolution bathymetry from multispectral satellite imagery: a comparison of empirical and optimisation methods through geographical error analysis. *Remote Sensing*, 7, 16257-16273. doi:10.3390/rs71215829.
- Heo, J., Kim, J.H., Kim, J.W., 2009. A new methodology for measuring coastline recession using buffering and non-linear least squares estimation, *International Journal of Geographical Information Science*, vol. 23, no. 9, pp. 1165-1177.
- Himmelstoss, E.A., Henderson, R.E., Kratzmann, M.G., and Farris, A.S. 2018. Digital Shoreline Analysis System (DSAS) version 5.0 user guide: U.S. Geological Survey Open-File Report 2018–1179, 110 p. doi: 10.3133/ofr20181179.
- Jackson Jr, C. W., Alexander, C. R., & Bush, D. M. 2012. Application of the AMBUR R package for spatio-temporal analysis of shoreline change: Jekyll Island, Georgia, USA. *Computers & Geosciences*, 41, 199-207.
- Kaliraj, S., Chandrasekar, N., & Magesh, N. S. 2014. Impacts of wave energy and littoral currents on shoreline erosion/accretion along the south-west coast of Kanyakumari, Tamil Nadu using DSAS and geospatial technology. *Environmental earth sciences*, 71(10), 4523-4542.
- Lafon, V., Dehouck, A., Robinet, A., Marieu, V., Curti, C., Durou N. 2014. Détection d'indicateurs géomorphologiques littoraux par télédétection à très haute résolution spatiale (pp. 601-610) - doi:10.5150/jngcgc.2014.066.
- Le Mauff, B., Juigner, M., Ba, A., Robina, M., Launeaub, P., Fattal, P., 2018. Coastal monitoring solutions of the geomorphological response of beach-dune systems using multi-temporal LiDAR datasets (Vendée coast, France), *Geomorphology* 304, 121–140, doi: 10.1016/j.geomorph.2017.12.037.
- Letortu, P. 2013. Le recul des falaises crayeuses haut-normandes et les inondations par la mer en Manche centrale et orientale : de la quantification de l'aléa à la caractérisation des risques induits. Géographie. Université de Caen, 2013. Français.
- Li R., Liu J.K., Felus Y. 2001. Spatial modeling and analysis for shoreline change detection and coastal erosion monitoring. *Journal of Marine Geodesy*, 24 (1), 1-12.
- Lippmann, T.C., Holman, R.A., 1989. Quantification of sand bar morphology: a video technique based on wave dissipation. *Journal Geophysical Research* 94, 995–1011.
- Liu J.K., 1998. Developing Geographic Information System Applications in Analysis of Responses to Lake Erie Shoreline Changes. 133 p. Thèse : Géographie : Columbus : 1998.
- López-Olmédilla, L., Andriolo, U., Silva, P.A., Fontán-Bouzas, A., Fernández-Fernández, S. 2019. Wave runup field measurements: a case study at Costa Nova Beach (West Portugal). Livro de Resumos da 5ª Conferência sobre Morfodinâmica Estuarina e Costeira – MEC 2019, 13-14.
- Lorensen, W.E., Cline, H.E., 1987. Marching cubes: a high resolution 3D surface construction algorithm. *Computer Graphics*, 21, 4, 163-169.



- Luijendijk, A., Hagenaaers, G., Ranasinghe, R., Baart, F., Donchyts, G and Aarninkhof, S. 2018. The State of the World's Beaches. *Scientific Reports* 8(6641.) doi:10.1038/s41598-018-24630-6
- Martino, S., Mazzanti, P. 2014. Integrating geomechanical surveys and remote sensing for sea cliff slope stability analysis: The Mt. Pucci case study (Italy), *Natural Hazards and Earth System Sciences*, 14 (4), 831-848.
- Marques F. M. S. F., Matildes R., Redweik P. 2013. Sea cliff instability susceptibility at regional scale: a statistically based assessment in the southern Algarve, Portugal. *Natural Hazards Earth System Science*, 13, 3185–3203.
- Marques, F. M. S. F., Matildes, R., Redweik., P. 2011. Statistically based sea cliff instability hazard assessment of Burgau-Lagos coastal section (Algarve, Portugal). *Journal of Coastal Research*, 927-931.
- Mavraeidopoulos, A.K., Oikonomou, E., Palikans, A., Poulos, S. 2019. A Hybrid Bio-Optical Transformation for Satellite Bathymetry Modeling Using Sentinel-2 Imagery. *Remote Sensing*, 11, 2746. doi: 10.3390/rs11232746
- Misra, A., Ramakrishnan, B., Vojinovic, Z., Luijendijk, A., Ranasinghe, R. 2019. Assessment of Complementary Medium-Resolution Satellite Imageries for Nearshore Bathymetry Estimation. *Journal of the Indian Society of Remote Sensing*, 47 (3), 537-540. doi: 10.1007/s12524-018-0920-x
- Neokosmidis, S., Elias, P., Parcharidis, I., Briole, P., 2016. Deformation estimation of an earth dam and its relation with local earthquakes, by exploiting multi-temporal synthetic aperture radar interferometry: Mornos dam case (central Greece). *Journal of Applied Remote Sensing*, 10(2) doi:10.1117/1.JRS.10.026010.
- Nikolakopoulos, K., Kyriou, A., Koukouvelas, I., Zygouri, V., Apostolopoulos, D. 2019. Combination of Aerial, Satellite, and UAV Photogrammetry for Mapping the Diachronic Coastline Evolution: The Case of Lefkada Island. *ISPRS Int. J. Geo-Inf.* , 8, 489
- Nunes, M., Ferreira, Ó., Schaefer, M., Clifton, J., Baily, B., Moura, D., Loureiro, C. 2009. Hazard assessment in rock cliffs at Central Algarve (Portugal): a tool for coastal management. *Ocean and Coastal Management*. doi: 10.1016/j.ocecoaman.2009.08.004
- Plat, E., avec la collaboration de Baudoin, V., Decotte, T., 2013. - Identification et cartographie des aléas liés aux talus et falaises du littoral de Loire Atlantique, rapport BRGM/RP- 62521-FR, 80 illustrations, 3 annexes.
- Otsu, N. A. 1979. Treshold Selection Method from Gray-Level Histograms. *IEEE Transactions on Systems, Man, and Cybernetics* Vol. SMC-9, No. 1. doi: 10.1109/TSMC.1979.4310076.
- Oyedotun, T. D. T., Ruiz-Luna A., Navarro-Hernández, A. G. 2018. Contemporary shoreline changes and consequences at a tropical coastal domain. *Geology, Ecology, and Landscapes*. doi: 10.1080/24749508.2018.1452483
- Payo, A, Jigena Antelo, B. J., Hurst, M., Palaseanu-Lovejoy, M., Williams, C., Jenkins, G., Lee, K., Favis-Mortlock, D., Barkwidth, A., Ellis, M. A., 2018. Development of an automatic delineation of cliff top and toe on very irregular planform coastlines (CliffMetrics v1.0). *Geosci. Model Dev. Discuss.*, <https://doi.org/10.5194/gmd-2018-83>.
- Pereira, P., Baptista, P., Cunha, T., Silva, P.A., Romão, S., Lafon, V. 2019. Estimation of the nearshore bathymetry from high temporal resolution Sentinel-1A C-band SAR data - A case study. *Remote Sensing of Environment*, 223, 166-178. doi: 10.1016/j.rse.2019.01.003.
- Poli, D., Remondino, F., Angiuli, E., Agugiario, G., 2015. Radiometric and geometric evaluation of GeoEye-1, WorldView-2 and Pleiades-1A stereo images for 3D information extraction. *ISPRS J. Photogramm. Remote Sens.*, 100, 35–47.
- Redweik, P., Matildes, R., Marques, F., Santos, L. 2009. Photogrammetric Methods for Monitoring Cliffs with Low Retreat Rate. *Journal of Coastal Research*, SI 56. 1577.
- Reimers, H.-C. (2003): Sedimentverteilung und Benthosverbreitung in den Watten der Dithmarscher Bucht als Indikator für morphodynamische Veränderungen. Abschlussbericht zum Forschungsvorhaben SEDIMORV, GKSS-Folrschungszentrum Geeshacht, GKSS 2003/18
- Robin, M., 2002a. Télédétection et modélisation du trait de côte et de sa cinématique. In : Baron-Yelles N., Goeldner-Gianella L., Velut S. (dir). *Le Littoral, regards, pratiques et savoirs. Etudes offertes à Fernand Verger*. Paris : Rue d'Ulm-Presses universitaire de l'École Normale Supérieure, 2002, p.95-115.



- Robin, M., 2002b. Étude des risques côtiers sous l'angle de la géomatique. *Annales de Géographie*, 2002, n°627-628, p.471-502.
- Román-Rivera, M.A., Ellis, J.T., 2019. A synthetic review of remote sensing applications to detect nearshore bars. *Marine Geology* 408, 144-153, [doi: 10.1016/j.margeo.2018.12.003](https://doi.org/10.1016/j.margeo.2018.12.003).
- Rosser, N. J., Petley, D. N., Lim, M., Dunning, S. A., Allison, R. J. 2005. Terrestrial laser scanning for monitoring the process of hard rock coastal cliff erosion. *Quarterly journal of engineering geology and hydrogeology*, 38 (4), 363-375.
- Ruessink, B., Bell, P., van Enckevort, I.M., Aarninkhof, S.G., 2002. Nearshore bar crest location quantified from time-averaged X-band radar images. *Coastal Engineering* 45, 19–32. [doi: 10.1016/S0378-3839\(01\)00042-4](https://doi.org/10.1016/S0378-3839(01)00042-4)
- Sagawa, T., Yamashita, Y., Okumura, T., Yamanokuchi, T. 2019. Satellite Derived Bathymetry Using Machine Learning and Multi-Temporal Satellite Images. *Remote Sensing*, 11, 1155. doi:10.3390/rs11101155
- Srivastava A., Niu X., Di K., Li R., 2005. Shoreline modeling and erosion prediction. In: ASPRS 2005 Annual Conference (Baltimore, Maryland), 11p.
- Tatui, F., Constantin, S., 2020. Nearshore sandbar crest position dynamics analysed based on Earth Observation data. *Remote Sense Environment* 237. doi:10.1016/j.rse.2019.111555
- Tătui, F., Vespremeanu-Stroe, A., Ruessink, G.B., 2016. Alongshore variability of cross-shore bar behavior on a nontidal beach. *Earth Surf Process Landforms* 41. [doi: 10.1002/esp.3974](https://doi.org/10.1002/esp.3974)
- Thieler, R.E., Himmelstoos, E.A., Zichichi, J.L., Ergul, A. 2009. The Digital Shoreline Analysis System (DSAS) version 4.0 - An ArcGIS Extension for Calculating Shoreline Change: U.S. Geological Survey Open-File Report 2008-1278.
- Toure, S., Diop, O., Kpalma, K., Seidou Maiga, A. 2019. Shoreline detection using remote sensing: a review. *ISPRS International Journal of Geo-Information*, 8(2), 75. doi: 10.3390/ijgi8020075
- Vos, K., Harley, M.D., Splinter, K.D., Simmonsland, J.A., Turner, L. 2019. Sub-annual to multi-decadal shoreline variability from publicly available satellite imagery. *Coastal Engineering*, 150, 160-174. doi: /10.1016/j.coastaleng.2019.04.004
- Walstra, D.-J., Wesselman, D., van der Deijl, E., Ruessink, G., Walstra, D.-J.R., Wesselman, D.A., Van der Deijl, E.C., Ruessink, G., 2016. On the Intersite Variability in Inter-Annual Nearshore Sandbar Cycles. *Journal of Marine Science and Engineering* 4, 15. [doi: 10.3390/jmse4010015](https://doi.org/10.3390/jmse4010015)
- Wang, Y., Liu, Y., Jin, S., Sun, C., Wei, X. 2019. Evolution of the topography of tidal flats and sandbanks along the Jiangsu coast from 1973 to 2016 observed from satellites. *ISPRS Journal of Photogrammetry and Remote Sensing*, 150, 27-43. doi: 10.1016/j.isprsjprs.2019.02.001.
- Warrick, J. A., Ritchie, A. C., Adelman, G., Adelman, K, Limber, P. W. 2017. New Techniques to Measure Cliff Change from Historical Oblique Aerial Photographs and Structure-from-Motion Photogrammetry. *Journal of Coastal Research*, 33(1), 39 – 55.
- Werner, C., Wegmüller, U., Strozzi, T., and Wiesmann, A., 2003. Interferometric point target analysis for deformation mapping. *Proceedings of IGARSS'2003*, 7, 4362–4364.
- Yuhi, M., Matsuyama, M., Hayakawa, K., Yuhi, M., Matsuyama, M., Hayakawa, K., 2016. Sandbar Migration and Shoreline Change on the Chirihama Coast, Japan. *Journal of Marine Science and Engineering* 4, 40. [doi: 10.3390/jmse4020040](https://doi.org/10.3390/jmse4020040)

- End -

